STRUCTURAL LIGHTWEIGHT CONCRETE WITH PUMICE AGGREGATE

LIU XIAOPENG

NATIONAL UNIVERSITY OF SINGAPORE

2005

STRUCTURAL LIGHTWEIGHT CONCRETE WITH PUMICE AGGREGATE

LIU XIAOPENG

A THESIS SUBMITTED

FOR THE DEGREE OF MASTER OF ENGINEERING

DEPARTMENT OF CIVIL ENGINEERING

NATIONAL UNIVERSITY OF SINGAPORE

2005

ACKNOWLEDGEMENTS

I wish to express my deep gratitude to my supervisor Associate Professor Wee Tiong Huan for his excellent guidance, invaluable suggestions, constant encouragement and criticism. The accessibility and infinite patience shown are beyond the expectations of supervisors. I own them a lot more than I can express in words. Particular thanks are given to Associate Professor Tan Kiang Hwee, who has given a lot of suggestions in my research program; Dr. Kong Kian Hau, Dr, Tamilselvan s/o Thangayah, Dr. Abdullah, and Mr. Lee Sun Nee have given a lot of valuable suggestions in the course of my research.

I gratefully acknowledge the co-operation and assistance of laboratory manager Mr. Sit and other technical officers in the Department of Civil Engineering. The assistance given by them in conducting the experiment work is honestly appreciated. My sincere thanks go to Mr. Ang Beng Onn, Ms. Annie Tan, Mr. Ow, Mr. Choo, Mr. Koh, and Mr. Kamsam for the help in the laboratory work.

My deepest gratitude is extended to my girlfriend Miss Jin Xue for her love, support and generous encouragement throughout this study.

I sincerely thank my colleagues and all my friends for their generous support during this work. I extend special thanks to my colleague Mr. Babu and Mr. Velu for their kind assistance in many occasions.

TABLE OF CONTENTS

SUMMARY

This thesis presents the results of extensive tests to investigate the mixing proportion, density, mechanical properties (compressive strength, modulus of elasticity, flexural strength and tensile strength), creep and drying shrinkage of high strength lightweight concrete made of pumice aggregates with the strength level of 18.5 to 27.4 MPa and the corresponding air-dry density of 1579 to 1836 kg/m^3. Material variables include the volume and composition of cementitious materials, pumice aggregate content by volume, replacement of sand by volume using fine pumice aggregates, and air content. Particular emphasis has been given to study the effect of concrete strength and density on modulus of elasticity, tensile strengths (flexural and splitting tensile), and Poisson's ratio of pumice concrete. Study on the size effect of specimens on compressive strength of concrete has also been done. The adequacy of some of the familiar relationship for predicting modulus of elasticity & tensile strength of concrete has been critically examined and suitable expressions are suggested.

To exploit the potential of using pumice concrete as structural element, further study has been carried out on the flexural behaviour of pumice concrete beams with limited experimental data. Flexural tests are conducted through four singly reinforced beams (three using pumice concrete beam and one using normal weight concrete (NWC) as the reference) and one doubly reinforced pumice concrete beam. The variables are the ratio of tensile steel content, ρ to the balanced steel content, ρ_b.

The ratio ranges between $0.10 \leq \rho / \rho_b \leq 0.49$ with a compression reinforcement ρ' being $0.21\,\rho_b$. The concrete strength is targeted at 25 MPa for all the beams. Test results are presented in terms of load-deformation behaviour, ductility index and cracking behaviour. Unlike reinforced NWC beam, for reinforcement ratio, ρ / ρ_b of 0.31, the displacement index (μ_d) of reinforced pumice concrete beam (with an average f_c' = 23.8 MPa) is significantly less than 3, the value specified by the code. The flexural design provisions of the ACI 318 building code are found to underestimate the measured deflections under short term service loads up to about 21.5 %, but give a safe prediction of the ultimate flexural strength, the code values being 20 % on average higher than the experimental results.

Key words: Pumice aggregate, lightweight concrete, mechanical properties, creep, shrinkage, flexural behaviour of beam

NOMENCLATURE

A_s	= Area of tensile reinforcement
A_s'	= Area of compression reinforcement
A	= Shear span
b	= Width of beam section
c	= Depth of neutral axis from the extreme compression fiber (at ultimate load)
C_c	= Resultant force due to concrete compressive force
C_s	= Force in compression steel
d	= Effective depth of beam section
E_c	= Modulus of elasticity of concrete
$E_{c,cal}$	= Calculated value of concrete modulus of elasticity
$E_{c,\exp}$	= Experimental value of concrete elastic modulus
E_S	= Modulus of elasticity of steel reinforcement
FM	= Fineness modulus
f_c'	= Concrete compressive strength obtained from cylinder test
f_{cck}	= Concrete compressive strength obtained from 150×150 mm cube test
f_{ct}	= Stress in the extreme tension fiber
f_{cu}	= Concrete compressive strength obtained from cube test
f_{cy}	= Concrete compressive strength obtained from cylinder test
f_p	= Stress at the proportional limit of the stress-strain curve
f_r	= Modulus of rupture of concrete

f_s = Stress in tension steel

f_s' = Stress in compression steel

f_{sp} = Splitting tensile strength of concrete

f_y = Yield strength of tensile steel

h = Height of beam section

I = Moment of inertia of beam section

I_{cr} = Moment of inertia for cracked section

I_e = Effective moment of inertia

I_g = Moment of inertia for gross concrete section

k = Neutral axis depth factor

k_1 = Ratio of average compressive stress to maximum stress in the compression zone of a beam section

k_2 = Ratio of the distance between the extreme compression fiber and the resultant of the concrete compressive force to the depth of the neutral axis

k_3 = Ratio of the maximum stress in the compression zone of a beam to the cylinder strength

L = Beam span (center to center distance of supports)

M_a = Maximum bending moment in the beam at particular load level M_{cr} cracking moment

$M_{cr,cal}$ = Calculated cracking moment

$M_{cr,\exp}$ = Experimental cracking moment

M_f = Moment at failure level

M_u = Ultimate (maximum) moment

$M_{u,\exp}$ = Experimental ultimate moment

P_{cr} = Cracking load

p_u = Ultimate (maximum) load

$P_{u,\exp}$ = Experimental moment

SD = Standard deviation

s_{av} = Average crack spacing

β_1 = Equivalent rectangular stress block depth factor suggested by ACI 318(1999)

δ = Maximum beam deflection

δ_s = Maximum beam deflection at service load level

$\delta_{s,cal}$ = Calculated deflection at service load

ε_c = Concrete compressive strain

ε_{cu} = Concrete compressive strain capacity under bending

ε_s = Strain in tensile steel

$\varepsilon_s^{'}$ = Strain in compression steel

μ_d = Deflection ductility index

$\omega_{cr,\exp}$ = Experimental crack width

$\omega_{cr,\max}$ = Maximum crack width

ρ = Tensile reinforcement ratio: A_s / bd

$\rho^{'}$ = Compressive reinforcement ratio: $A_s^{'} / bd$

ρ_b = Balanced compressive reinforcement ratio: A_b / bd

List of Tables

List of Figures

CHAPTER ONE

INTRODUCTION

1.1 Background

Concrete with a density between 1350 and 1900 kg/m^3 and a minimum compressive strength of 17 MPa is defined as structural lightweight concrete (ACI 213R-87, 1998). The past two decades have witnessed the widespread extension of the knowledge of the properties and application of high-strength, lightweight concrete based on artificial lightweight aggregates (Gjerde, 1982; Finn, 1987; Hoff, 1992). Improved structural efficiency (strength-mass ratio) has provided economic advantages to many commercial structures, with the improvements in concrete properties aided by the development of new admixtures (e.g. high range water reduce admixture (HRWRA)).

Pumice is a natural sponge-like material of volcanic original composed from molten lava rapidly cooling and trapping millions of tiny air bubbles. Pumice aggregates are abundant at the outskirt of volcanic maintains, particularly in Mediterranean area, Rocky Mountains in US, and most part of Turkey and Indonesia.

The utilization of LWAC based on natural lightweight aggregate materials such as pumice has been rather limited, partly due to insufficient quality obtainable in the early years when the material and production know-how is low and partly due to lack of enthusiasm and industrial interests. In recent years, the existing limited research has shown that structural concrete with compressive strength up to 25 MPa can be produced with adequate economic benefits (Yeginobal and Sobolev, 1988; Ramazan, 2001; Haktanir and Altun, 2002; Hossain, 2003).

When structural lightweight concrete with pumice is used in construction and

maintenance of civil engineering structures, the resultant benefits of reduced overall costs, better heat and sound insulation and better resistance to fire can be realized. Despite of its lower compressive strength and lower modulus elasticity, pumice concrete can be potentially used in many kinds of structural elements. For example, the disadvantage of possible excessive deformation in such elements as beams and slabs due to its low elasticity modulus can be compensated by keeping the span as small as possible, and by keeping the slab depths just a little greater than customary values. Further more, in structural wall systems, the expected stress level usually proves to be very low, and consequently, high material strength is not required. As a matter of fact, in this case the flexural effects under horizontal loads are reduced by the relatively large available internal lever arm. The reduced self-weight of walls also leads to a remarkable reduction in the stress. Under these conditions, the size of the foundation can be reduced too, and moving and mounting are made easier when precast elements are used.

Although the strength of pumice concrete has been reported, there exists no literature reporting the complete mechanical properties of high-strength pumice aggregate concrete. Besides, the results of drying shrinkage and creep of pumice concrete have not been reported before. The knowledge of these properties is important for the practical usage of structural pumice concrete.

Concrete structures are generally designed to take advantage of its compressive strength. The primary structural property of concrete a designer is generally concerned with is the compressive strength of concrete at a specific age. However, there are several other properties described below which a designer needs to know to design efficient and safe structures.

The present design methodology ensures that a structure behaves elastically under

service loads. Consequently the static modulus of elasticity and Poisson ratio are important parameters in determining short term deformations.

Although the tensile strength of concrete is assumed to be negligible in ultimate strength calculations, in design of pre-stressed concrete and also in calculating the cracking moment of flexural members, the tensile and flexural strength are of considerable importance.

The stress-strain curve of concrete in compression is a fundamental property needed for ultimate design of concrete structures. The stress-strain curves of concrete in compression give an indication of the ductility of concrete components heavily loaded in compression such as column under minimum eccentric loading. Both the compressive strength and the ductility of the concrete can be enhanced by a confining pressure provided by lateral reinforcements such as ties or stirrups. The compressive strength and the ductility enhancement as governed by the reinforcement amount and pattern are important properties required by a designer.

There are several other properties such as creep and shrinkage which a designer needs to have for the efficient design of concrete structures

1.2 Research Significance

The development and use of lightweight concrete is important to the construction and maintenance of civil engineering structures. Lightweight concrete has the potential to increase the economy and durability of the structural systems and are mainly focused on by researchers throughout the world. Pumice being a natural aggregate of abundant resource around the world, is cost-effective and environmentally friendly. However, pumice is far from being fully utilized in lightweight concrete at the time being. The current investigation provides information on the density, mechanical properties, creep

and drying shrinkage of pumice concrete with consideration for structural application, obtained from a controlled set of experiments that includes a number of material variables.

1.3 Objective And Scope Of Research

Many researchers have reported research works on lightweight concrete with pumice aggregates (Yeginobal and Sobolev, 1988; Ramazan, 2001; Haktanir and Altun, 2002; Sahin and Uysal, 2003; Hossain, 2003). However, the full range of mechanical properties and production guidance is limited. The main objective of this study is to develop high strength structural pumice aggregate concrete, investigate its mechanical properties and explore the possibility of its structural application. The research program is given in Figure 1.1.

The scope of the research work is divided into three parts:

(1) To produce high strength structural pumice aggregate concrete in the laboratory. This includes reviewing available literature on lightweight aggregate concrete (LWAC) to identify mix parameters which are found to have significant influence on the structural properties.

(2) To investigate the mechanical properties of pumice aggregate concrete, such as density, compressive strength, tensile strength, modulus of elasticity, Poisson's ratio, stress-strain relationships, as well as drying shrinkage and creep.

(3) To investigate the flexural behaviour of reinforced pumice LWAC beam.

1.4 Outline Of Thesis

The present thesis is divided into six chapters:

(1) Chapter One introduces the background, research scope and objectives of this study.

(2) Chapter Two gives literature review on previous and recent studies dealing with the production, mechanical properties of LWAC and the flexural behaviour of reinforced pumice LWAC beam.

(3) Chapter Three presents a detailed description of the production of structural pumice aggregate concrete in the laboratory.

(4) Chapter Four involves investigating the mechanical properties of the pumice LWAC. Analysis and discussions of the experimental results are also included.

(5) Chapter Five aims at investigating the full flexural response of reinforced pumice LWAC beam with the comparison to that of a normal weight reinforced concrete beam of similar strength.

(6) Chapter Six summarizes the main findings of this study and provides some recommendations for future works.

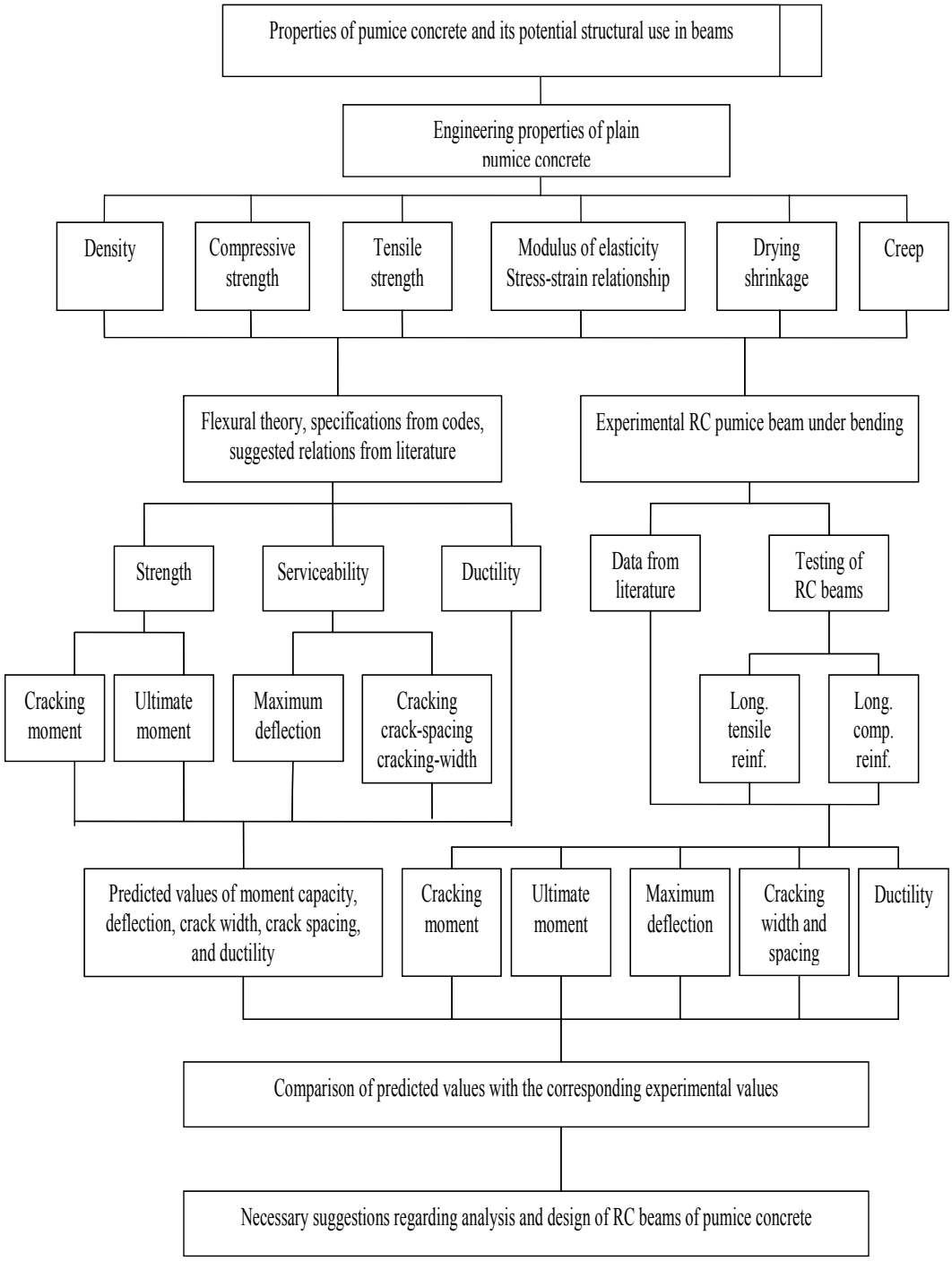

Figure 1.1 Research program

CHAPTER TWO

LITERATURE REVIEW

Up to now, studies on lightweight concrete with pumice aggregate have been scarce. However, considerable research work has been carried out on normal weight concrete (NWC) and artificial lightweight aggregate concrete (LWAC). Knowledge in the difference between LWAC and NWC is helpful for the study of high-strength pumice aggregate concrete. In this study, the difference between LWAC and NWC is presented and studies on both artificial LWAC and natural pumice aggregate concrete are reviewed.

2.1 Difference Between Lightweight Aggregate Concrete and Normal Weight Concrete

Differences between LWAC and NWC concern the mixing stage, hardening stage, ductility, failure modes et al.

In the mixing stage, the porous, water-absorbing lightweight aggregates can affect the workability of the concrete (Neville et al., 1987) as well as the effective water/binder ratio (ACI211.2, 1998). In the hardening stage, the relatively low specific heat and high insulating capacity of LWAC will cause a higher hydration temperature. The water initially present in the porous aggregate particles may affect the moisture state in the hardening system to a large extent. Volume changes take place with the changes in the state of water in the pore system in the early stage of hardening.

In the hardened concrete, the differences between LWAC and NWC are mainly due to differences in the strength and elastic modulus of the aggregate, and particularly

to differences of the matrix-aggregate interfacial zone. These differences determine the degree of heterogeneity of concrete. The properties of the interfacial zone are determined by the surface characteristics of the aggregate, as well as the pore structure and the initial water content of the aggregates (Isserman and Bentur, 1996). Depending on the pore structure of the aggregates, some reaction products e.g. calcium hydroxide, will even penetrate into the pores of the aggregates. This is more likely in aggregates with higher absorption and bigger pores (Isserman and Bentur, 1996).

The strength of many lightweight aggregates (LWA) is about the same as the strength of the hardened paste. The matrix-aggregate interfacial zone is of a higher quality than in the case of NWC. The bleeding effect on aggregate surfaces is also reduced due to the reduced response of the LWA to vibration energy during compaction of the concrete. It means that in many LWAC, the interfacial zone is not the weakest link. With comparable modulus of elasticity for the LWA and the mortar, the stress will be more evenly distributed in LWAC than in NWC. Often, the LWA has even lower modulus of elasticity than the mortar phase, causing the mortar to attract more stress. The resulting local transverse tensile stress will act in the mortar, and not in the interface zone. As a matter of fact, in this case, the interface zone will partly be confined by transverse compressive stress (FIP, 1983).

The strength and fracture toughness of LWA are substantially lower than those of normal weight aggregate (NWA) of natural origin, and possibly even the mortar phase. The crack initiation of LWAC takes place at a rather high stress level due to the elastic compatibility of the phases. The strength of LWA can be the strength limit of LWAC (Bremner and Holm, 1986; Chi and Huang, 2003).

2.2 LWAC Mix Design And Production

Comprehensive reports reporting the properties of lightweight concretes and lightweight aggregates have been published by Shideler (1957), Reichard (1964), Holm (1983) and Valore (1988). In general, proportioning rules and techniques used for ordinary concrete mixes apply to lightweight concrete with added attention given to the concrete unit weight and the influence of the water absorption characteristics of the lightweight aggregate *(*ACI 213R-87, 1994*).* Specifications for structural-grade lightweight concrete usually require minimum values for compressive and tensile splitting strength, maximum limitations on slump, specified ranges of air content and a limitation on maximum fresh unit weight.

2.2.1 Constituents of LWAC

The essential components in LWAC are similar to that of NWC, aside from the difference in coarse aggregate.

(1) Binder

The most commonly used binder is cement, but other supplementary materials such as silica fume, fly ash and slag can also be included as long as their acceptability has been demonstrated. The addition of supplementary materials as partial replacement to the binder can enrich the concrete with various desirable properties in its fresh and hardened states (Narayanan and Ramamurthy, 2000).

(a) Cement

ACI 213R-87 (1994) states that, the same criteria for choosing type of cement, fly ash, ground granulated blast furnace slag and silica fume applies for LWAC as for NWC. ACI 523.1R-92 (1992) recommends the use of Portland cement or Portland blast furnace slag cement which conforms to the respective ASTM Specifications: C 150 (1994), Type I or Type III; Type IA or Type IIIA; C 595 (1994) , Type IS or Type IS-A. It also points out that high-early-strength cements for e.g. Type III or III A, are often used to advantage in the production of low density concrete. Cement content less than 250 kg/m^3 should not be used (Dossier, 1997). In modern codes, there is a trend to focus more on the effective water/binder ratio rather than on the cement content or strength grade while formulating requirements for durability.

(b) Silica fume

The silica fume particles assist in reducing the bleeding and segregation by segmenting the water flow in fresh concrete and ensure a densely packed microstructure in hardened concrete (Mehta and Aitcin, 1990). The high silica content and the larger surface area of silica fume make it a highly reactive pozzolan reacting with the calcium hydroxide liberated from the hydration of cement to produce more cemetitious materials. Tests reported by Wolsiefer and Clear (1995) demonstrated significant improved physical properties when silica fume is added to concrete containing structural lightweight aggregate (LWA). It is reported that 5 to 10 % replacement of cement by silica fume (SF) is economic and practical (Zhang, 1990).

(c) Ground granulated blast furnace slag

Blast furnace slag takes an active part in hydration and makes substantial modifications to the resulting microstructure (Taylor, 1990). In most cases, ground granulated blast furnace slag (GGBS) has been used in proportions of 25 %~70 % by mass of total cementitious materials, generally at the upper end of the range for maximum benefit (ACI 233R-95, 1996). It has been shown that slag imparts several technical advantages to Portland cements in concrete including low heat of hydration, resistance to sulfate attacks and reduced alkali silica reaction (ASR) (Numata et al., 1986). Blast furnace slag cement (60 % to 70 % slag), in combination with 10 % to 20 % silica fume, has found to reduce the expansion caused by ASR (Ramachandran, 1995)

(2) Lightweight aggregate

(a) Shape and size of the grains

The shape of the grains is a well-known factor that influences the properties of LWAC. It affects, like in NWC, the workability of LWAC. Together with the particle size distribution and the water absorption of the aggregates, the particle shape determines the content of cement and the amount of mix water (Weigler et al., 1972). Normally, the recommended maximum particle size is limited by the concrete strength requirement, since larger particles tend to be weaker. Large particles also tend to increase the segregation driven by the internal density differences, since the surface area/volume ratio of the particles decreases with increasing particle size. Like NWC, the specific surface of the aggregate affects the workability. This is even more when the grain surface exhibits an open pore structure.

(b) Surface properties of the LWA

The surface properties of the aggregates affect the workability of concrete and the bond between paste and aggregate. The mortar penetrating into the pores of the grain would not improve workability but density would increase (Weigler et al., 1972). Ideally the aggregate particles should be spherical, with a hard and closed external skin providing a good bond with the cement paste, while the interior of the particles should have a high proportion of voids (Cemburau 1974). Besides these mechanical properties of the LWA surface, some LWA's have a pozzolanic reactive surface. This pozzolanic reactivity will lead to an interaction of the LWA and the cement paste, thus forming a very dense and strong interfacial transition zone (Zhang, 1992).

(c) Water absorption

One important effect of the aggregate absorption is the loss of concrete workability (Asgeirsson, 1984; Punkki et al., 1995,). Another effect is the reduction of the effective water/binder ratio as water penetrates into the LWA during setting (Hammer et al., 1992). The rate of initial absorption is important to foresee the loss of workability of the fresh mix (Weigler et al., 1972). In mix design, water absorption by LWA during setting is often assumed equivalent to that absorbed in the case of pure water after 1 hour. However, the water absorption in concrete may vary (Punkki et al., 1995).

(d) Effect of LWA strength on LWAC strength

The strength limiting effect of LWA increases with decreasing water/binder ratio (Smeplass, 1997a). Such results will form the basis for practical guidelines for the choice of aggregates within each strength grade. Definition of an upper strength grade of LWAC will depend on the strength of available LWA and the strength potential of a

particular kind of LWA is close to its particle density (Smeplass, 1997b). So that while a 20 MPa mix might be achieved for a density of 1200 kg/m^3, this value would increase to 1800 for an 80 MPa mix (Lazarus, 1993). The lowest densities require lightweight sand, whereas the higher densities require natural sand.

(3) Natural sand

In most cases a combination of normal density and lightweight aggregate is used when batching LWAC. Factors influencing the optimum split between normal weight aggregate (NWA) and LWA are the density and strength requirements of the concrete, and the quality and grading availability of the LWA. Often fine grades of LWA are only available as crushed coarse LWA. In these cases, the water demand will increase and the workability characteristics are impaired. An optimum mix design is therefore normally achieved by combining coarse LWA with normal density sand. The requirements for the normal density (ND) sand will then be the same as that for NWC. To reduce segregation, a continuous grading of the total aggregate, calculated on a volume basis, is preferred (FIP, 1983). The maximum particle size of the normal density sand should then correspond to the minimum particle size of the LWA. The optimum amount of fines should, like for NWC, fit the amount of cement paste, i.e. for cement rich mixes, low-fine sand is preferred and vice versa.

(4) Mixing water

According to ACI 523.3R (1993), mixing water for concrete should be fresh, clean and drinkable. The minimum water to cement (w/c) ratio required for full hydration of the cement paste is 0.36 (Mehta, 1986; Neville, 1987). In the production of normal strength concrete this limit is always exceeded, as a higher w/c ratio is required to

satisfy the workability requirements. However, as reported by other researchers (Carrasquillo et al. 1981; Ahmad and Shah, 1985) the workability can be achieved at low w/c ratios by incorporating a water-reducing admixture. It has been observed that the strength of concrete continues to increase with the reduction of w/c ratio below the 0.36 limit. The empirical relationships between w/c ratio and the compressive strength, available for normal strength concrete, may not be applicable for high strength concrete below the full hydration limit of 0.36 (Mehta and Aitcin, 1990).

(5) Admixtures or additives

Good workability of concrete can not be achieved with a water to cement ratio below about 0.45 without the use of superplasticizer (Neville, 1987). Hence, to achieve high strength lightweight concrete, a superplasticizer is required, since w/c ratio will be below 0.45.

In general the effect of using superplasticizer in LWAC is similar to that of using them in NWC (FIP, 1983). It is possible that part of the fluid admixtures may be absorbed by LWA, thus reducing their action if the LWA is unsoaked. The absorption of a part of the free water with the dissolved additive will decrease the effectiveness of the latter (FIP, 1983). ACI 304.5R (1991) recommends the use of unsoaked LWA to avoid absorption of the additives into the LWA. Delayed addition of superplasticizers will also reduce the problem.

Air entraining agents can be used with LWAC. Its use reduces the density proportionally to the weight of the paste it replaces, enhances the workability and reduces the segregation and bleedings. Very often, air-entraining agents are used to provide higher frost resistance concrete (Weigler et al., 1972). Most air-entraining agents are formulated to give a total of 3 % to 6 % air by volume in most concrete

mixtures at their recommended dosage level. In ACI 211 (1998), recommended ranges of total air content is 4-8 % by volume for usually structural lightweight concrete with maximum aggregate size of 20 mm. Air content of LWAC is determined in accordance with the procedure of ASTM C260 (1994). The air-entraining agent named MICRO AIR, meeting the requirement of ASTM C260 is used in this study.

2.2.2 Mix proportion of LWAC

Workability, compressive strength and density are the three main design variables that need to be fulfilled by a suitable proportioning method for LWAC. By the traditional proportioning methodologies, the concrete strength is related to water-cement ratio; however, it is not valid for LWAC since they do not incorporate the mechanical properties of the lightweight aggregates.

The common methods used to proportion NWC are also applicable to LWAC, taking into account the following aspects:

(1) The density is an additional variable and depends on the mix design.

(2) The properties of the fresh and hardened concrete are heavily influenced by the LWA characteristics.

(3) The water absorption characteristics of the LWA

ACI 211.2 (1998) gives rather detailed advice for two practical procedures for selecting the proportions for LWAC. "Method 1 - Weight method" is applicable for lightweight coarse aggregate and normal density fine aggregate, while "Method 2 Volumetric method" is for use for all-lightweight aggregate concrete. The procedures include test and trial batching. Guidance for mix design of LWAC is also given in the FIP Manual of LWAC (1983).

2.2.3 Production

The volumetric proportioning of LWA is advisable. In the case of batching by weight, frequent checks on the bulk density of aggregates are mandatory in some standards in order to adjust for variations in the moisture content. Frequent control of LWA density and moisture content is the recommended normal procedure in most countries.

Control of the moisture content in the aggregate is of paramount importance in view of quality control. The lower the water/cement ratio, the more sensitive the mixes are to variations in the moisture content of the aggregate. Contrary to the North American tradition of feeding water saturated LWA into the mixer, the Norwegian system is to use dry LWA with less than 8 % moisture (Johnsen, 1995)

The procedures used to determine the consistency of NWC, such as compaction, flow table or the slump methods, are also valid for LWAC. The consistency of the LWAC measured by these tests is generally "softer", due to the shape of the aggregate and the density (Weigler et al., 1972). Normally the slump test tends to underestimate the workability of LWAC (Pankhurst, 1993). In practice, LWAC normally loses its workability faster than NWC.

2.3 Mechanical Properties Of LWAC

The mechanical performance of LWAC differs from that of conventional concrete. The following mechanical properties and mutual relationships between these properties will be reviewed here: compressive strength and density, tensile strength, correlation between tensile and compressive strength, modulus of elasticity and Poisson’s ratio, compressive stress-strain curve, creep and drying shrinkage.

2.3.1 Compressive strength

(a) Homogeneity (matrix-aggregate bond)

Excellent particle-matrix bond and similarity of particle and paste elastic moduli ensure that the matrix is used efficiently (Newman, 1993). As a result, LWAC does not rupture due to dislocation between the phases, but as a result of the collapse of the arching structure of mortar over the grain of LWA, which has a limited strength. The fracture line, therefore, goes through the aggregate (like in high strength concrete), the opposite of conventional concrete, where the failure is produced by the fracture in the mortar and separation between both phases, resulting in a line around the aggregate grains (Dossier, 1997).

(b) Effect of LWA strength on LWAC strength

The effect of the particular properties of the LWA on strength can be seen in Section 2.2.1-(2)-(d).

(c) Effect of size of test specimen

Compressive strength of LWAC is more independent of test specimen size as compared to NWC (Thorenfeldt, 1995). The correlation between cylinder and cube strengths is found to have average values of 0.9 for LWAC of LECA 800 and of 0.95 for LWAC of LECA 700 (Smeplass, 1997). The fact that the correlation between cylinder and cube strength is different for LWAC and NWC is considered a very important point since some standards use strength values based on cylinder tests, but use a fixed value for the ratio between cylinder and cube strength. This may lead to incorrect estimates of the strength.

(d) Effect of water/binder ratio and cement content

In general, in order to reach the same strength, a LWAC needs more cement or binder than conventional concrete. Weaker LWA will require even stronger mortars and higher cement contents (Newman, 1993). For concretes with strength higher than 40 MPa, this proportion of cement content increases. The increase in strength for a given increase in cement content depends on the LWA type. On the average, a 10 % increase will provide a 5 % increase in strength (Newman, 1993). Today the water/binder ratio is considered to be even more important than the absolute cement content.

(e) Strength development with age

LWAC has a faster hardening factor in the initial setting phase than conventional concrete, normally reaching 80 % of the 28 day strength within 7 days. The strength growth from 28 to 90 days is generally low and decreases with increasing concrete strength level. This is assumed to be a consequence of the strength limiting effect of the lightweight aggregate (Thorenfeldt, 1995). A lower long-term strength gain in LWAC results in a lower auxiliary capacity of the LWAC as compared to NWC designed to comply with the same strength grade.

2.3.2 Tensile strength

Tensile strength of concrete is important when considering cracking. LWAC presents a flexural and tensile splitting strength slightly inferior to that of NWC of the same compressive strength (Clarke, 1993; Zhang et al., 1995). The Norwegian design code, NS 3473 (1998) reduces the tensile strength of LWAC compared with NWC of the same compressive strength multiplying with a factor (0.3 + 0.7 D/2400) if the tensile

strength is not determined by testing, where D is the density of the concrete in kg/m^3. For the ratio between flexural and splitting tensile strength of high performance LWAC, values of 1.5 to 1.6 have been found (Curcio et al., 1998).

According to Weigler et al. (1972), the compressive strength of LWAC increases faster than the tensile strength. The ratio tensile/ compressive strength is normally in the 5 % to 15 % range for LWAC with compressive strength over 20 MPa. According to Curcio et al. (1998) the splitting tensile strength of high performance LWAC is about 6 % to 6.5 % of the cylinder compressive strength. The flexural strength of the same concrete is 9.8 % to 10.5 % of the compressive strength.

2.3.3 Modulus of elasticity and stress-strain relationship

The modulus of elasticity is a function of the individual moduli of its ingredients, their relative proportions and the bond between aggregate and matrix. Because of the high volume percentage of the aggregate in the concrete, the lower stiffness of most LWA will result in a lower modulus of elasticity of LWAC compared to NWC (Zhang et al., 1995). Chi et al., (2003) reported that the properties of lightweight aggregates and the water/binder ratio are two significant factors affecting the compressive strength and elastic modulus of concrete. A good correlation between modulus of elasticity and compressive strength has also been found by Curcio et al., (1998).

Anson and Newman (1966) reported that the stiffness and proportion of coarse aggregate have a considerable effect on the Poison ratio of the concrete. According to them, stiffer aggregates are found to be more effective in reducing the lateral expansion and hence result in a lower Poisson ratio. Hoff et al., (1995) reported an average Poisson's ratio of 0.20 for LWAC, with only slight variations due to age,

strength level, curing environment, or LWA used.

Stress-strain relationships for LWAC are generally characterized by a more linear ascending curve, more limited plastic strain and a steeper descending branch than NWC. The linear, brittle behaviour is usually enhanced with increasing strength. This will appear in concrete with moderate strength too if moderate density LWA is combined with high strength cementitious matrix (Thorenfeldt, 1995).

2.3.4 Drying shrinkage

Drying shrinkage is caused by the withdrawal of water from concrete kept in unsaturated air. It is an important property besides strength and durability for the practical construction of concrete. Shrinkage of concrete due to self-desiccation is known as autogenous shrinkage. Since its magnitude is of the order of 100 mirostrains for NWC, it has been ignored for practical purposes (Davis, 1940).

There are three microscopic scale mechanisms of drying shrinkage as follows: the variation in capillary depression, the variation in surface tension of colloidal particles, and the variation in disjoining pressure (Hua et al., 1995).

When structural lightweight aggregate concretes are proportioned with cementitious binder amounts similar to that required for NWC, the shrinkage of lightweight concrete is generally, but not always, slightly greater than that of ordinary concrete due to the lower aggregate stiffness. Cembureau (1974) reported that the final shrinkage of LWAC is about 1 to 1.5 times the final shrinkage of NWC of the same strength. Hoffmann and Stock (1983) reported for LWAC with cylinder strength of 40 to 50 MPa, that the drying shrinkage is 30 % higher than NWC. In ENV-1-4 (1992), it is stated that the final drying shrinkage values for lightweight concrete can be obtained

by multiplying the values for normal density concrete with a factor η_3 defined by η_3=1.2 (valid for compressive strength of 25 MPa or higher). Unlike NWC, data on the shrinkage behaviour of pumice concrete are very limited.

2.3.5 Creep

Several theories on creep behaviours have been proposed (Neville et al., 1983), and these generally fit into two categories, the seepage theory (Glucklich, 1962) and the viscous shear theory (Ruetz, 1968). Creep characteristics of any concrete type are principally influenced by aggregate characteristics, water and cement content (paste volume fraction), age at time of loading, type of curing and applied stress-to-strength ratio. The creep strain in concrete can be several times larger than the elastic strain under load, causing an increase in long-term deflection, loss of prestress, reduction in stress concentration and change in chamber.

Recent data on creep of LWAC made with different LWA and compared with with that of NWC surport the trend that creep of LWAC seems to continue to increase even at later ages. Short et al., (1963) states that creep is invariably higher for LWAC than for NWC. A difference of 20 % to 60 % of the creep of the NWC is generally to be expected. The ultimate creep is higher, the lower the strength.

2.4 Flexural Behaviour Of Reinforced LWAC Beam

2.4.1 Behaviour of reinforced concrete beam at different stage of loading

(a) Prior to loading

After initial hardening, concrete begins to shrink and causes compressive stress in reinforcement and tensile stress in concrete. These stresses usually vary along the beam depth – from the maximum value in the lowermost fiber to a minimum value in the top fiber. Due to the existence of these stresses, the cracking moment capacity of reinforced concrete (RC) beam will be reduced. Sometimes, these stresses alone can cause cracking in a RC member before it is called upon to carry any load.

When the reinforcement is asymmetrically arranged, shrinkage causes a non-uniform strain distribution, which results in warping of the member. The effective concrete modulus of elasticity of interest should refer to the portion of concrete in tension (ACI Committee 435, 1966). For the analysis of shrinkage curvature, comparisons with experimental data (Branson, 1963) indicated that good results can be obtained by considering gross section properties and using a reduced modulus E_{ct} equal to $E_c/2$ to account for the associated creep effect in which, E_{ct} is the sustained modulus for the effect of creep and E_c is the concrete modulus of elasticity obtained from 28 day cylinder test.

(b) Cracking and cracking moment

A RC beam responds elastically prior to cracking and the normal stresses generated by bending will be shared by both the steel reinforcement (rebar) and concrete in

proportion to their elastic modulus. Cracking occurs when the stress in the extreme tensile fiber reaches the modulus of rupture of the concrete, f_r. Although, the use of un-cracked transformed section properties taking into account presence of steel rebar, would be theoretically more accurate, the corresponding cracking moment, M_{cr}, is usually determined using elastic theory based on the properties of gross concrete section as followings:

$$M_{cr}=\frac{f_r I_g}{y_t} \tag{2.1}$$

where I_g is the moment of inertia of gross concrete section ignoring steel reinforcements; and y_t is the distance of the extreme tension fiber from the neutral axis.

Depending on the amount and arrangement of reinforcement, shrinkage-induced stress, $f_{sh,}$ at the extreme tension fiber may be substantial. If the effect of shrinkage is included to obtain more accurate prediction of cracking moment, Equation 2.2 should be employed. The sign convention is positive for tensile shrinkage and is negative for compressive shrinkage.

$$M_{cr}=\frac{(f_r - f_{sh})I_g}{y_t} \tag{2.2}$$

The influence of shrinkage induced stress on cracking moment can be seen from the test observations reported by Paulson (1989) and Ashour (2000). In both studies, it uses the ACI 318 (1999) equation for modulus of rupture as follows.

$$f_r = 0.62\sqrt{f_c'} \tag{2.3}$$

where f_c' is the cylinder compressive strength of concrete in MPa.

(c) Post -cracking behaviour under service load

As the load is increased, cracks propagate quickly upwards towards the neutral axis, which in turn shifts upward with progressive cracking. In well-designed beams, the widths of these cracks are so small that they are not objectionable from the viewpoint of either corrosion protection or appearance. The spacing of cracks may be irregular because of random variation in concrete tensile strength. The stresses in tensile steel vary locally along the beam, reaching its maximum value at the cracked section. Under the usual service load, the stress in the extreme compression fiber remains small enough to assume a linear variation. At a cracked section, there is a small region of concrete directly above the crack but below the neutral axis (Figure 2.1), which is subjected to tensile stress, but its effect is usually neglected.

Crack spacing and crack width-The maximum crack width in a RC beam under service load should be limited for aesthetic and durability concerns. It is well known that the closer the crack spacing, the smaller is the resulting maximum crack width. In a flexural member, cracks are classified into primary cracks and secondary cracks. The spacing of primary cracks depends on the depth of the member, while that for the secondary crack, which forms between two primary cracks, solely depends on the interfacial bond strength between the surface of tensile steel and the surrounding concrete. The present ACI Code methods for crack control has shown that crack width

is generally proportional to the amount of stress and the amount of the cover on the steel. There is very little experimental information available regarding the cracking behaviour of pumice concrete flexural members.

Maximum deflection and service load-The most critical issues in calculating maximum deflection of a beam are the determination of cracking moment (M_{cr}), elastic modulus (E_c) and moment of inertia at cracking (I_{cr}). The use of LWC results in lower values of M_{cr} , and E_c consequently a lower moment of inertia. Consequently, LWC beams are likely to undergo larger deflection at service load compared to identical NWC beam. For a simply supported beam subjected to four-point flexural loading, elastic bending theory gives the following equation to estimate the maximum (mid-span) deflection.

$$\delta_{\max} = \frac{pa}{24EI}(3L^2 - 4a^2) = \frac{M_a}{24E_c I_e}(3L^2 - 4a^2) \tag{2.4}$$

where $\delta_{\max}$ is the maximum deflection at midspan in m; p is the applied point loads; M_a is the applied maximum (mid-span) moment in MPa; L is the beam span in m; a is the shear span in m; E_c is the elasticity of modulus of concrete in MPa. I_e is the effective moment of inertia of the beam section in m^4 . The ACI code (ACI 318, 1999) specifies equations to predict I_e as follows:

$I_e = I_g$ (for uncracked beam) (2.5)

$I_e = I_{cr} + (I_g - I_{cr})\left(\frac{M_{cr}}{M_a}\right)^3 \le I_g$ (for cracked beam) (2.6)

where I_g and I_{cr} are the moments of inertia of gross and cracked section respectively; M_{cr} is the cracking moment capacity of the beam obtained by using the gross concrete section.

In calculating the maximum deflection of a RC beam, an accurate assessment of the flexural stiffness ($E_c I_c$) of the beam is of utmost importance. Based on experimental results, it has been reported that the specification in ACI 318 (1999) underestimate the maximum deflection at service load for high strength normal weight concrete (HSC) beams (Pastor et al., 1984; Paulson et al., 1989; Ashour, 2000). Ahmad (1991) reported that ACI code predicts well the maximum deflection at the service loads for high strength LWAC beams. Further study is needed to investigate the behaviour of pumice concrete beams.

2.4.2 Behaviour at overload

As the applied moment, M is increased above the service load, the compressive concrete becomes more highly stressed and behaves in an increasingly non-linear manner particularly for NWC. For LWC, concrete stress increases more or less proportionally with strain, so that the stress block remains almost triangular until the extreme compression fiber reaches its peak stress. In the case of under-reinforced beam, a moment M_y is eventually reached when the steel yields. At this stage, the section is in a condition of high overload. Nevertheless, it can usually accept a further small increment in moment and the moment capacity, M_u is slightly higher than the moment at first yield, M_y. In order for the moment to increase above M_y, the internal lever arm, between the compressive and tensile stress resultants, must increase. This can occur

because the compressive capacity of the concrete is not exhausted at moment M_y.

(a) Flexural strength

Flexural strength is determined from the stress strain distribution across the depth of concrete section. At ultimate level, the unconfined concrete is assumed to fail when its compressive strain reaches a limiting value. In ACI 318 (1999), this ultimate compressive strain (ε_{cu}) is considered as 0.003, while in BS 8110 (1997), the ultimate compressive strain of concrete is assumed as 0.0035. Either of these values will be conservative for NWC but it will be unconservative for high strength LWAC. This is because the ultimate compressive strain capacity of unconfined LWAC decreases with an increase in concrete strength.

At ultimate load, the compressive stress block may be assumed to be rectangular, trapezoidal, parabolic or any other shape that results in prediction of strength in substantial agreement with the results of comprehensive tests (ACI 318, 1999). Thus rather than using a representative stress-strain curve, simple geometrical shapes which are easier to use in computations are acceptable. ACI 318 (1999) permits the use of the equivalent rectangular concrete stress distribution for ultimate strength calculations. It also specifies a uniform concrete compressive stress of $\alpha_1 f_c^{'}$ ($\alpha_1 = 0.85$) distributed over an equivalent compression zone bounded by edges of the cross section and straight line located parallel to the neutral axis at a distance $\alpha = \beta_1 c$ from the fiber of maximum compression strain (see Figure 2.1). For this relation, c is the neutral axis depth from compression face and β_1 is the equivalent stress block depth factor. The factor β_1 is considered equal to 0.85 for concrete with compressive strength as high as 27.6 MPa.

(b) Ductility

Ductility of RC member is a measure of its ability to undergo large deformations without failure. For flexural members, these deformations may be the deflection or the curvatures. Ductility becomes important for LWAC members because an increase in concrete strength increases its brittleness and higher strength concrete has less ultimate strain capacity in compression. The displacement ductility index, μ_d can be expressed as:

$$\mu_d = \frac{\delta_f}{\delta_y} \tag{2.7}$$

where δ_f is the maximum beam deflection at failure in m and δ_y is the maximum deflection at the yielding of tensile reinforcement in m.

Ahmad (1991) found that both normal and high strength lightweight aggregate concrete beams exhibit insufficient displacement ductility (less than 3) when reinforced with $\rho / \rho_b > 0.40$. Beams with 75.9 MPa concrete strength exhibit ductility that is marginally acceptable when reinforced with ρ / ρ_b of 0.22. For this relation ρ and ρ_b is the steel reinforcement ratio and balanced steel reinforcement ratio across the section, respectively.

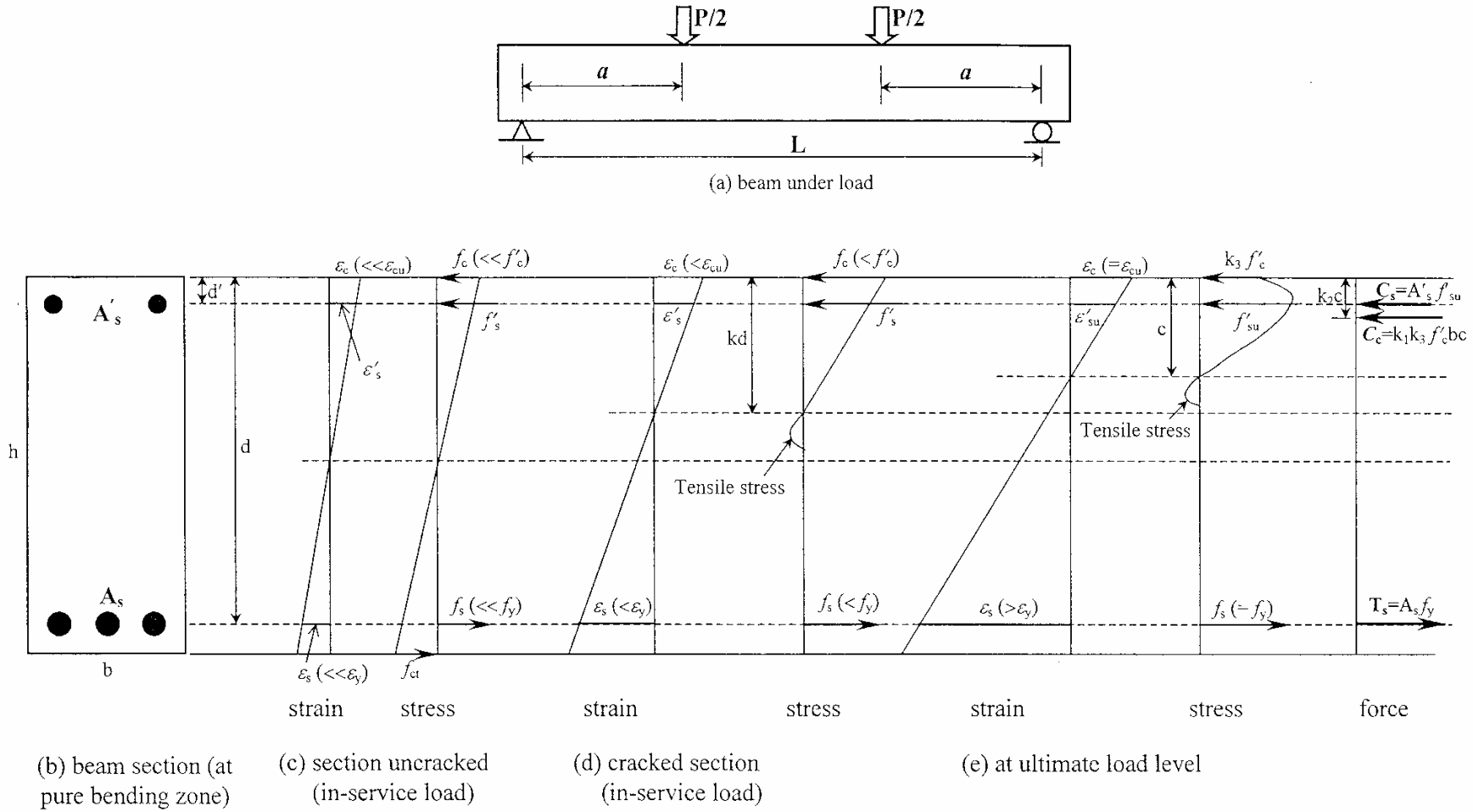

Figure 2-1. Rectangular beam subjected to pure bending

CHAPTER THREE

PRODUCTION OF PUMICE LIGHTWEIGHT AGGREGATE CONCRETE

In this chapter, the selection of the materials, mix proportioning guidelines and the production procedure adopted in the thesis reported herein are described. The 28-day compressive strength, fresh, air-dry and oven-dry densities are reported for all the chosen mixes.

3.1 Selection Of Materials

3.1.1 Pumice aggregate

Pumice is a natural material of volcanic origin produced by the release of gases during the solidification of lava (Asgeirsson, 1994). Their treatment is only via mechanical handling, crushing and screening (Spitzner, 1995).

(a) Chemical properties

Pumice is a pozzolanic material because of its reaction with lime (calcium hydroxide) liberated during the hydration of cement (Jackson, 1983). Amorphous silica present in the pozzolanic materials combines with lime and forms cementitious materials. Table 3.1 presents the chemical properties of pumice given by Jackson (1983).

(b) Porosity and water absorption

The porosity and water absorption characteristics greatly affect the properties of the fresh mix, as well as the hydration properties. According to ASTM C566 (1997), the result of water absorption is given in Table 3.2.

(c) Shape and surface properties

Figure 3.1 shows the shape and surface texture of pumice aggregates used in this study.

(d) Size of aggregate particles

After having determined the average gradation and dry particle density of each pumice group as summarized in Table 3.3 and Table 3.4. Computation of many linear systems of two equations results in the choice of 20 % 1 to 5 mm size pumice, 35 % 5 to 10 mm size pumice and 45 % 10 to 20 mm size pumice, by weight. The gradation chart of this combination based on the absolute volume basis is given in Figure 3.2. The proportioning of these pumice aggregates of different sizes is done so as to have a mixed aggregate whose granulometric curve is within the "favorable region" based on the absolute volume by ASTM C33 (1993).

(d) Density of aggregates

The bulk density of LWA is the relation between the mass of a pile of aggregates and the volume it fills, including the voids between aggregates. It should be measured without compaction, to avoid the influence of this parameter. The real density of LWA should be determined either by ensuring a saturated surface dry state of the aggregate (ASTM 127, 2001) or using a viscous fluid (DIN 4226, 1983) to avoid effects of water absorption. Table 3.4 gives the test results of density of pumice aggregates by ASTM

127 (2001).

(e) Aggregate strength

BS 812 (Part III), 1990 describes a method for the determination of ten percent fines value (TFV) of aggregates, which give a relative measurement of resistance of an aggregate to crushing under a gradually applied compressive load. The values of TFV of pumice aggregate are given in Table 3.5.

3.1.2 The cement

In Singapore, Type A Ordinary Portland Cement (OPC) is most readily available to produce high strength concrete, both in the laboratory and at the construction site. Therefore Type A OPC from the same source is selected for all mixtures. Table 3.6 gives the composition of the OPC used.

3.1.3 Natural sand

The physical properties of the natural sand are given in Table 3.7. The specific gravity and fineness modulus are 2.62 and 2.6 respectively.

3.1.4 Superplasticizer

In this study, anaphthalene based superplasticizer, Daracem-100 from GRACE Company, complying with ASTM C 494 type A and F (1994), is used to achieve the required workability.

3.1.5 Silica fume

The composition of condensed silica fume in this study is given in Table 3.8.

3.1.6 Ground granulated blast-furnace slag (GGBS)

Specifications of ground granulated blast furnace slag used in this experiment are given in Table 3.9.

3.1.7 Air-entraining agents

The air-entraining agent named MICRO AIR, meeting the requirement of ASTM C 233 (2001) is used in this study to achieve the desired air content in concrete.

3.2 Proportioning Guidelines Adopted

3.2.1 Variables

The main objective of the research program is to investigate structural properties of LWAC with pumice aggregates, with compressive strength more than 20 MPa which could be used in reinforced concrete (RC) structures. Consequently, several mix variables are studied. Three mixes (referred to as A, B and C) are designed to have compressive strength in the range of 20 to 30 MPa. Three different water to binder (w/b) ratios are selected. The pumice content, amount of replacement of natural sand by fine pumice, air content as well as the replacement of cement by cementicious materials are the obvious factors affecting the properties of pumice concrete. However, there have been no reports about results relating to these factors. So the above factors are also chosen as variables.

3.2.2 Proportions used

With consideration to the factors discussed in Section 2.2 and 2.3, the following procedure is adopted in proportioning the mixes.

Water to binder ratios of 0.43, 0.33 and 0.27 are selected as for these water to binder ratios, formulas by Chandra and Berntsson (2001) and Videla and Lopez (1997) indicate approximate 28 day compressive strengths of 20 to 30 MPa with fresh density of 1800 kg/m^3. If the volumetric method for mix proportioning of ACI 211.2(1998) is followed, the next step would be to determine the amount of mixing water to achieve a desired workability. The workability of high strength LWAC is almost totally dependent on the amount of superplasticizer used. Hence, this step of workability control is omitted in high strength LWAC. The next step is to determine the cement content for a given water to cement ratio. The cement content-strength relationship is similar for a given source of lightweight aggregate but varied widely between sources. In DIN 4219 (1979), Section 5.2.2, the minimum cement content of 300 kg/m^3 and a maximum content of 450 kg/m^3 is required. Then binder contents of 350, 450 and 550 kg/m^3 are selected in this study.

The supplier's specification for use of the chosen superplasticizer is 0.6 to 1.2 litres/100 kg of binder.

The content of pumice has a direct effect on both the compressive strength and density. According to ACI 213R-87 (1994), the absolute volume of LWA should normally take up 40 % ± 5 % of the concrete and can be adjusted to achieve the required density. Due to the lower ceiling strength of the pumice aggregate, a small alteration in the content of pumice content would result in significant change in compressive strength. Moreover, the combined grading curve has to meet the requirement of Fuller curve to safeguard good workability. A subsidiary program to

investigate the influence of the pumice content is designed with two further mixes with 35 % and 45 % pumice content.

To further decrease the LWAC density, partial or whole sand amount can be replaced by fine pumice aggregates. A mix with 50 % volume replacement of sand by fine pumice aggregate is designed. Air entraining agent (AEA) is commonly used in LWAC to enhance its workability and improve its durability. However, the entrained air bubbles affect the density and compressive strength of the LWAC. ACI 213R-87 (1994), Section 3.2.15, confines the entrained air content from 2-8 % by volume in concrete when the maximum size of coarse LWA is less than 19 mm. A mix with 8 % air content is made to study the effect of the air content on the properties of the pumice concrete.

Cementitious materials have been used extensively throughtout the world nowadays. The pozzolanic reaction has several characteristics that affect the strength. The comprehensive characteristics of cementitious materials are reported by Rachel & Bhatty (1996) and ACI 363.R (1992). In this study, three mixes are designed to study the effect of cementicious materials on the properties of pumice concrete, with cement replacement by 65 % GGBS, 10 % silica fume, and the combination of 10 % SF and 55 % GGBS respectively.

Basic details of all mixtures are given in Table 3.10. In the mix ID number, the first letter identifies the binder content, “A” for 450 kg/m^3, “B” for 550 kg/m^3, “C” for 350 kg/m^3. The first number behind the first letter denotes the influencing phases, where “1” for variation in coarse pumice aggregate content, “2” for variation in the replacement of natural sand by fine pumice aggregate, “3” for variation in the replacement of cement by cementitious materials, “4” for variation in the air content in concrete. The second number stands for the sub-mix number.

3.2.3 Production workability

The workability of pumice concrete is measured by the "slump test" in conjunction with visual assessment (Figure 3.3). It is attempted to keep the slump at about 150-200 mm in all mixes by adjusting the dosage of superplasticizer.

The required amount of superplasticizer to obtain a slump of 150-200 mm is increased with a decrease in the content of coarse pumice aggregates. Increases in superplasticizer dosages up to 1 litre/m^3 are observed when the pumice content decreased from 45 % to 35 %, as it is expected that with the reduction in fine particles, the workability would decrease, hence more superplasticizer is needed to maintain its workability. Mixes of A3 series with the involvement of cementitious materials are found to present a better workability with deceased superplasticizer dosage; this is because of the lubricating effect of the GGBS and silica fume due to their spherical particle shape and the prevention of coagulation of cement by GGBS and SF. It is also found that the increase in air content and the replacement of sand by fine pumice could decrease the superplasticizer demand to some extent.

3.2.4 Laboratory mixes

All the mixes are mixed in the laboratory using the twin shaft mixter (model SD-100 by PME Pte Ltd, Japan) with a capacity of 0.15 m^3 using following procedure:

1. Before the commencement of the mixing, the mix pan and mixer blades are dampened prior to mixing and the internal surface of the mixer are coated with a mix of cement slurry (2 kg of cement mixed with l kg water) to compensate for the residual cement paste after discharging the fresh concrete.

2. The water to be added to the mix is combined with half to 2/3 of

superplasticizer or/and AEA prior to its addition into the mix.

3. The lightweight coarse aggregate is added to the mix pan along with two thirds of the water (including superplasticizer and AEA). After a brief period of mixing, the pan is covered with plastic sheeting and allowed to stand for 1.5 minutes.

4. The required cement and/or GGBS and/or SF is then added, immediately followed by the required sand.

5. The mixture is then mixed for 60 seconds after which the rest of the water and superplasticizer is added. The mix is then mixed for a further 30 seconds**.** The mix is then hand mixed to ensure full mixing of the constituents.

6. The mixture is finally mixed for a further 90 seconds.

7. The workability of fresh concrete is adjusted according to the slump requirement, through further addition of the remaining superplasticizer.

3.3 Compressive Strength And Density

The mean 28 day compressive strength is determined by testing three 100 (diameter)×200 (height) mm standard cylinder cured in a 100 % relative humility fog room at 23 °C. The strength for each mix is plotted in Table 3.11. The compressive strength achieved at 28 days ranged from 18.6 to 27.4 MPa. The coefficient of variation ranged from 0.42 % to 6.65 %.

A decrease of 5 % pumice content in the concrete with 40 % pumice in volume, with the same cement content and w/c ratio, is found to increase by 18 % in compressive strength and 3 % in its fresh density. By increasing up to 5 % of pumice content, there will be a 6.2 % decrease in compressive strength and a 4 % decrease in fresh density. Meanwhile, the replacement of 50 % sand by fine pumice in volume

resulted in a 28.3 % decrease in compressive strength and 9 % decrease in fresh density. The differences in the mean compressive strength between similar mixes with the replacement of cement by cementicious materials are within 8 % and differences in fresh density within 7 %. Out of 350 kg/m^3, 450 kg/m^3 and 550 kg/m^3 cement dosage in the pumice concrete, an appreciable jump in strength is observed from 350 kg/m^3 to 450 kg/m^3 dosage LWC, 34 % increase comparing mixes A1-1 and C1-1. However, the change from 450 kg/m^3 to 550 kg/m^3 dosage concrete is only 6.6 % as shown by mixes A1-1 and B1-1. For the mixes A1-1, B1-1 and C1-1, the fresh density varies within 5 % of each other. Increasing the air content from 2 % to 8 % in LWC led to a decrease of compressive strength of 20 % and the fresh density of 10 % as shown in mixes A1-1 and A4-1. The 28 day compressive strength of all the mixes expressed in the form of Chandra and Berntsson's equation is plotted in Figure 3.4.

$$f_{la} = a10^{b\rho/1000} \tag{3.1}$$

$$f_M = A.10^{-B.W/C} \tag{3.2}$$

$$\log f_{con} = v_{la}.\log f_{la} + v_M.\log f_M \tag{3.3}$$

where, f_{la} is the strength of the LWA in MPa; f_M is compressive strength of mortar in MPa; f_{con} is the compressive strength of the LWAC in MPa; a and b are coefficients and a=1.0 and b=1.25 for a bulk density of 300 kg/m^3; A =140 and B=0.87; W is the water content in kg/m^3 and C is the cement content in kg/m^3; v_{la} is the volume of the LWA in concrete in m^3/m^3 and v_M is the volume of mortar in concrete in m^3/m^3. ρ is the particle density of LWA in kg/m^3.

Table 3-1. Pumice chemical properties (Jackson, 1983)

Chemical compound	Chemical composition, %
Calcium oxide (CaO)	4.44
Silica (SiO_2)	60.82
Alumina (AL_2O_3)	16.71
Iron oxide (Fe_2O_3)	7.04
$SiO_2 + Al_2O_3 + Fe_2 O_3$	84.5
Sulphur trioxide (SO_3)	0.14
Magnesia (MgO)	1.94
Sodium oxide (Na_2 O)	5.42
Potassium oxide (K_2 O)	2.25
Loss on ignition	1.52

Table 3-2. Water absorption of pumice aggregate

Size	60 minutes (%)	24 hours (%)
10~20 mm	83	87
5~10 mm	80	86
1~5 mm	52	60

Table 3-3. Grading of pumice aggregates

Sieve Opening Size (mm)	Cumulative passing (%)			
	Pumice aggregate size (mm)			
	1-5 mm (P1)	5-10 mm (P2)	10-20 mm (P3)	20 % P1+35 % P2+45 % P3
25	---	---	100	100
19	---	---	72.8	86.5
14	---	100	19.9	60.3
12.5	---	98.8	11.1	55.5
9.5	---	43.7	0.24	29.1
7.5	100	8.7	0.19	15.7
4.75	43.5	8.4	0.19	8.6
2.36	8.1	5.1	0.19	3.0
1.18	5.3	0.5	0.00	0.8
0.60	5.0	---	---	0.6
0.30	4.7	---	---	0.6

Table 3-4. Density of pumice aggregates

Density (kg/m^3)	Pumice Aggregate Size		
	1-5 mm	5-10 mm	10-20 mm
Bulk density	397	350	346
Oven dry particle density	1013	571	565

Table 3-5. TFV values for pumice aggregates

Pumice aggregate size	TFV values
6.3~10 mm	76.1
10~14 mm	78.0
14~20 mm	87.0

Table 3-6. Chemical compositions of Ordinary Portland Cement

Composition	**Content (%)**	**Physical properties**	**Content (%)**
Loss on ignition	0.75	Fineness (cm^2/g)	3150
SiO_2	20.57	Specific gravity	3.15
Al_2O_3	5.00		
Fe_2O_3	3.23		
CaO	64.31		
MgO	2.35		
SO_3	2.57		
K_2O	0.71		
Na_2O	0.07		
Insoluble residue	0.31		
Total	99.86		

Table 3-7. The physical properties of the natural sand

Size (mm)	**Cumulative retained (%)**	**Cumulative Passing (%)**
9.5	0.0	100
4.75	2.0	98.0
2.36	8.5	91.5
1.18	25.5	74.5
0.60	51.5	48.5
0.30	78.3	21.7
0.15	94.0	6.0
0.00	100.0	0.0
Fineness modulus/ Specific gravity		2.60/2.62
Specific gravity		2.62

Table 3-8. Chemical composition and physical properties of silica fume

Specific gravity (g/cm^3)	2.2
Specific surface area (cm^2/g)	20
Loss on ignition (%)	1.89
SiO_2 content (%)	93.1
SO_3 content (%)	0.27
Fe_2O_3 content (%)	0.9
CaO content (%)	0.35
C content (%)	1.22
Total alkali	0.9
Moisture content (%)	0.3

Table 3-9. Specifications of ground granulated blast furnace slag

Property	GGBS-4000
Specific gravity (g/cm^3)	2.90
Specific surface area (cm^2/g)	4480
Loss on ignition (%)	1.25
MgO content (%)	6.25
SO_3 content (%)	0
Cl^- content (%)	0.008

Note: 4000 refers to the fineness of the GGBS

Table 3-10. Mix proportion of the various concrete mixes

Mix No.	Cementitous materials			w/b	Pumice aggregate content (m^3/m^3)	Natural sand content (m^3/m^3)	Mix Proportions C:FA:CA (By volume)	Natural sand volume percentage of fine aggregate	Air content %	SP (l/m^3)	Fresh Density (kg/m^3)
	Ceme-nt	GGBS	SF								
	Kg/m^3										
A1-1	450	---	---	0.33	0.40	0.287	1:2.01:2.80	100%	2	5	1825
A1-2	450	---	---	0.33	0.45	0.232	1:1.62:3.15	100%	2	6	1770
A1-3	450	---	---	0.33	0.35	0.332	1:2.32:2.45	100%	2	4.5	1900
A1-1	450	---	---	0.33	0.40	0.287	1:2.01:2.80	100%	1825	5	1825
A2-1	450	---	---	0.33	0.40	0.287	1:2.01:2.80	50%	1660	3.5	1660
A1-1	450	---	---	0.33	0.40	0.287	1:2.01:2.80	100%	2	5	1825
A3-1	405	---	45	0.33	0.40	0.287	1:1.89:2.68	100%	2	4	1828
A3-2	157.5	292.5	---	0.33	0.40	0.287	1:1.77:2.58	100%	2	4	1830
A3-3	157.5	247.5	45	0.33	0.40	0.287	1:1.76:2.56	100%	2	4	1838
A1-1	450	---	---	0.33	0.40	0.287	1:2.01:2.80	100%	2	5	1825
A4-1	450	---	---	0.33	0.40	0.227	1:1.59:2.80	100%	8	2	1660
A1-1	450	---	---	0.33	0.40	0.287	1:2.01:2.80	100%	2	5	1825
B1-1	550	---	---	0.27	0.40	0.249	1:1.42:2.29	100%	2	4.5	1850
C1-1	350	---	---	0.43	0.40	0.319	1:2.87:3.60	100%	2	5.5	1813

Note:

C=cement; FA=fine aggregate (sand); C=coarse aggregate; SP = superplasticiser; GGBS=ground granulated blast furnace slag; SF=silica fume; w/b=water/binder ratio.

Group A1-1, A1-2, A1-3 varies with parameter of pumice aggregate content; Group A1-1, A1-2 varies with parameter of replacement of sand by fine pumice aggregate; Group A1-1, A3-1, A3-2, A3-3 varies with parameter of cement replacement by cemetitious materials; Group A1-1, A1-2 varies with parameter of entrained air content; Group A1-1, B1-1, C1-1 varies with parameter of cement content.

Table 3-11. Compressive strength and density of pumice concrete

Mix No.	Compressive strength (MPa)	Density (kg/m^3)		
	28-day	Fresh	Air-dry	Oven-dry
A1-1	25.8	1825	1801	1606
A1-2	21.2	1770	1721	1582
A1-3	27.4	1900	1836	1710
A1-1	25.8	1825	1801	1606
A3-1	18.5	1660	1579	1366
A1-1	25.8	1825	1801	1606
A3-1	26.6	1828	1808	1596
A3-2	25.4	1830	1792	1631
A3-3	26.3	1838	1750	1598
A1-1	25.8	1825	1801	1606
A4-1	18.6	1660	1542	1405
A1-1	25.8	1825	1801	1606
B1-1	27.8	1850	1815	1683
C1-1	19.2	1813	1751	1611

Figure 3.1. Pumice aggregates

Note: (a) cut-section view of 10-20 mm pumice aggregates; (b) view of 5-10 mm pumice aggregates. (c) view of 1-5 mm pumice aggregates; (d) contrast of the 3 grades of pumice aggregates

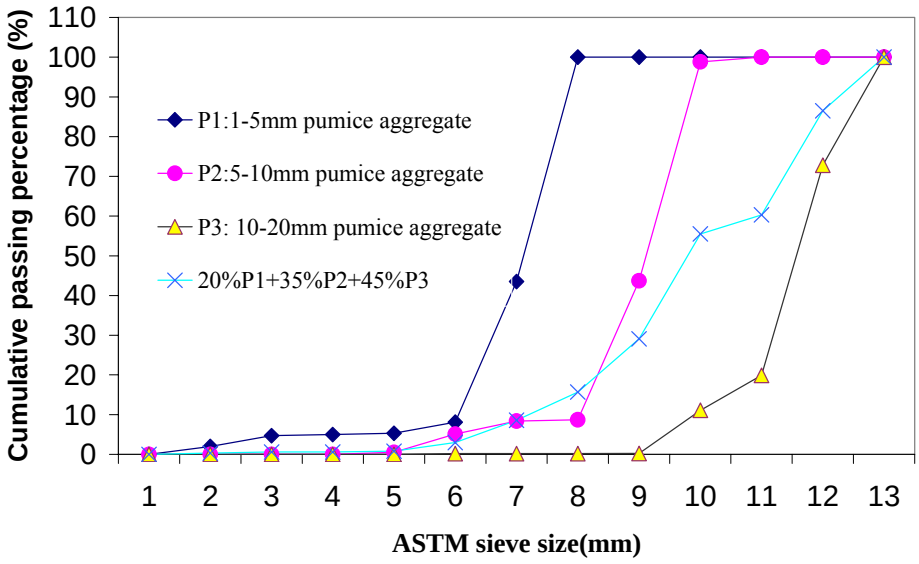

Figure 3.2. Grading curves of pumice aggregates and their combination

(a) Slump test on pumice concrete (b) A view of fresh pumice concrete before casting

Figure 3.3. Fresh pumice concrete

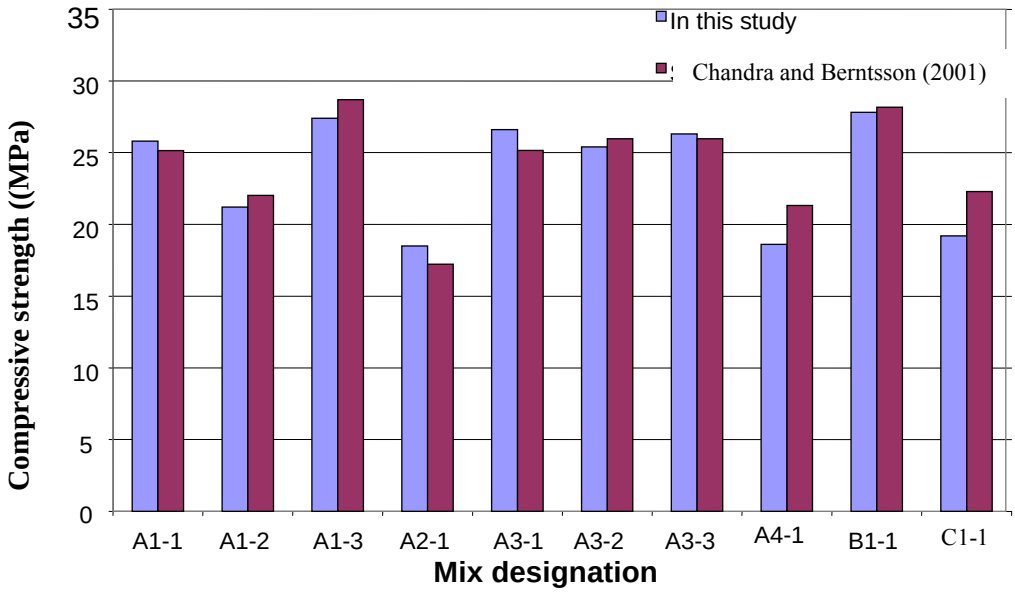

Figure 3.4. Comparison of the experimental results and Chandra and Berntsson's formula

CHAPTER FOUR

MECHANICAL PROPERTIES OF PUMICE LIGHTWEIGHT AGGREGATE CONCRETE

This Chapter presents experimental details and the test results to investigate the mechanical properties (compressive strength, modulus of elasticity, flexural strength, tensile strength, creep and drying shrinkage) of high strength lightweight concrete based on pumice aggregates. Material variables include the total amount and composition of cementitious materials, pumice aggregate content, replacement of sand by fine pumice aggregates and air content. The experimental results are compared with code relations and other proposed equations for high strength pumice concretes. Based on the results of these tests, recommended relationships of mechanical properties are given.

4.1 Experimental Details

4.1.1 Compression testing

All are cast in steel moulds. The 100 mm (diameter) $\times$200 mm (height) cylinders and 100 mm$\times$100 mm$\times$100 mm cubes are filled in two layers and the 150 mm (diameter) $\times$300 mm (height) cylinders in three layers. All the specimens are placed on a variable speed vibrating table and the moulds are vibrated after each layer is filled. The top of the cylinder or cube is finished with a trowel to obtain a smooth surface. Each cylinder or cube is covered with a polythene sheet secured with a rubber band and kept at room temperature.

Specimens are demoulded after 24 hours and are immediately transferred to a 100 % relative humidity fog room which had a constant temperature of 28 °C. They are cured until taken out to be prepared for testing.

One draw back in using cylindrical specimens to determine the compressive strength of concrete is that one of the loaded surfaces is finished by hand toweling. ASTM 617 (1998) requires the cylinders to be grinded into a plane surface or capped with a high strength capping material which is as strong as the concrete tested.

All compressive tests are carried out in a 3000 kN capacity Avery-Denison compression testing machine (see Figure 4.1). The specimens are loaded at a displacement rate of 2.5 mm in 5 minutes for 150 mm (diameter)× 300 mm (height) cylinders and 2.5 mm in 10 minutes for 100 mm (diameter) × 200 mm (height) cylinders. These operating rates of the machine are closest to that recommended in ASTM C39 (2001). The rate of the loading is approximately 200 kN/min whereas those recommended in ASTM C39 (2001) is 260 ± 60 for 150 mm (diameter)×300 mm (height) cylinders. Mak (1993) has shown that there is little difference in strength obtained using the two loading rates, 2.5 mm per 5 minutes and 2.5 mm per 10 minutes for 100 mm (diameter)× 200 mm (height) cylinders. All the pumice concrete shows explosive brittle failure.

4.1.2 Compressive stress-strain relationship testing

All the ten mixes in this study are included in the experimental program. A compressometer such as that recommended for elastic modulus test following ASTM C469 (2002) is considered unsuitable for measurement of the average vertical displacement of the concrete specimens since explosive failure is expected at the peak

stress which will damage the system. Therefore, electrical resistance strain gauges are used as strain measuring device to measure the strain up to the peak load. Strain gauges recommended for concrete with a gauge length of 65 mm are chosen.

The ends of the concrete specimens are grinded to be parallel. In the middle of one third of the height of the concrete specimen, two strain gauges of 65 mm gauge length are fixed longitudinally on two diametrically opposite sides. A second hardened plate is placed on the top of the concrete specimen.

All the specimen are cured in the fog room until 90 days, specimens had to be dry before attaching strain gauges, as the glue is found to be affected by moisture. Specimens are grinded at both ends and are kept at room temperature for a week before testing.

The positions of the longitudinal strain gauges are marked in two diametrically opposite sides in the middle one third of the height of the cylinders. The surface of the cylinder at these positions is grinded to obtain a smooth surface. Epoxy glue is used to cover the minute pores on the surface and left to cure for 24 hours. The surface is then ground again until the concrete is exposed leaving the pores covered with the resin. Strain gauges are then glued on to specimen.

Cylinders are placed on the lower platen of the testing machine and the testing is carried out under deformation control at 2.5 mm in 10 minutes (see Figure 4.2). The strain gauges and a linear variable differential transducer (LVDT) are connected to a personal computer. Strain gauges and load readings are recorded at one second intervals and load displacement data is plotted on the screen simultaneously. All specimens exploded at peak stress in a brittle failure. It is not possible to obtain the descending portion of the stress strain curve in this test.

4.1.3 Tensile strength

Splitting tensile strengths are conducted for all mixes at 3, 7, 28 and 91 days. Specimens are 100 mm (diameter) × 200 mm (height) cylinders. Specimen preparation and testing for all mixes is carried out according to ASTM C496 (1996) recommendations on a Denison compression testing machine. Three specimens are sampled from each mix for one test. The specimens are moist cured for 7 days, air dried at 30 ± 2 °C and exposed in 65 ± 5 % relative humidity for the following 21 days before the test is carried out on the 28^{th} day. A typical failure mode for the splitting tensile test as well as the cross-sectional failure planes is shown in Figure 4.3.

Modulus of rupture tests for all mixes are carried out at 3, 7, 28 days by a Denison compression testing machine. Three specimens are used for each mix. The test specimens are 100 × 100 × 400 mm prisms and are moist cured in a fog room until the testing day. The testing procedure conforms to ASTM C78 (2002) (see Figure 4.4). The loading span is 300 mm and the rate of loading is 12 N/minute.

4.1.4 Modulus of elasticity and Poisson ratio

The static modulus of elasticity of all mixes is determined experimentally at 3, 7, 28 and 90 days. 100 mm (diameter) × 200 mm (height) specimens are prepared as described in compression specimens.

A compressometer with four vertical LVDT is used to measure the average vertical strains over the middle third portion of the specimens. An extensometer mounted horizontally on a ring is positioned to measure the lateral strains (see Figure 4.5) the LVDT are connected to a Doric data logger which enabled the readings to be recorded. The vertical LVDT are calibrated to an accuracy of 0.002 mm and horizontal LVDT to 0.001 mm.

A 5000 kN capacity Instron universal testing machine is used for this test. The rate of loading adopted is the same as that of the compression testing of cylinders, which is approximately 240 kN/min for 100 mm (diameter) $\times$ 200 mm (height) cylinders. This is the closest operating rate of the testing machine to that recommended in ASTM 469 (2002), which recommends a loading rate of 241 ± 34 kN/min.

The specimens are initially loaded up to 40 % of the average failure load of the standard cylinder and then unloaded with no recording of any data during the first and second loading cycles. Load and LVDT readings are recorded at 1 second intervals for two subsequent loading cycles up to 40 % of the estimated failure load. Three specimens from each mix are tested from all other mixes for a particular age.

4.1.5 Drying shrinkage

Prismatic specimens of $100 \times 100 \times 400$ mm are used to monitor the drying shrinkage of the hardened pumice concrete. A total nine prismatic specimens are prepared for each mix, of which 3 specimens are used for 3 exposure ages (after 1, 7 and 28 days of curing). The specimens are covered with a plastic sheet to prevent water evaporation until demoulding. After demoulding, the specimens for the 1 day tests are tested and the rest are stored in a fog room until the age of testing. The tests for the drying shrinkage measurements are conducted in a room equipped with air circulating system which consisted of fresh and exhaust air blowers, with temperature maintained at $30 \pm 2\ ^{\circ}$C and relative humidity of $65\ \% \pm 5\ \%$.

Upon the demoulding of the concrete specimens for one day curing, Demec pins are glued onto the side surfaces of the specimens. A fast setting epoxy Araldite is used so that initial measurement can be taken within 1 hour after attaching all the pins on

the surface. As for the drying shrinkage test of the concrete that are cured in fog room for 7 and 28 days, the specimens are removed from fog room on the day of testing. Demec pins are quickly glued onto the side surface of the specimen after drying the points of contract. A Demec gauge is used to measure the deformation of concrete specimens (see Figure 4.6). It has a gauge length of 200 mm and a resolution of 0.002 mm, which corresponds to 10 microstrains.

4.1.6 Creep

Creep test in compression of pumice concrete is carried out basically in accordance with ASTM C512 (1994) except that the temperature and relative humility adopted are different. According to the ASTM standard, the curing and storing of specimens shall be carried out under temperature of $23 \pm 1.7^{\circ}$C, However, the average temperature in Singapore is higher and therefore, $30 \pm 2^{\circ}$C is adopted for curing and storing. Besides, the standard recommends that the relative humility for storing the specimens shall be 50 ± 4 % relative humility. In Singapore, a relative humility of 65 % $\pm$ 5 % is adopted.

Cylinder specimens with the dimensions of 150 mm (diameter) $\times$ 300 mm (height) are moist cured at the temperature of $30 \pm 2^{\circ}$C until the 7 days. The specimen are then moved to the creep room with ambient temperature of $30 \pm 2^{\circ}$C and relative humility of 65 ± 5 %. The specimens are loaded at the age of 28 days (see Figure 4.7). The compressive strengths of the specimens are determined immediately before loading the creep specimens in accordance with ASTM C39 (2001). Stress applied on the specimen is 40 % of its compressive strength at 28 days. The values of compressive creep are calculated by subtracting the free drying shrinkage from the total deformation (excluding the elastic strain upon loading).

4.2 Results and Discussion

4.2.1 Compressive strength

Results of all the compression strength tests carried out as part of the experimental work reported in the thesis are tabulated in Table 4.1 and 4.2.

(a) Size effects

In ASTM C39 (2001), the standard specimen for measurement of strength is a 150 mm (diameter)×300 mm (height) cylinder. If the height of the specimen is sufficient, the stress distribution in the middle is reported to be free of the end effects and is in fairly uniform compression (Kotsovos, 1983). 100 mm (diameter)×200 mm (height) cylinder and 100 mm×100 mm×100 mm cube specimens are also permitted provided that the maximum aggregate size is less than 20 mm.

The statistical weakest link theory associated with failure of brittle materials (Tucker, 1945; Neville, 1959) predicts that the larger the volume of the material subjected to a certain stress, the larger the possibility of having flaws which initiate failure and therefore lower the apparent strength. However, the variability in strength results is said to be higher in smaller specimen in a phenomena called size effect (Malhotra, 1976). The weakest link theory is mostly associated with tensile failure. And since failure of a concrete compression test specimen is a combination of shear and tensile splitting, size effect would have a certain influence.

The effect of curing on the strength of cylinders of two specimen size will not different so much for lightweight aggregate concrete. The water absorbed during mixing and transportation provides a reservoir of free water available during curing to assist in the hydration of the paste. Experiments with mixes having a blend of LWA have shown a reduced sensitivity to curing processes (Weber et al., 1995).

The correlation between cylinder and cube strengths of LWAC seems to be more related to the type and amount of LWA than the strength level of concrete. Smeplass (1992 and 1997b) found average values of 0.90 for a substantial number LWAC containing LWA of the Leca 800 and Liapor 8 types, and average values of 0.95 for LWA of the Leca 700 type. LWAC containing both coarse and fine LWA may have ratios as high as 1.0 (Thorenfeldt, 1995; Smeplass, 1992). The fact that the correlation between cylinder and cube strength is different for LWAC and NWC is considered a very important point since some standards use strength values based on cylinder tests, but use a fixed value for the ratio between cylinder and cube strength. This may lead to incorrect estimates of the strength.

From all the mixes, nine cylinders from each mix of the two sizes (100 mm (diameter) $\times$200 mm (height) and 150 mm (diameter)$\times$300 mm (height)) and nine 100$\times$100 $\times$100 mm cubes are tested to observe the effect of specimen size. Results are given in Table 4.1. These results indicate values for the 100 mm$\times$100 mm $\times$100 mm cube/ 100 mm (diameter)$\times$200 mm (height) cylinder at 28 day's strength has a strength ratio of 1.07 with a standard deviation (S.D) of 0.057 and coefficient of variation (COV) of 5.33; for 150 mm (diameter) $\times$ 300 mm (height)/100 mm (diameter)$\times$200 mm (height) cylinder the strength ratio is 0.97 with S.D of 0.026 and COV of 2.70.

(b) Strength development with age

The strength development of the pumice concrete is shown in Figure 4.8. For the various mixes, the pumice concrete has a faster hardening factor during the initial setting phase than conventional concrete, normally reaching 63 % to 83 % of the 28 day strength of NWC within 3 days, and 75 % to 93 % of the 28 day strength of NWC

within 7 days. Among the mixes, the strength development of concrete mix A2-1 (50 % sand replacement by fine pumice aggregates) is fastest in comparison to the ones with natural sand, since the lighter and rather weak fine pumice aggregates reduce the benefit of the stronger cement paste. Incorporation of mineral admixtures in concrete influences the rate of hydration of the cement and thereby the strength development. It is easy to recognize that the rate of strength development as well as the ultimate strength of concrete made with mineral admixtures can be related to the progress of pozzolanic reaction by which the continual process of pore refinement and improvement in structure at the transition zone occur (Telford, 1988). However, in this study it is found that, the strength development of concrete with mineral admixtures is similar to that of concrete without mineral admixtures, due to the strength limit of the pumice aggregates.

For all mixes, there is almost no strength gain after 28 days. This is due to the fact that, at earlier ages, the strength is limited by the strength of the paste component (Thorenfeldt, 1995). As the lightweight mixes has lower water to cement ratios, the paste strength, therefore dominates the strength development during the first 7 day period. Beyond about 7 days, the strength of the paste in the lightweight concrete begins to approach the strength of the aggregate and a ceiling is reached shortly after. This indicates that the strength development over the longer term has been limited by the strength of the lightweight aggregate. The missing long term strength growth in LWAC results in a lower auxiliary capacity of the concrete material as compared to ordinary concrete designed to reach the same strength grade. An optimal strength/ density ratio in LWAC is often obtained exploiting the strength properties of the aggregates to the limit.

(c) Effect of cement content on the compressive strength of pumice concrete

Out of the 350 kg/m^3, 450 kg/m^3 and 550 kg/m^3 cement dosage in the pumice concrete mixes, an appreciable jump of 6.6 MPa in compressive strength from 350 kg/m^3 cement dosage LWC to 450 kg/m^3 is observed. However, the increase in strength from 450 kg/m^3 to 550 kg/m^3 dosage of cement in LWC is relatively lower, only 2 MPa.

The design curve correlating the compressive strength and water to cement ratio of dense gravel concrete do not apply to LWAC. In general, in order to reach the same strength, a LWAC needs more cement or binder than conventional concrete (Newman, 1993). The increase in strength for a given increase in cement content depends on the LWA type. On average, a 10 % increase in cement content will provide a 5 % increase in strength (Newman, 1993). It is observed in this study that a 12 % increase in strength resulted from a 10 % increase in cement content from 350 kg/m^3 to 450 kg/m^3.

Today the water/binder ratio is considered to be even more important than the absolute cement content. Zhang et al. (1995) and Newman (1993) confirmed the strength of the LWA as the primary factor controlling the upper strength limit of the LWAC. The strength limiting effect of LWA increases with decreasing water/binder ratio (Smeplass, 1997a). Such results will form the basis for practical guidelines for the choice of aggregates within each strength grade. Definition of an upper strength grade of LWAC will depend on the strength of available LWA (Smeplass, 1997b). Compared with NWC, there is a lower increase in strength with an increase in the amount of cement. This is because the potential of the pumice aggregate dominates the attainable strength and the long term strength (Faust, 2002). A minor effect of the water/binder ratio on the strength has also been reported by Rønne et al. (1993). In this study, it shows that a limiting compressive strength of 25 MPa of pumice concrete can be achieved with a cement content of 450 kg/m^3.

(d) Effect of pumice content on the compressive strength of pumice concrete

Since the pumice aggregate is the weakest link in the pumice concrete, its content in concrete significantly affects the compressive strength. In the study, there is a 22 % and 6.2 % increase in compressive strength when pumice content decreased from 0.45 to 0.4 m^3/m^3 and from 0.4 to 0.35 m^3/ m^3 in concrete, respectively. By contrast of the ratio of compressive strength to air dry density, a pumice content of 0.4 seems to be optimal among the 3 mixes with pumice aggregate content of 0.35, 0.4 and 0.45 m^3/ m^3 , respectively.

Several researchers (Videla and Lopez, 1997; Chelouah, 1996) have investigated the effect of LWA content on the compressive strength, proposing the formula of compressive strength with variables of the strength and volume of mortar and LWA in concrete. Moreover, Chelouah (1996) found that, in the case of expanded clay and shale, the mixes with different volume ratio of aggregates and binder show nearly minor effect on compressive strength, attributing this to the better elastic compatibility of the components. But for pumice concrete, due to the weakness of pumice aggregate and stronger mortar, there can be a difference in the elasticity of the components, leading to an increase in strength with an increase in mortar content.

(e) Effect of sand replacement by fine pumice aggregates on compressive strength

In order to decrease the LWAC density, sometimes, it is necessary to replace fine lightweight aggregates with sand (ACI 213R, 1987). The compressive strength decreased by 27 % from 25.8 MPa in mix A1-1 to 18.8 MPa in mix A2-1 with corresponding oven-dry density decreasing 15 % from 1606 kg/m^3 to 1366 kg/m^3. The loss in strength is more pronounced than the decrease in density. Faust (2000) reported that replacement of natural sand by lightweight fine aggregate reduces the compressive strength of mortar. Simultaneously, the influence of the effective water-

binder ratio becomes more insignificant in the case of lighter matrices

(f) Effect of the air content on the compressive strength

There are three major reasons for intentionally entraining air into concrete, i.e. for durability, cohesion and density modifications. It is always assumed that the entrainment of air in concrete leads to a considerable reduction in compressive strength. Popovics (1969) reported that each percent of air will reduce the strength by about 5 % for normal weight concrete. A similar result is found in this study that the compressive strength decreased from 25.8 to 18.6 MPa when the entrained air increased from 2 to 8 % in the pumice concrete, an average of 4 % compressive strength loss with the increase of 1 % air content (see Table 4.1).

However, a better result is gained by Olafur (2002), an average of 1.82 % compressive strength loss per 1 % air –entrainment, when a pumice concrete with fresh density of 1773 kg/m^3 and compressive strength of 25.9 MPa had its entrained air content increased from 2 % to 13.7 % in volume. Olafur (2002) replaced the 13 % concrete content by the entraining air in the mix and decreased the pumice aggregate content by 15 %, instead of replacing sand by the air content in this study. The difference in the strength loss rate by air-entrainment in the two methods (Popovics, 1969; Olafur, 2000) can be attributed to the different elasticity match of the air-entrained mortar and pumice aggregate.

(g) Effect of cement replacement by cementitious materials on compressive strength

The result shows the influence of replacement of cement by 10 % silica fume, 65 % GGBS and a combination of 10 % silica fume and 55 % GGBS on compressive

strength of pumice concrete.

In this study, the strength of mix A3-1 with 10 % silica fume and mix A3-3 with a combination of 10 % silica fume and 55 % GGBS showed marginal difference when compared to that of mix A1-1 without mineral admixture, a maximum 3 % difference is achieved. Silica fume concrete with normal weight aggregate is considerably stronger than the equivalent Ordinary Portland Cement (OPC) concrete at the same water to cement ratio due to enhanced interfacial zone (Tasdemir, 1998). Isserman and Bentur (1996) found that the physical and chemical interfacial processes have an influence on the overall strength beyond that of the aggregate strength. From this observation, it may be concluded that coarse pumice aggregate can be the weakest link in pumice concrete.

The incorporation of 65 % GGBS seems to have little effect on the 28 day compressive strength. There is only a 1 % difference in compressive strength between the mix A1-1 without mineral admixture and mix A3-2 with 65 % GGBS. Ramachandran (1995) reported that at 65 % replacement level by GGBS, up to 3 days in age, the contribution of the slag to the strength of mortar is low. However, at 7 days, strengths almost equal to that of reference mortar is achieved. At later ages, GGBS increased the strength of mortar significantly to values higher than that of reference mortar made with only Portland cement as binder. Due to the weak pumice particle, the strength of pumice concrete depends on the strength and volume of the mortar and the pumice aggregate (Videla and Lopez 1997). Consequently, there is no significant difference in compressive strength for pumice concretes with and without 65 % GGBS replacement.

The above discussion indicates that the strength of pumice aggregate is the limiting factor in the concrete; the transition zone becomes no longer the weakest link

in the pumice concrete. When the mortar strength reaches a certain value, the corresponding strength of pumice concrete will not increase any more.

4.2.2 Stress- strain relationship

The ascending portion of the stress strain curve of the pumice concrete is almost linear up to the peak stress for all the mixes (see Figure 4.9 to 4.13)

In order to compare the linearity of the different curves, the stress (f_p) at which each curve deviates from linearity (the limit of proportionality of stress to strain), as a fraction of the peak stress is calculated. For the stress-strain curve, linear regression fits are obtained for each experiment at curve using data up to 0.4 $f_c^{'}$, where $f_c^{'}$ is the cylinder compressive strength. The point at which the experimental stress-strain curve deviates from this regression line is taken as the proportional limit for each curve. These values are reported in Table 4.3.

(a) Effect of the cement content on the stress-strain curve

It can be observed in Figure 4.9 that the stress-strain curve of Mix C1 has higher limit of proportionality of compressive stress to the compressive strain, compared to that of mix A1-1 and B1-1, whereas the stress-strain curves of Mix A1-1 and B1-1 show a close similarity. Obviously, with the increase in cement content or the decrease in effective water/cement ratio, the pumice concrete becomes more brittle as the strength of LWAC depends on aggregate strength and less on cement paste strength.

The deviation in the stress-strain curve away from linearity has been associated with microcracking at the interfacial zone or in the mortar (Carrasquillo et al., 1981)**.** The internal stress in concrete largely depends on the relationship between the rigidity of its components i.e. aggregate and cement paste matrix. In LWAC, compressive loads are carried mainly by the more rigid mortar matrix corresponding to the stiffness

relationship between the aggregates and matrix, which causes transverse stresses in the aggregates and matrix. The mechanical interlock causes the strong nature of the transition zone, because the cement paste penetrates into the pores on the aggregate surface. The second reason is that there is no way for water to accumulate on the grain skin because of the porosity of the LWA. Finally, it is believed that LWA are pozzolanically reactive. Due to the strong bond forming between the matrix and the LWA, failure occurs mostly after the tensile capacity of the aggregates is exceeded, if no stress redistribution from the aggregates to the matrix is possible.

With decreased cement content or increased effective water/cement ratio, both the strength and modulus of elasticity of the mortar can be decreased. Thus more tensile stresses can be imposed on the pumice aggregate under the same load. Moreover, at a higher water/cement ratio, micro cracks can occur in the mortar under lower levels of the load. The above factors make the behaviour of mix C1-1 less brittle than that mix A1-1 and B1-1.

The stress-strain curves of mix A1-1 and B1-1 are almost the same in spite of the higher cement content of the mix B1-1. This is explained by the way that cracks develop in pumice aggregates first when the mortar has enough strength.

(b) Effect of pumice content on the stress-strain relationship

Mix A1-3 concrete with 35 % pumice aggregate shows a lower stiffness and also relatively high deviation from linearity (lower proportional limit) together with a smaller maximum strain than mix A1-1 with 40 % of pumice and A1-2 with 45 % of pumice (see Figure 4.10). Meanwhile, the stress-strain curves of mix A1-1 and A1-2 seem to be very much similar.

As discussed above, the change in the mortar content of pumice concrete would

definitely affect the behaviour of the internal stress. The less the mortar content, with more pumice aggregate content, the more transverse stress will be imposed on the pumice aggregates, culminating in a less homogenous structure. As shown in Figure 4.10, the stress-strain curve from A1-3 presented a higher deviation of the linearity; however, the stress-strain curves of A1-1 and A1-2 are similar.

(c) Effect of sand replacement by pumice fine aggregate on the stress-strain relationship

The stress-strain curve of mix A2-1 (concrete with 50 % sand replacement by fine pumice aggregate) had a lower limit of proportionality compared to the stress-strain curve of corresponding Mix A1-1 (see Figure 4.11). This observation indicates that the pumice concrete with a high stiffness mortar (cement, sand and water) becomes stiffer.

As discussed in Section 2.1, the failure mechanism of LWAC is different from that of NWC, which is largely dependent on the stiffness relationship between the pumice aggregates and the mortar. With 50 % of the sand replaced by fine pumice aggregate, the stiffness of the mortar decreases, and the mortar itself becomes more heterogenous, in which cracks can probably occur through the fine pumice aggregates and the mortar. Consequently, the concrete becomes more heterogenous compared to concrete without sand replacement by fine pumice aggregates.

(d) Effect of cement replacement by cementitious materials on the stress-strain relationship

Figure 4.12 shows the similarity in most of the stress-strain curves among the pumice concrete with and without cementitious material replacement. The observation indicates that, unlike NWC, the transition zone is no longer the weak phase in pumice

concrete and that the compressive stress-strain behavior is largely dependent on the pumice aggregate itself.

The stress-strain curve of Mix A3-3 pumice concrete with a cement replacement of the 10 % by silica fume and 55 % by GGBS has comparably less deviation than that of mix A1-1 without replacement and the limits of proportionality of the curves of mix A1-1, A3-1, A3-2 are only marginally different. At 90 days, the difference in the compressive strength of mix A1-1, A3-1, A3-2, and A3-3 is very small within experimental variability. This may be explained due to excellent aggregate-matrix bond and similarity of aggregate and paste moduli ensuring that the matrix is used efficiently (Newman, 1993). As a result, LWAC does not fracture due to dislocation between the phases, but as a result of the collapse of the arching structure of mortar over the aggregate, which has limited strength. The fracture line, therefore, goes through the aggregate similar to high strength concrete (Dossier, 1997). Use of superplasticizer and silica fume will enhance the interface in concrete and provide elastic compatibility between the aggregates and matrix. Thus low stress concentrations developing at the interface zone (Tasdemir, 1982).

The proportional limit of the stress-strain curves corresponding to Mix A1-1 and A3-2 are also comparable as shown in Figure 4-12. Since the deviation from linearity of the stress-strain curves of these concrete is mainly influenced by the similar properties of the mortar in the two mixes, the influence of the GGBS is not evident.

(e) Effect of different air content on the stress-strain curves

Figure 4.13 shows the relatively lower deviation from linearity in the stress-strain curve of mix A4-1 with 8 % air content than that of A1-1 with 2 % air content. With increasing air content, the stiffness of the mortar decreased, making the pumice

concrete more homogenous. Hence, the micro-cracks of the pumice aggregates in mortar can occur at a relatively higher level of the compressive stress in relative to the strength of the pumice aggregates by itself.

(f) Strain at the peak stress in uniaxial compression

In this study, Table 4.3 gives the strains at the peak stress of the stress-strain curves of different mixes. The strain at the peak stress in the study is found to be in the range of 0.0016 to 0.0020, similar to the results given by Tesdemir (1982). However, the maximum strains of pumice concrete are significantly lower than those of NWC or other LWAC with artificial LWA at the maximum stress. In a 100 MPa high strength concrete, the strain typically ranges from 3×10^{-3} to 4×10^{-3} and in a 20 MPa NWC, the strain is about 3×10^{-3} (Neville,1996). A strain 2.5×10^{-3} to 3.5×10^{-3} for LWAC containing fine fly ash aggregates of compressive strength 25 to 30 MPa is reported by Swamy (1983). Rønne (1993) reported that the strain at maximum stress for LWAC with lightweight sand and with strength grades of 30 to 40 MPa may have strains at ultimate stress 40 % higher than for a NWC of equal compressive strength. In addition, the higher strain at the peak stress is obtained due to the elastic modulus compatibility of the constituents. The relatively lower strain of pumice concrete can be due to the limiting strain capacity of the pumice aggregates.

An accurate value of the strain at maximum stress is important for the plot of stress-strain curve of concrete under uniaxial compression. Several investigators such as Ahmad and Shah (1985), Almusallam (1995), Tasdemir (1998), Faust (2000) and the CEB –FIB (1999) have proposed linear relationships to predict the strain at the peak stress in terms of the compressive strength, covering LWAC as well as NWC and HSC. These relationships of peak strain with respect to compressive strength given in

Equation 4.1 to 4.5 predict that the strain at the peak compressive stress (ε_{cu}) increases with compressive strength. This trend is not observed in the results reported in this thesis based on different pumice concretes tested.

$$\varepsilon_c = -(0.001732 + 1.1122 \times f_c)/1000 \quad \text{by Ahmad and Shah (1985)} \tag{4.1}$$

$$\varepsilon_c = -(-0.067 f_c^{\,2} + 29.9 f_c + 1053) \times 10^{-6} \quad \text{by Almusallam (1995)} \tag{4.2}$$

$$\varepsilon_c = -0.0035.(0.4 + 0.6.w_c / 2200) \quad \text{by Tasdemir (1998)} \tag{4.3}$$

$$\varepsilon_c = \text{-}(0.025\ f_{cck} + 1.5)/1000 \quad \text{by CEB –FIP (1999)} \tag{4.4}$$

$$\varepsilon_c = \text{-}(0.398\ f_c + 18.147) \times 10^{-4} \quad \text{by Faust (2000)} \tag{4.5}$$

where ε_c is the strain at the peak stress in uniaxial compression; f_c is concrete compressive strength obtained from cylinder test in MPa; f_{cck} is concrete compressive strength obtained from 150 × 150 × 150 mm cube test in MPa; w_c is the air-dry density of concrete in kg/m^3 .

The strain at the peak stress increased from 0.0016 for the 19.2 Mpa strength to 0.0021 for pumice concrete with compressive strength of 19.2 to 27 MPa respectively.

The homogenous structure of the lightweight matrix deviates from the elastic modulus tests of different matrixes depending on the elastic compatibility which governs the shape of the ascending branch of the curve which can be described by means of the plasticity factor k (Popovics, 1969).

$$k = E_0 \varepsilon_c / f_c \quad \text{by Popovics (1969)} \tag{4.6}$$

where E_0 is initial modulus of elasticity of concrete in the stress strain model in MPa; ε_c is the compressive strain of concrete under peak load; f_c is the compressive stress of concrete under peak load in MPa.

The value of k is a measure of the linearity of the ascending portion of the stress-strain curve. For NWC, this value is close to 2 (Smith and Young, 1956). For a perfectly linear curve the above mentioned ratio would be equal to 1. Therefore, the plasticity factor k for concrete should vary from 2 for NWC and to nearly 1 for LWAC.

Regression analysis is carried out to find the best fit relationship, indicating the brittleness of pumice concrete increasing with increase of compressive strength. The following relationships are found to be best fit for the results obtained.

$$\frac{E_0 \varepsilon_c}{f_c} = 1.0858 \, f_c^{\,0.0533} \tag{4.7}$$

$$E_0 = w_c^{\,1.5} \, 0.043 \, \sqrt{f_c} \tag{4.8}$$

where E_0 is the initial static modulus of elasticity of the concrete in MPa; ε_c is the peak strain in uniaxial compression of the concrete; f_c is the compressive strength of the concrete in MPa; w_c is the air dry density of the concrete in kg/m^3.

Figure 4.14 shows the proposed relationships and available data. The relationships proposed by Almusallam (1995), Tasdemir (1998), CEB –FIP (1999) and

Faust (2000) are also shown.

The most important aspect in the design of LWAC is how to account for the reduced ductility in LWAC as compared to NWC. With regard to the greater brittleness in LWAC, the design should aim to exclude sections with a high percentage of tensile reinforcement. Only in this case, the compressive zone is more relevant and plays a bigger role in the design. A limitation on the ultimate concrete compressive strain or the height of the compressive zone is the approach used in design.

4.2.3 Tensile strength

The tensile strength of concrete is small and often assumed to be negligible compared to its compressive strength. As pointed by other researchers such as Oluokun et al (1991) and Alfes (1990), the cause of the failure of concrete is often in tension. LWAC presents a flexural and splitting tensile strength slightly inferior to that of NWC of the same compressive strength (Zhang et al., 1995; NS 3473, 1998; Uijl et al., 1995). The experimental results of tensile strength are given in Table 4.4.

4.2.3.1 Flexural tensile strength

(a) Effect of cement content on the flexural tensile strength

Figure 4.15 shows the modulus of rupture results plotted against the cement content for mix A1-1, B1-1 and C1-1. Similar to the compressive strength test results, the modulus of rupture also increased with an increased cement content. This is similar to the trend observed for normal weight concrete.

(b) Effect of pumice aggregate content on the flexural tensile strength

Figure 4.16 shows the effect of the pumice aggregate content by percentage volume on the flexural tensile strength of pumice concrete. Among mixes A1-1, A1-2 and A1-3,

mix A1-2, which has the highest pumice aggregate content and the lowest compressive strength, also has the lowest value of flexural tensile strength at the 7 and 28 days. With the pumice aggregate content decreasing from 0.45 to 0.4 m^3/m^3, the flexural tensile strength increases by about 20 %, similar to the compressive strength (an increase of 20 %) as shown in Table 4.1. A further 5 % decrease in pumice content results in an 8.5 % increase in the flexural tensile strength whereas the compressive strength increases by 23 % with the pumice content decreasing from 0.4 to 0.35 m^3/m^3 in the concrete. Regarding the strength development, the 7-day flexural tensile strengths are about 83 %, 80 % and 92 % of that at the 28 days for mixes A1-1, A1-2, and A1-3 respectively, close to the corresponding values of 81 %, 81 %, and 83 % for compressive strength. The observations above indicate that the influence of the content of the pumice aggregate on the flexural strength of pumice concrete is similar to that of the compressive strength

The behavior can be explained by considering the failure modes of concrete in compression and flexure. The main difference between the failure modes in the modulus of rupture test and the compression test is that in the former, propagation of one single crack will be sufficient to cause failure whereas in the latter, a large number of combined cracks will only form a failure mode plane (Jones and Kaplan, 1957). The pumice aggregate itself rather than the interfacial zone is the weakest link in the pumice concrete and the fracture line goes through the aggregate. The stress-strain curve of mix A1-2 concrete in Figure 4.11 shows a lower limit of proportionality of compressive stress to compressive strain which is attributed to the cracking of aggregates. Earlier microcracking initiated in the pumice concrete is reflected in the lower proportional limits (see Section 4.3.2 and Table 4.3). This will lead to a lower modulus of rupture value for pumice concrete with increasing pumice content.

(c) Effect of sand replacement by fine pumice aggregate on the flexural tensile strength

Comparing mixes A1-1 and A2-1, the results show that the 28-day flexural tensile strength decreases by 20 % when the percentage of the sand replaced by fine pumice aggregate increases from 0 % to 50 % meanwhile the corresponding compressive strength decreases by 30 %. Moreover, compared to mix A1-1, the flexural tensile strength and compressive strength of mix A2-1 drops by 11 % and 7 % respectively at 7 days, 28 % and 20 % respectively at 28 days. The results indicate that there is a similar trend for the flexural tensile strength and compressive strength development when the mortar strength decreases due to the sand replacement by fine pumice aggregate.

(d) Effect of air content on the flexural tensile strength

When the air content increased from 2 % to 8 % in mix A4-1, the 28-day flexural tensile strength is found to decrease from 6.12 MPa to 5.06 MPa, resulting in an average 2.8 % decrease with 1 % air content increase in pumice concrete. As compared to the compressive strength, the strength loss in flexural tensile strength seemed to be less influenced by the increase of air content.

(e) Effect of cement replacement by cementitious materials on the flexural tensile strength

Pumice concrete with silica fume shows a slightly higher flexural tensile strength compared to the equivalent mix without silica fume at 28 days, an average 5 % increase is observed as shown in Figure 4.17. The 15 % increase in the flexural tensile strength at 7-days is found to be larger than that at 28 days, due to the fast strength

development of silica fume concrete. The cement replacement by GGBS does not seem to influence the flexural tensile strength, and only 4 % difference is found.

The comparable flexural tensile strength values of mixes A1-1, A3-1, A3-3 confirm that the weakest link in pumice concrete is the pumice aggregate rather than the interfacial zone of the aggregate and matrix. Thus, further significant increase in flexural tensile strength is not obtained by replacement of silica fume.

4.2.3.2 Splitting tensile strength

(a) Effect of cement content on the splitting tensile strength

The plot of splitting tensile strength with respect to the cement content at 7, 28, 56 and 91 days is shown in Figure 4.18. When cement content increases from 350 kg/m^3 to 450 kg/m^3, the splitting tensile strength increases by 18 %, and a further 100 kg/m^3 increase in cement content leads to only 7 % increase in splitting tensile strength. The behavior of the increase in splitting tensile strength with cement content is similar to that of compressive strength as shown in Table 4.1, demonstrating the close relationship between compressive strength and splitting tensile strength. Further more, the mean splitting tensile strength of the mixes with cement contents of 350 kg/m^3 and 550 kg/m^3 does not show an obvious increase after 28 days. A few of individual specimen test results show mean strengths reducing with age from 28 to 91 days due to the statistical scatter of the results.

(b) Effect of pumice aggregate content on the splitting tensile strength

Similarly to the flexural tensile strength and compressive strength, the splitting tensile strength increases with a decrease in the pumice aggregate content in the concrete (see Figure 4.19). Both 17 % and 10 % increase in the splitting tensile strength are noted

when the pumice aggregate content decreases from 0.45 to 0.4 and from 0.4 to 0.35 m^3/m^3 in concrete, respectively.

(c) Effect of sand replacement by fine pumice aggregate on the splitting tensile strength

The 28-day splitting tensile strength decreases by 21 % (see Figure 4.20) due to the 50 % sand replacement by fine pumice aggregate whereas the corresponding flexural tensile strength and compressive strength decreases by 28 % and 27 %, respectively

(d) Effect of air content on the splitting tensile strength

The splitting tensile strength seems to be less affected by the increasing entrained air content. Mixes A1-1 and A4-1 are compared. The 28-day splitting tensile strength decreases by 22 % when the entrained air content increases from 2 % to 8 %. In contrast, the corresponding decrease in flexural tensile strength and compressive strength is about 30 %.

(e) Effect of cement replacement by cementitious materials on the flexural tensile strength

One expected observation is that the pumice concrete with silica fume (mix A3-1) did not obviously have higher splitting tensile strength than the corresponding mix without silica fume. The compressive strength and flexural tensile strength of pumice concrete with silica fume are only slightly higher than those of equivalent mix without silica fume. It is hypothesized in Chapter Two that the enhanced interfacial zone alone could not raise the compressive strength of pumice concrete with 10 % silica fume at the low water to binder ratio. The observation indicates that the interfacial zone does

not have a significant influence on the splitting tensile strength of pumice concrete. Failure planes of pumice concrete specimens tested under both tension and compression pass through pumice aggregate without any sign of bond failure/interfacial zone. The effect of cement replacement by cementitious material is shown in Figure 4.21.

Visual examination of splitting tensile test specimens of dry mature specimens of pumice concrete clearly show visible signs of high moisture contents on the split surface and in the pumice aggregates. This shows that well-compacted mixtures with a high binder content, particularly mixes which incorporate mineral admixtures (silica fume, GGBS), are impermeable and will release moisture very slowly. The high strength concrete specimens drying in the laboratory air for over several months are still visibly moist over 90 percent of the split diameter (Holm and Bremner, 1994). In tests on air-dried LWAC of 30 to 50 MPa compressive strength, the reductions in splitting strength caused by differential drying moisture gradients in the concrete prior to reaching hygral-equilibrium are significantly delayed and diminished in high binder content high strength lightweight aggregate concrete (Holm, 2000). Due to the high internal moisture available for hydration from the water-absorption by pumice aggregates, the splitting tensile strength of pumice concrete can be less affected by the curing conditions.

The results indicate that the factors influencing the failure of pumice concrete under a uniform tensile stress are significantly similar to those affecting failure under compression and flexure. The weak strength of pumice aggregate can be a dominating factor in micro-cracking under the three modes of failure i.e compression, flexural tensile failure and splitting tensile failure.

4.2.3.3 Relationship between splitting tensile strength and flexural tensile and strength

It is generally established that for NWC, the splitting tensile strength is lower than the flexural tensile strength of concrete (Oluokun, 1991). The same relationship between the two tensile strengths also applies to the pumice concrete in this study.

The ratios of 1.5 to 1.6 of the ratio flexural strength/splitting tensile strength, of high performance LWAC with Leca LWA have been found (Curcio et al., 1998). In tests conducted by CUR (1995), no significant difference was observed between NWC and LWAC with reference to splitting tensile strength of plain concrete. For NWC, the ratio of flexural and splitting tensile strength is 1.52 as reported by McNeely and Lash (1963) and 1.34 as reported by Raphael (1984).

Results of pumice concrete reported here indicates a ratio of flexural strength to splitting tensile strength (f_r / f_{sp}) varying from 1.76 to 2.54 at the 7 days and from 2.17 to 2.34 at the 28 days, a narrow range. The plots of the f_r / f_{sp} ratios reported here against cylinder compressive strength is shown in Figure 4.22 and indicates that the f_r / f_{sp} ratios at 28 days are larger than that at 7 days and much scatter. In comparison, for NWC, the f_r / f_{sp} ratio increases with compressive strength (Burnett, 1990).

4.2.3.4 The relationship between the flexural tensile strength and compressive strength

The traditional relationship between flexural tensile strength, f_r and cylinder compressive strength, f_c is of the form:

$$f_r = k(f_c)^n \tag{4.9}$$

where k and n are coefficients. Values of n between 0.5 to 0.75 have been suggested. ACI 318 (1999) proposes a value of 0.6 for k and 0.5 for n which is valid for NWC. For LWAC, different modified equations of 4.10 to 4.13 are proposed by FIP (1983), Zhang (1991) and RILEM (1993) respectively.

f_r =0.46 $f_{cu}^{2/3}$ by FIP (1983) (4.10)

f_r =0.73 $f_{ck}^{1/2}$ by Zhang (1991) (4.11)

f_r =0.27+0.21 f_{cu} by RILEM (1993) (4.12)

f_r =0.6 $f_{cck}^{1/2}$ by ACI 318 (1999) (4.13)

where, f_{cck} is the cylinder compressive strength (100×200 mm) in MPa; f_{cu} is the cube compressive strength (150 ×150 ×150 mm^3) in MPa; f_{ck} is the cube compressive strength (100 ×100×100 mm^3) in MPa.

In this thesis regression analysis is performed using the limited flexural tensile strength values from pumice concrete, and an equation of the form of Equation 4.8 had k of 0.55 and n of 0.75 with a coefficient of correlation of 0.64 and a standard error of 0.3 MPa .Most of the current available formula for NWC underestimates the flexural tensile strength with respect to its corresponding compressive strength (Figure 4-23). The formula by RILEM (1993) seemed able to the flexural tensile strength of the pumice concrete.

$$f_r = 0.55 f_{cu}^{0.75} \quad (4.14)$$

where f_r is the flexural tensile strength in MPa; f_{cu} is the cube compressive strength in MPa.

4.2.3.5 The relationship between the splitting tensile strength and compressive strength

According to Weigler et al. (1972), the rate of increase in compressive strength of LWAC is faster than the rate of increase in tensile strength. This tendency is observed more frequently with high quality concrete. The ratio tensile strength / compressive strength is normally in the range of 5 to 15 % for LWAC of compressive strength greater than 20 MPa. Smeplass (1992) found that the tensile strength for LWAC with natural sand as well as with lightweight sand is about the same as for a concrete with normal density in the same strength class. According to Curcio et al. (1998), the splitting tensile strength of high performance LWAC is about 6 to 6.5 % that of the cylinder compressive strength, whereas the corresponding flexural strength of the same concrete is 9.8 to 10.5 % of the cylinder compressive strength.

The generally accepted relationship between the splitting tensile strength and compressive strength is shown in the form of Equation 4.8. The values of 0.42 for k and 0.5 for n are adopted by ACI 318 (1999) for NWC whereas FIP (1983) proposed values of 0.23 and 0.67 for k and n respectively for lightweight aggregate concrete.

The following equations are for LWAC and NWC.

$$f_{sp} = 0.23 f_{cu}^{2/3} \quad \text{by FIP (1983)} \quad (4.15)$$

f_{sp}=0.51 $f_{cy}^{1/2}$ by Slate et al (1986) (4.16)

$f_{sp} = 0.42 f_{cy}^{0.5}$ by ACI 318 (1999) (4.17)

f_{sp}=0.47 $f_{cy}^{0.56}$ by Rashid et al (2002) (4.18)

where f_{cu} is the cube compressive strength ($150\times150\times150\ mm^3$) in MPa; f_{cy} is the cylinder compressive strength (150 mm (diameter)$\times$300 mm (height)) in MPa.

In this study, regression analysis is performed using the limited splitting tensile strength values of pumice concrete and an equation in the form of Equation 4.8 had k of 0.253 and n of 0.732 with a coefficient of correlation of 0.43 and a standard error of 0.2 MPa.

$$f_{sp} = 0.2534(f_c)^{0.7318} \quad (4.19)$$

where f_{sp} is the splitting tensile strength in MPa; f_c is the cylinder compressive strength in MPa.

Figure 4.24 shows the experimental results of splitting tensile strength vs. compressive strength and the other relationships proposed. It presents a comparison of the results obtained in this study with those by the formula from FIP (1983), Repheal (1984), Slate et al. (1986) and ACI 318 (1999) respectively. Equations 4.16 and 4.18 seem to predict results of this study well. Meanwhile, equations proposed by FIP (1983) and ACI 318 (1999) underestimate the pumice concrete splitting tensile strength, derived based on the corresponding compressive strength.

4.2.4 Modulus of elasticity and Poisson's ratio

Longitudinal and lateral strains for cylinders under compression are calculated at each load level. Stress-strain curves are drawn up to a load level of 40 % of the compressive strength. The slope of the regression line is determined and compared with the standard chord line modulus. The coefficient of correlation for the regression fit to the stress-strain curve up to 40 % of the failure load is 0.99 in all cases and also the regression slop is within ± 1 % of the standard chord modulus. Therefore, modulus of elasticity, E_c is taken as the slope of the regression line to the stress-strain curve of pumice concrete up to 40 % of the failure load.

The Poison's ratio, v_c is calculated following procedure given in ASTM 469 (2002). Results for the average E_c and v_c are given in Table 4.5.

The scatter of test results for the static modulus of elasticity of NWC is reported to be very high (Walker, 1923; Ahmad and Shah, 1985). Statistical measures will be helpful in establishing the range in which the result of modulus of elasticity and Poisson's ratio could be expected to fall. For small sample sizes, the t distribution has been recommended for establishing the confidence interval (Wright, 1954). The 95 % confidence interval of the results of each sample is calculated from each set of six specimens of the 10 pumice concrete mixes using the equation.

$$T=X\pm\frac{ts}{\sqrt{n}} \tag{4.20}$$

where, X is the mean of the results of a specimens; s is the standard deviation of the sample; t is value obtained from t distribution for n-1 numbers of freedom and 95 % confidence interval; n is the sample size.

Table 4.5 gives the mean and the 95 % confidence interval for the experimental results of static modulus of elasticity and Poisson's ratio of all mixes at 28 days. It is observed that the 95 % confidence interval of a sample is less than 1.5 GPa for the static modulus of elasticity of pumice concrete and is less than 0.024 for the Poisson's ratio. This indicates that 95 % of the measured values of the static modulus of elasticity fall within the range of about ± 5 % from the mean whereas 95 % of the experimental values of Poisson's ratio have a range of up to ± 13 % from the mean.

(a) Effect of cement content on the static modulus of elasticity

Modulus of elasticity of pumice concrete is found to have a direct relationship with cement content, and not increase much after 28 days (see Figure 4.25). This is similar to the trend shown for compressive strength and flexural strength.

(b) Effect of pumice aggregate content on the static modulus of elasticity

It is evident from Figure 4.26 that the pumice content has a significant influence on the E_c of pumice concrete. The highest E_c generally corresponded to concretes containing less pumice aggregate content (see Figure 4.27 and Table 4.6 for mix A1-2, A1-1 and A1-3). Therefore, it seems that the pumice aggregate content in the concrete is a dominating factor influencing the static modulus of elasticity of pumice concrete. This has also been observed by other researchers e.g. Aitcin and Mehta (1990), Baalbaki et al. (1992), Hirsch (1962), Bremner and Holm (1986).

(c) Effect of sand replacement by fine pumice aggregate on the static modulus of elasticity

The results shows that the static modulus of elasticity, E_c decreases by 39 %, 25 %,

22 %, 19 % and 18 % at 3, 7, 28, 56 and 91 days when 50 % sand by volume in the pumice concrete is replaced by fine pumice aggregates (see mix A1-1 and A2-1). The results also indicate that there is a similar trend for the static modulus of elasticity and compressive strength and tensile strength when the sand in the concrete is replaced by fine pumice aggregates.

(d) Effect of air content on the static modulus of elasticity

As expected, when the air content increases from 2 % to 8 %, the 28-day static modulus of elasticity is found to decrease from 17.18 MPa to 12.33 MPa, resulting in an average 3.7 % decrease in the static modulus of elasticity with 1 % air content increase in pumice concrete. Compared to the 28-day compressive strength which decreases by 4 % with 1 % air content increase, the strength loss of the static modulus of elasticity seems to be similarly influenced by the increased air content. Whiting (1998) reported that for NWC the effect of air content on elastic modulus in compression is similar to that of compressive strength, and the modulus will usually decrease by 2.5 to 6 % for every 1 % of air content. Unlike the pumice concrete with 2 % air content, the static modulus of elasticity of the pumice concrete with 8 % air content does not increase significantly much after 7 days. This can be due to the fact that the ceiling strength of higher air content concrete is achieved at earlier age.

(e) Effect of cement replacement by cementitious materials on the static modulus of elasticity

Figure 4.27 shows a comparison of the modulus of elasticity between mixes A1-1, A3-1, A3-2 and A3-3 using three types of cement replacement. Pumice concrete with silica fume shows higher values of E_c when compared with concrete without silica

fume. However, mix A3-1 with 10 % silica fume has higher E_c values, by 5.3 % at 28 days and 7.2 % at 91 days, compared to those of corresponding mix without silica fume, e.g. mix A1-1. The corresponding compressive strength are also higher by 8.2 % at 28 days and 7 % at 91 days. Mix A3-3 with cement replacement by 10 % silica fume and 55 % GGBS gives the highest values of E_s at the later ages, up to 13 % increase at 91 days compared to that of mix A1-1. The cement replacement by 55 % GGBS leads to a marginally higher elastic modulus at different ages compared to mix A1-1 without any cement replacement. It should be noted that in mixes with cement replacement by silica fume or/and GGBS, the volume of the paste is comparably higher than in corresponding mix without silica fume or GGBS. Consequently, this contributes to an enhancement of the static modulus of elasticity of the pumice concrete to some extent.

(f) Experimental values of modulus of elasticity and existing empirical relationships

Several empirical formulae proposed for calculating the E_c of NWC and LWAC as a function of cylinder compressive strength, f_c and the air dry unit weight ρ_c are given in Table 4.7 and are shown in Figure 4.28.

$$E_c = 9500 f_{cck}^{0.3} (\rho / 2400)^{1.5} \quad (f_{cck} < 85 \text{ MPa}) \quad \text{by NS3473} \tag{4.21}$$

$$E_c = w_c^{1.5} 0.043 \sqrt{f_c} \quad (f_c < 41 \text{ MPa}) \text{ by ACI 318 (1987)} \tag{4.22}$$

$$E_c = 3320 \sqrt{f_c} + 6895 (w_c / 2320)^{1.5} \quad (21 < f_c < 62 \text{ MPa}) \text{ by Slate (1986)} \tag{4.23}$$

$$E_c = 1.19^{2/3}\sqrt{f_{ck}} \quad (60< f_c <100 \text{ MPa}) \text{ by Zhang (1991)} \tag{4.24}$$

where E_c is modulus of elasticity in MPa; ρ and w_c is the air dry density of concrete in kN/m^3; f_{ck} is the cube compressive strength (100 mm $\times$ 100 mm $\times$ 100 mm) in MPa; f_{cck} is the cylinder compressive strength (100 mm (diameter) $\times$ 200 mm (height)) in MPa; f_c is the cylinder compressive strength (150 mm (diameter) $\times$ 300 mm (height)) in MPa.

The equations above show a comparison of various equations given in Norwegian Concrete Code 3473 (1992), ACI 318 (1983), equations given by Slate (1986) and Zhang (1991). In Table 4.6 a comparison between the experimental and the various empirical calculated values is also given. The calculations are based on the following assumptions that the ratio of f_{ck}/f_{cck}=1.07 and f_c/f_{cck}=0.97.

For the various concrete mixes, the Norwegian Code appears to give a fairly good prediction of elastic modulus within a maximum of 6 % difference, while the ACI code significantly underestimates the elastic properties. The equation given by Slate (1986) significantly overestimates the actual results. The equation from Zhang (1999), gives a reasonable prediction of the elastic modulus for high strength lightweight aggregate concrete of 60 to 100 MPa in compressive strength. If used for pumice concrete, it will lead to an underestimation of more than 2 times that of the actual values. The discrepancy between the predicted values of E_c of LWAC from the above formulas can be attributed to the difference of types of the LWA used.

(g) Relationship of Poisson's ratio with compressive strength

Figure 4.29 shows the experimental values of Poisson's ratio, v_c plotted against compressive strength, f_c. Results show a high scatter with values varying from 0.16 to 0.27 and there is no definite trend with the compressive strength at different ages. As shown in Table 4.5, the confidence limits for a sample of five pumice concrete specimens can be as high as ± 45 %. A suggested value of 0.21, irrespective of the compressive strength, appears to be the median of the results and may be used as the Poisson's ratio of pumice concrete. In comparison, a suggested value of 0.2 (RILEM, 1990; Holm, 1994) is recommended as the Poisson's ratio of NWC and high strength normal weight concrete (HSC) as well as LWAC.

4.2.5 Drying shrinkage

BS 8810 Part 2 (1985), Section 7.4 states that the 6 month drying shrinkage of NWC for an effective section thickness of 150 mm can be about 175 microstrains under 70 % ambient relative humility. For illustration, such a concrete will have an original water content of about 190 L/m^3 (where 1 $m^3 = 1000L$), where concrete is known have a different water content, shrinkage may be regarded as proportional to water content within the range 150 L/m^3 to 230 L/m^3 . The drying shrinkage of pumice concrete in this study is found to vary between 500 and 1200 microstrains at 168 days, significantly higher than that of NWC.

(a) Effect of cement content on the drying shrinkage

The drying shrinkage measurements are carried out on prismatic specimens for a period of 168 days according to ASTM 157M (1999). Figures 4.30 (a) to (c) present the drying shrinkage of 1, 7 and 28 days moist cured pumice concrete with different cement content but having the same water content. These figures show that the drying

shrinkage decreases with an increase in cement content within the 168 days observed. The drying shrinkage values for mix A1-1, B1-1 and C1-1 are 1076, 857 and 1047 microstrains respectively for 1 day curing; 1076, 857 and 1007 microstrains respectively for 7 days curing; 889, 500 and 872 microstrains respectively for 28 days curing. Brooks (1989) demonstrated that the shrinkage of hydrated cement paste is directly proportional to water to binder ratio (w/b) between the values of about 0.2 to 0.6 for NWC. At higher water to binder ratio, the additional water is removed from capillary pores upon drying resulting in more shrinkage. El-Hind et al. (1994) reported that for NWC, a lower water to binder ratio leads to smaller drying shrinkage. It is also found that increasing the water to cement ratio by 24 % (from 0.33 to 0.41) increase the drying shrinkage at 300 days by 84 % for NWC (Roy et al., 1993)

Figure 4.31 compares the rates of drying shrinkage of concretes with cement content of 350, 450 and 550 kg/m^3 at the constant water content 150 kg/m^3 for 1, 7 and 28 days of curing before performing the drying shrinkage test. The figure shows that the drying shrinkage rates of these concretes decrease with time. In the first month, mix C1-1 (350 kg/m^3 cement content) gives the highest drying shrinkage rate and mix B1-1 (550 kg/m^3 cement content) corresponds to a lowest rate. However, with time advancing, there is a reverse trend in the drying shrinkage for the concrete with different cement content at different ages. At the 6th month of drying, the rate of drying shrinkage of mix B1-1 is higher than that of mix A1-1, while mix C1-1 has the lowest corresponding rate.

It is found that the values of drying shrinkage decreases with an increase in cement content and curing duration before drying. Increasing the cement content (from 350 to 450 kg/m^3 with the corresponding water to cement ratio increasing from 0.43 to 0.28), decreases the drying shrinkage significantly at 168 days by 44 % when

under 28 days of curing. On the other hand, at later ages, the higher the cement content is, the higher the rate of drying shrinkage. The trend from the above results is consistent with the findings by Neville (1995) in that the final drying shrinkage is unaffected by the cement content under a constant water content and after a long period, for e.g. 6 months, the water content in the matrix has become constant.

(b) Effect of pumice aggregate content on the drying shrinkage

Figures 4.32 (a) to (c) present the drying shrinkage over age (test duration or drying period) for concrete with pumice aggregate content of 0.35, 0.40 and 0.45 m^3/m^3, which have been moist cured for 1, 7, 28 days. It is observed that for concretes for different moist curing durations, the drying shrinkage generally increased with pumice aggregate content. This can be due to the more free water stored at higher content by the pumice aggregates, as well as the possible shrinkage of the pumice aggregate itself with a relative lower modulus elasticity (Reichard, 1964). However, the difference of drying shrinkage observed between concretes with 0.35 and 0.45 m^3/m^3 pumice aggregate wanes away at later drying days, of which 5 %, 7 %, and 15 % differences are achieved at 168 days drying for concrete with curing duration of 1, 7, 28 days respectively. This may suggest that the influence of pumice aggregate content in concrete plays an important role in the early age drying shrinkage rate, whereas the final drying shrinkage values can be mainly controlled by the properties and content of the cement paste in the concrete. According to Richards (1964), shrinkage is inversely proportional to the modulus of elasticity of concrete. Due to the porous structure of LWA, these aggregates are prone to shrinkage themselves. The stiffer the aggregate, the more the contraction of the matrix is restrained and the lower the resulting shrinkage of the concrete will be (Cembureau, 1974). This has been mentioned as one

of the reasons why the shrinkage of LWAC is generally higher than that of NWC (Liu et al., 1995). Since transport of water is the basis for the occurrence of shrinkage, the higher moisture content in LWA has a great influence on drying shrinkage. A higher moisture content in LWA will lead to a decrease in drying shrinkage.

(c) Effect of 50 % sand replacement by fine pumice aggregate on the drying shrinkage

In Figure 4.33, the drying shrinkage values of mix A2-1 are significantly higher than that of mix A1-1 during the drying period, with 46 %, 53 % and 59 % higher values at 84 drying day and 20 %, 20 % and 30 % higher at the 168 drying day for the curing durations of 1, 7 and 28 day respectively. Within the first 90 days of drying, Mix A2-1 with half sand replaced by fine pumice aggregate by volume, showed higher drying shrinkage rate and magnitude than Mix A1-1. Similar observation has also been reported by Kruml (1968) in that replacement of the natural sand fraction by LWA sand increases shrinkage by 14 %. The results suggest that the replacement of sand by fine pumice aggregate lead to higher shrinkage. This is largely due to the fact that the fine pumice aggregate, having a lower modulus of elasticity, offers less restraint to the potential shrinkage of the cement paste and sand replacement by fine pumice aggregate also leads to a larger void content in concrete (Neville, 1995).

(d) Effect of different air content of fine pumice aggregate on the drying shrinkage

Figure 4.34 shows the effect of air content increasing from 2 % to 8 % on the drying shrinkage is similar to that of the effect of 50 % sand replacement by fine pumice aggregate. The differences of 11 %, 12 %, and 20 % in drying shrinkage value at 168 drying day are found comparing between mix A4-1 and A1-1 for the moist curing

duration of 1, 7 and 28 days respectively. This result seems to contradict the findings by Sutherland (1974) that air entrainment seems not to influence the drying shrinkage strains to a large extent. A possible reason can be the weak pumice aggregate and the sand replacement by air bubbles which undermine the restraint of shrinkage of cement paste (Shideler, 1957).

(e) Effect of cement replacement by cementitious materials on the drying shrinkage

Figures 4.35 (a) to (c) present the drying shrinkage of concretes containing various replacement percentages of GGBS and silica fume after moist curing for 1, 7 and 28 days. After 168 days drying, the drying shrinkage values for mix A3-1 are 1047, 956 and 829 microstrains for 1, 7 and 28 days of moist curing respectively. Correspondingly, for mix A3-2, the strains are 827, 560, 298 microstrains and for mix A3-3, the strains are 527, 419 and 286 microstrains for 1, 7 and 28 days of moist curing respectively. A general trend of decreasing drying shrinkage with increase duration of moist curing is observed for all the mixes. The concrete with 65 % GGBS by weight (mix A3-2) showed decreases in drying shrinkage by the largest extent, 25 % and 43 %, when the curing days are prolonged from 1 to 7 and 28 days respectively.

The drying shrinkage of silica fume concrete mix A3-1 at 168 drying days is similar to that of the control mix A1-1 for 1, 7 and 28 days of moist curing. This is in good agreement with the result from Carette and Malhotra (1983a). Silica fume reduces the permeability and the pore size in the concrete, thus reducing the rate of drying shrinkage. On the other hand, it densifies the microstructure of the concrete and reduces the size of capillary pores, thus increasing capillary pressure and causing a larger amount and rate of drying shrinkage (Sugair, 1995). Sugair (1995) pointed out

that both mechanisms are possible in describing the effect of silica fume on drying shrinkage. From his explanation, the higher content of water reserved in the pumice aggregate can balance the two contradictory effects of the silica fume in the drying shrinkage of pumice concrete.

The 168-day drying shrinkages of mix A3-2 with 65 % GGBS by weight are 21 %, 44 % and 64 % lower than that of control mix A1-1 for 1, 7 and 28 days of moist curing respectively. According to Neville (1995), the shrinkage of concrete containing GGBS is initially increased but, in general, shrinkage is not adversely affected by the use of GGBS. However, Penttala and Rautanen (1990) reported that the drying shrinkage of high strength GGBS concrete using slag cement which started drying at 7 days and measured after 1 years is only half that of NWC.

The replacement of cement with 55 % GGBS and 10% silica fume (mix A3-3) further reduced the drying shrinkage in the study. Manmohan et al (1981) found that an increase in the replacement percentage of GGBS increases the volume of fine pores in concrete and therefore reduces the evaporation rate of moisture from concrete. Further-more, the pozzolanic reactions of silica fume and GGBS lead to much more pore refinement, making mix A3-3 the one with the lowest drying shrinkage.

Figure 4.36 shows that the drying shrinkage rates decrease significantly during the first three months, but in the later three months, the rate does not show an obvious drop. On the other hand, pumice concrete having a higher value of drying shrinkage at an early age presents a lower value of drying shrinkage at a later age. The results indicate that a longer time is required for the drying shrinkage of pumice concrete to develop compared to NWC. A possible reason is that moisture movement from the paste to the environment is at first partly compensated for by the water stored in the porous aggregates. This causes a time lag in the shrinkage of LWAC as compared to

NWC (Cembureau, 1974; Theissing et al. 1971). This has the benefit of counteracting early-age shrinkage effects with a lower shrinkage during the period when the tensile strength of concrete is still low.

4.2.6 Creep

The compressive strengths of the specimens are determined immediately before loading the creep specimens in accordance with ASTM C39 (1992). Stress applied on the specimen is 40 % of its compressive strength at 28 days. The results are given in Table 4.8. Figure 4.37 shows the creep curve in concrete subjected to a sustained load.

(a) Instantaneous strain and creep recovery

Table 4.8 shows that the measured values of instantaneous strain (ε_{ci}^{m}) for creep specimens in compression are larger than the calculated ones (ε_{ci}^{c}). However, the calculated instantaneous strain constitutes a major part of the measured values. This can be explained by taking into account the fact that creep would have occurred during the time of loading, although the loading is completed within a few minutes. The instantaneous strain upon unloading (ε_{ce}^{m}) is less than that upon loading (ε_{ci}^{m}). The proportion of $\varepsilon_{ce}^{m} / \varepsilon_{ci}^{m}$ ranges from 0.61 to 0.94 in this study. This observation is consistent with the description by Neville (1995) that the decrease in strain upon unloading corresponds to the improved modulus of elasticity and the removal of stress at the age.

Total creep consists of delayed elastic deformation (creep recovery) and viscous flow (Neville, 1995). Delayed elastic deformation is a result of the potential energy stored in the aggregate particles. Therefore, it depends on the elastic properties of the

aggregate. Delayed elastic deformation of NWC is about 0.4 times the time-dependent deformation. In LWAC with medium to very strong aggregates, a ratio of 0.2 to 0.3 has been found (Cembureau, 1974). Hofmann et al. (1983) found values of creep recovery of LWAC to be between 0.3 and 0.4. For NWC creep recovery values of 0.24 would hold for a concrete with a water-cement ratio of 0.31, for a concrete with water - cement ratio of 0.53 the creep recovery value is 0.41. The DIN 4226 (1983) gives a value of 0.4. In this study, values of creep recovery between 0.13 and 0.22 are found, which can be due to the high porosity of the pumice aggregates in the concrete.

(b) Effect of cement content on the compressive creep

Figure 4.38 shows the compressive creep of concretes with a constant water content of 150 kg/m^3 and cement content of 350, 450, and 550 kg/m^3 respectively. It is noted that the compressive creep increases with a decrease in cement content. It should be noted that it is the hydrated cement paste which undergoes creep. The role of aggregates in the concrete is primarily that of restraint. Creep is a function of the volumetric content of cement paste in concrete, but the relation is not linear (Neville, 1964). For the same applied stress to strength ratio, creep is independent of the water/cement ratio (Neville, 1995). The creep of NWC would increase with an increase in cement content for concretes with the same water content and the same applied stress to strength ratio in test. This is because a higher strength with more cement content will reduce the applied stress to strength ratio. However, the test results on pumice concrete seem to be contradictory with the above statement. The observation in this study might be explained in the way that for pumice concretes with water to cement ratio of 0.43, 0.33 and 0.27. The strength difference of the cement paste in the concretes can be obviously larger than that of the concretes which is limited by the maximum strength

of pumice aggregate. As a result, the cement paste of mix C1-1 is subjected to higher applied stress to strength ratio than that of mix B1-1. The reason is that due to its lower cement content, its strength is lower and at constant applied stress, the ratio of applied stress to strength ratio is higher. It is the applied stress to strain ratio of the cement paste, which has a direct proportionality with the creep (Neville, 1960), that plays a principle role in the creep of the pumice concrete.

(c) Effect of pumice aggregate content on the compressive creep

From Figure 4.39 it is observed that in the concretes with various pumice aggregate content, mix A1-2 with 0.45 m^3/m^3 pumice aggregate content present the highest compressive creep and mix A1-3 with 0.35 m^3/m^3 pumice aggregate content showed the lowest creep. This indicates that the pumice aggregate content may have the apparent influence on compressive creep, where by the differences in creep of 22 % at 56 days and of 10 % at 168 days are found between mix A1-2 and A1-3. Although cement paste is the main location where creep takes place, the restrain effect of the aggregates due to its different modulus of elasticity also plays an important role too in creep development (Counto, 1964). It followed that the rate and magnitude of creep must be higher, the lower the modulus of elasticity of the aggregate.

Experimental data has revealed a significant effect of the modulus of elasticity of the aggregate on creep development in LWAC. First of all, unlike normal density aggregate (NDA), some LWA itself exhibit some creep (Kordina, 1960). This will affect the creep potential of the concrete made with these aggregates. The theory on the effect of the elastic modulus of the aggregate on creep deformations has been significantly contributed by Neville et al. (1982). Neville referred to the work of several authors, e.g. Counto (1964), who represented concrete as a two-phase system.

On the basis of such a two-phase model, the transfer of stresses from the matrix phase to the aggregates, and the effect of this transfer on creep can be easily explained. The enhanced transition zone between the matrix and pumice aggregate may also contribute to the lower creep of the pumice concrete by prohibiting moisture in the pumice aggregate from transferring to the cement paste. In the CEB/FIP (1987) manual on LWAC, the specific creep of LWAC is stated to exceed that of NWC of similar mix composition by about 10 to 30 %. Richard (1964) concluded that after 1 year the creep of LWAC is generally 20 % higher than that of NWC.

The high porosity of pumice aggregates leads to a low modulus of elasticity, hence a higher creep. Besides this, the transfer of the moisture in the pumice aggregates within the concrete may be associated with creep as it produces conditions conductive to the development of drying creep (Neville, 1995). The possible creep of the pumice aggregates themself can affect the creep potential of the pumice concretes with various pumice aggregate content (Kordina, 1960).

(d) Effect of sand replacement by fine pumice aggregate on the compressive creep

Figure 4.40 shows the compressive creep of pumice concrete with and without 50 % sand replacement by fine pumice aggregate. The significant increase of 64 % at 28 days to 65 % at 168 days in creep when comparing between mix A2-1 and A1-1 is observed. This is because mix A2-1 has more fine pumice aggregates which lead to a low modulus of elasticity, higher transfer of moisture in the aggregate and higher creep potential of LWA. All these contribute to higher creep.

(e) Effect of air content on the compressive creep of pumice concrete

The increase of entrained air content from 2 % to 8 % is found to increase the

creep to some extent in Figure 4.41, with 17 % difference at 28 days and 29 % difference at 168 days. Neville (1970) concluded that air entrainment seems not to influence the creep to a large extent. Some studies have shown larger creep with air-entrained concrete, but the reasons are confused with changes in mix design brought by air entrainment (Ramachandra, 1995). In this study, part of sand is replaced by entrained air, resulting in a possible weaker restraint on the creep of the cement paste.

(f) Effect of cement replacement by cementitious materials on the compressive creep

Figure 4.42 presents the compressive creep of the pumice concrete with and without cement replacement by cementitious materials. mix A3-1 with 10 % OPC replaced by silica fume shows a slightly lower compressive creep compared to mix A1-1, with 14 % decrease at 28 days and 4 % reduces at 168 days. Mix A3-2 with 65 % OPC replaced by GGBS by weight further reduces the compressive creep, with a decease of 14 % at 28 days and of 13 % at 168 days. Similar to drying shrinkage, mix A3-3 with 65 % OPC replaced by 55 % GGBS and 10 % SF deceased the compressive creep most significantly, with a decrease of 62 % at 28 days and 46 % at 168 days when compared to mix A1-1.

The result of creep decrease in pumice concrete with silica fume is consistent with findings by Tomaszewicz (1985) and Wiegrink (1996). As the adsorption of water from voids in the matrix gel is one of the mechanisms that causes creep, the finer the voids, the more difficult it is for the water to be removed, thus the less the creep per unit applied stress. Neville (1995) explained that the reduced creep in SF pumice concrete can be explained in the way that hydration reaction of SF reduces the amount of water available for movement out of the gel.

65 % cement replacement by GGBS results in a decreased creep in mix A3-2. Klieger and Isberner (1967) reported that for NWC, few differences were observed when GGBS is partly used as compared with OPC. Fulton (1974) also observed generally greater creep where various blends of GGBS are used. Similar to SF, GGBS can also refine the microstructure of the gel particles, reducing the amount of water available for movement out of the gel.

In mix A3-3, there is 10 % SF and 55 % GGBS replacement of OPC, the total amount of replacement being the same as mix A3-1. However, the fineness of the GGBS and SF is higher than that of OPC; thus the hydration product would be expected to be denser for mix A3-3.

(g) Specific creep in compression

Specific creep is the value of creep per unit applied stress (microstrain/MPa). As compared to creep at the same stress/strength level which describes the effect of material properties other than strength, specific creep reflects a greater influence of strength on the creep of material. Fig 4.42 presents the trend of specific creep of various mixes, which is similar to that of compressive creep. A range of typical values for one year specific creep of 65-90 microstrain/MPa is reported by CEB/FIP (1977) for LWAC. However, a larger range of specific creep, 45 to 143 microstrain/ MPa, is found using pumice concrete in this study. It is worth mentioning that among the factors investigated affecting creep and specific creep, the sand replacement by fine pumice aggregate, the increased entrained-air content as well as higher water to cement ratio can significantly increase specific compressive creep by almost two times after 168 days of loading.

4.3 Conclusions On The Mechanical Properties Study Of Pumice Concrete

Based on the limited investigation, the following conclusions are drawn as following:

Structural pumice concrete with compressive strength of 18.6 MPa to 27.8 MPa and oven-dry density of 1366 kg/m^3 to 1710 kg/m^3 can be achieved. The compressive strength increases with a decrease in the pumice content, however, the trend becomes less obvious when the pumice content reductions are less than 0.4m^3/m^3. Replacement of 50 % sand by fine pumice aggregate can decrease the density by 160 kg/m^3 together with a decrease of 28.3 % in compressive strength. Cementitious materials, especially silica fume is not effective in enhancing the compressive strength. An average 4 % compressive strength loss with an increase of 1 % air content is found when the air content is increased from 2 % to 8 %. A lower strain at the peak stress of 0.0016 to 0.0020 with significant scatter is found and the relationship $\frac{E_0\varepsilon_c}{f_c}=1.0858\ f_c^{\ 0.0533}$ (where E_0 is initial modulus of elasticity of concrete in the stress strain model in MPa; ε_c is the compressive strain of concrete under peak load; f_c is the compressive stress of concrete under peak load in MPa) is proposed for the pumice concrete. The method proposed by Chandra and Berntsson (2001) can be used for mix proportioning of structural pumice concrete.

The flexural tensile strength and splitting tensile strength both increase with an increase in cement content and a reduction in pumice aggregate content and decreases with an increase in air content and the replacement of sand by fine pumice aggregate. Silica fume did not seem to have beneficial effect on the flexural tensile strength and splitting tensile strength. The flexural tensile strength of pumice concrete seems to be two times higher than that of NWC at the same compressive strength. The

relationships f_r =0.55 $f_{cu}^{0.75}$ and $f_{sp} = 0.25 f_{cu}^{0.73}$ (where f_r is the flexural tensile strength in MPa; f_{cu} is the cube compressive strength of concrete in MPa; f_{sp} is the flexural tensile strength in MPa) are proposed for pumice concrete.

The Norwegian code NS 3473 (1998), $E_c = 9500 f_{cck}^{0.3} (\rho / 2400)^{1.5}$ (where E_c is modulus of elasticity of concrete in MPa, f_{cck} is the cylinder compressive strength of concrete and ρ is the air-dry density of concrete in kg/m^3) give good prediction of the static modulus of elasticity of the pumice concrete in this study. The Poisson's ratio of pumice concrete shows a larger scatter ranging from 0.16 to 0.27; a value of 0.21 may be suggested as the Poisson's ratio of pumice concrete.

A drying shrinkage of 500 to 1047 microstrains after 90 days drying is found for pumice concrete with cement content ranging from 350 to 450 kg/ m^3. The pumice aggregate content in concrete is found to influence the drying shrinkage to a limited extent. After the 168 drying days for a curing duration of 28 days, the 50 % sand replacement by fine pumice aggregates and an increase in air content from 2 % to 8 % lead to the increase of drying shrinkage by 30 % and 20 % respectively. The pumice concrete with 10 % silica fume, 55 % GGBS and 35 % OPC shows the lowest drying shrinkage, 66 % lower than that without cement replacement.

The values of specific creep in compression of pumice concrete are mainly found to vary between 45 and 110 microstrain/MPa at 168 days of loading and the corresponding ratio of instantaneous strain upon unloading to instantaneous strain upon unloading vary between 0.61 and 0.94. The corresponding values of creep recovery vary between 0.13 and 0.22. The increase in entrained air content from 2 % to 8 % and 50 % sand replacement by fine pumice aggregate significantly increase the compressive creep by 29 % and 65 % respectively at 168 days of loading.

Table 4.1 Comparison of compressive strength of three size sizes of pumice specimens

(a) 3 days compressive strength (MPa)

3 days	100×100×100 cubes			100×200mm cylinders			150×300mm cylinders		
Mix No	Mean	S.D	C.O.V (%)	Mean	S.D	C.O.V (%)	Mean	S.D	C.O.V (%)
A1-1	18.9	0.93	2.77	16.8	1.03	3.43	16.2	0.98	2.10
A1-2	17.4	0.88	5.54	16.1	0.78	5.55	15.4	0.87	4.44
A1-3	19.0	1.23	2.76	17.4	0.96	3.31	17.0	1.21	5.53
A2-1	15.2	0.55	1.97	14.2	1.21	2.12	14.2	0.54	6.01
A3-1	20.4	0.88	4.55	18.0	0.45	6.65	17.8	0.65	2.33
A3-2	17.7	0.89	4.32	16.5	0.76	2.89	16.4	0.61	3.87
A3-3	18.0	0.92	3.78	17.3	0.32	4.30	15.4	1.11	2.88
A4-1	12.0	0.76	4.02	11.7	1.43	5.40	11.3	0.87	4.01
B1-1	23.0	0.94	4.32	21.5	0.79	4.56	21.1	0.32	3.52
C1-1	16.6	0.77	3.47	16.0	1.12	3.09	15.3	0.99	5.01

(b) 7 days compressive strength (MPa)

7 days	100×100 ×100 cubes			100×200mm cylinders			150×300mm cylinders		
Mix No	Mean	S.D	C.O.V (%)	Mean	S.D	C.O.V (%)	Mean	S.D	C.O.V (%)
A1-1	25.7	1.54	5.87	21.0	2.04	6.78	19.9	0.53	4.58
A1-2	21.4	0.99	4.07	20.0	1.12	5.45	19.6	0.65	2.33
A1-3	28.4	0.56	1.76	22.8	1.01	3.33	22.5	1.43	5.32
A2-1	17.4	0.43	3.65	17.2	0.89	4.39	16.6	1.38	3.87
A3-1	22.8	1.78	9.78	21.8	0.77	3.38	20.2	0.78	5.21
A3-2	21.1	1.13	6.33	20.3	1.34	6.54	19.8	0.93	3.56
A3-3	22.9	1.45	4.23	21.7	0.45	2.98	21.3	0.63	4.11
A4-1	15.1	0.54	3.89	14.0	0.98	4.49	14.0	1.74	8.33
B1-1	24.8	0.74	3.44	24.0	0.76	5.55	22.9	0.34	3.22
C1-1	17.3	1.11	4.09	17.2	0.82	3.89	17.3	0.98	5.22

(c) 28 days compressive strength (MPa)

28 days	100×100 ×100 cubes			100×200mm cylinders			150×300mm cylinders		
Mix No	Mean	S.D	C.O.V (%)	Mean	S.D	C.O.V (%)	Mean	S.D	C.O.V (%)
A1-1	26.2	0.65	3.32	25.8	1.02	4.55	23.9	0.87	4.67
A1-2	23.3	152	5.53	21.2	0.32	3.78	21.2	0.98	5.66
A1-3	30.1	0.76	4.31	27.4	0.78	5.32	26.7	1.65	3.83
A2-1	19.4	0.64	3.76	18.5	0.56	4.69	18.3	0.56	5.93
A3-1	27.0	0.93	5.32	26.6	0.82	3.69	25.2	0.87	4.83
A3-2	26.7	1.11	4.44	25.4	0.47	5.64	24.3	0.77	4.84
A3-3	29.5	0.87	4.21	26.3	0.58	4.64	26.1	0.39	3.76
A4-1	19.4	0.65	5.65	18.6	0.46	3.68	18.2	0.79	5.83
B1-1	28.2	133	5.43	27.8	1.04	5.77	26.4	1.23	2.74
C1-1	19.6	0.78	2.17	19.2	0.83	6.42	19.2	0.56	5.33

Notes: S.D is standard deviation; C.O.V is coefficienct of variation.

Table 4.2 Compressive strength test results with 100×200mm cylinders (MPa)

Mix No	3-day			7-day			28d			91d		
	Mean	S.D	C.O.V (%)	Mean	S.D	C.O.V (%)	Mean	S.D	C.O.V (%)	Mean	S.D	C.O.V (%)
A1-1	16.8	1.03	3.43	21.0	2.04	6.78	25.8	1.02	4.55	25.6	1.23	3.45
A1-2	16.1	0.78	5.55	20.0	1.12	5.45	21.2	0.32	3.78	21.9	0.88	3.76
A1-3	17.4	0.96	3.31	22.8	1.01	3.33	27.4	0.78	5.32	27.8	0.56	1.65
A2-1	14.2	1.21	2.12	17.2	0.89	4.39	18.5	0.56	4.69	18.6	0.79	3.41
A3-1	18.0	0.45	6.65	21.8	0.77	3.38	26.6	0.82	3.69	27.4	0.64	4.21
A3-2	16.5	0.76	2.89	20.3	1.34	6.54	25.4	0.47	5.64	26.2	0.87	0.42
A3-3	17.3	0.32	4.30	21.7	0.45	2.98	26.3	0.58	4.64	27.3	0.54	1.45
A4-1	11.7	1.43	5.40	14.0	0.98	4.49	18.6	0.46	3.68	20.7	1.16	5.43
B1-1	21.5	0.79	4.56	24.0	0.76	5.55	27.8	1.04	5.77	27.3	1.07	3.87
C1-1	16.0	1.12	3.09	17.2	0.82	3.89	19.2	0.83	6.42	19.7	0.95	4.21

Note: S.D is the standard deviation; V.O.V is the coefficient of variation.

Table 4.3 Strains at the peak stress and proportional limit in uniaxial compression (at 90days)

Mix No.	f_c (MPa)	f_p / f_c	Strain at the peak stress
A1-1	25.78	68%	0.00168
A1-2	21.21	76%	0.00197
A1-3	27.38	62%	0.00168
A2-1	18.51	52%	0.00195
A3-1	26.60	75%	0.00187
A3-2	25.41	70%	0.00160
A3-3	26.28	86%	0.00162
A4-1	18.55	76%	0.00165
B1-1	27.81	71%	0.00200
C1-1	19.21	51%	0.00163

Note: f_c is cylinder compressive strength, f_p is the stress at proportional limit of concrete stress strain curve.

Table 4.4 Flexural / splitting tensile strength of pumice concrete

(a) 7 days strength

Mix ID No.	7 day						
	f_c MPa	f_{sp}, MPa			f_r, MPa		
		Mean	S.D	COV%	Mean	S.D	COV%
A1-1	21.0	2.42	0.57	4..83	4.70	0.68	10.2
A1-2	17.3	2.33	0.46	3.98	4.10	0.54	9.65
A1-3	22.8	2.69	0.58	5.22	5.52	0.57	8.64
A2-1	17.2	1.96	0.23	2.17	4.17	0.47	6.66
A3-1	21.8	2.58	0.61	10.8	5.45	0.33	5.32
A3-2	20.3	2.02	0.53	7.10	4.74	0.37	5.32
A3-3	21.3	2.45	0.46	6.34	5.30	0.10	4.34
A4-1	14.1	1.87	0.42	5.51	4.75	0.32	3.78
B1-1	24.0	2.91	0.48	6.22	5.58	0.61	7.64
C1-1	17.2	2.20	0.64	8.52	4.52	0.34	4.43

(b) 28 days strength

Mix ID No.	28 day						
	f_c MPa	f_{sp}, MPa			f_r, MPa		
		Mean	S.D	COV (%)	Mean	S.D	COV (%)
A1-1	25.8	2.71	0.81	6.32	6.12	1.12	11.5
A1-2	21.2	2.35	0.15	3.86	5.11	0.84	12.4
A1-3	27.4	2.90	0.78	7.88	6.64	0.62	8.56
A2-1	18.5	2.14	0.97	8.73	4.92	0.32	4.58
A3-1	26.6	2.81	0.71	7.95	6.67	0.46	5.76
A3-2	25.4	2.66	0.43	6.78	5.89	0.22	4.42
A3-3	26.3	2.74	0.98	8.36	6.33	0.67	6.67
A4-1	18.6	2.09	0.44	5.43	5.06	0.81	7.83
B1-1	27.8	2.91	0.22	4.37	6.80	0.58	6.43
C1-1	19.2	2.30	0.40	6.13	5.01	0.79	6.11

(c) 56 days strength

Mix ID No.	f_c MPa	f_{sp}, MPa		
		Mean	S.D	COV (%)
A1-1	25.7	2.68	0.38	6.78
A1-2	21.8	2.30	0.43	7.87
A1-3	27.4	2.93	0.12	2.63
A2-1	18.4	2.10	0.42	6.55
A3-1	27.5	2.75	0.33	5.67
A3-2	26.0	2.71	0.42	6.01
A3-3	27.2	2.71	0.47	8.92
A4-1	20.1	2.10	0.14	3.10
B1-1	27.4	2.88	0.37	6.14
C1-1	19.6	2.33	0.71	5.51

(d) 91 days strength

Mix ID No.	f_c MPa	f_{sp}, MPa		
		Mean	S.D	COV (%)
A1-1	25.6	2.72	0.21	1.79
A1-2	21.9	2.36	0.36	5.70
A1-3	27.8	2.85	0.67	8.54
A2-1	18.6	2.09	0.54	9.17
A3-1	27.4	2.79	0.22	4.21
A3-2	26.2	2.64	0.35	5.36
A3-3	27.3	2.78	0.56	6.01
A4-1	20.7	2.13	0.12	1.98
B1-1	27.3	2.85	0.50	8.91
C1-1	19.7	2.28	0.61	8.74

Note: f_c is the cylinder compressive strength in MPa, f_{sp} is the splitting tensile strength in MPa, f_r is flexural tensile strength in MPa.

Table 4.5 Static modulus of elasticity and Poisson's ratio

Mix No.	Static modulus of elasticity and Poisson's ratio									
	3-day		7-day		28-day		56-day		91-day	
	E_c (GPa)	ν_c	E_c (GPa)	ν_c	E_c (GPa)	ν_c	E_c (GPa)	ν_c	E_c (GPa)	ν_c
A1-1	13.00	0.254	13.66	0.223	17.18	0.213	17.20	0.205	17.50	0.224
A1-2	12.44	0.261	13.10	0.234	15.21	0.236	15.78	0.224	15.57	0.232
A1-3	15.04	0.239	17.60	0.219	20.27	0.224	20.88	0.228	20.52	0.220
A2-1	7.97	0.242	10.19	0.225	13.50	0.220	13.94	0.218	14.37	0.214
A3-1	15.53	0.252	17.76	0.234	18.09	0.214	18.67	0.205	18.76	0.214
A3-2	13.00	0.203	13.81	0.165	17.22	0.175	17.69	0.171	17.89	0.164
A3-3	13.91	0.227	15.35	0.183	18.26	0.179	19.61	0.184	19.84	0.175
A4-1	8.43	0.243	11.83	0.204	12.33	0.190	12.51	0.203	12.60	0.213
B1-1	15.96	0.252	17.04	0.252	20.33	0.242	20.83	0.235	21.40	0.225
C1-1	11.78	0.266	13.00	0.242	16.39	0.238	16.60	0.203	16.77	0.212

Note: E_c is the modulus of elasticity, ν_c is the Poisson's ratio.

Table 4.6 Statistical analysis of the test results at 28 days

Mix No.	Static modulus of elasticity E_c (GPa)			Poisson's ratio ν_c		
	Mean, X	Standard deviation S.D	$\pm ts/\sqrt{n}$	Mean, X	Standard deviation S.D	$\pm ts/\sqrt{n}$
A1-1.	17.184	0.838	0.964	0.213	0.014	0.016
A1-2.	15.209	0.743	0.854	0.236	0.012	0.013
A1-3.	20.267	1.103	1.268	0.224	0.016	0.018
A2-1.	13.504	0.960	1.104	0.220	0.011	0.012
A3-1.	18.088	0.676	0.777	0.214	0.014	0.016
A3-2.	17.218	0.661	0.760	0.175	0.015	0.017
A3-3.	18.262	1.286	1.479	0.179	0.022	0.024
A4-1.	12.334	0.563	0.647	0.190	0.014	0.015
B1-1.	20.326	0.948	1.090	0.242	0.008	0.009
C1-1.	16.387	0.702	0.807	0.238	0.010	0.012

Table 4.7 Comparison of experimental and calculated modulus of elasticity at 28 days for pumice concrete

Mix No.	Compressive strength, (MPa)	Density (Kg/m^3)	Observed modulus of elasticity (GPa)	Calculated modulus of elasticity (GPa) and the corresponding ratio of calculated/ observed modulus of elasticity							
				NS3473		ACI318-87		Slate (1986)		Zhang (1991)	
A1-1.	25.78	1801	17.18	18.24	1.06	16.43	0.96	21.32	1.24	10.86	0.59
A1-2.	21.21	1721	15.21	15.97	1.05	13.93	0.92	19.46	1.28	9.54	0.63
A1-3.	27.38	1836	20.27	19.16	0.94	17.43	0.86	21.96	1.08	11.31	0.56
A2-1.	18.51	1579	13.50	13.41	0.99	11.43	0.85	17.94	1.33	8.71	0.65
A3-1.	26.60	1808	18.09	18.54	1.02	16.79	0.93	21.61	1.19	11.09	0.61
A3-2.	25.41	1792	17.22	18.08	1.05	16.19	0.94	21.16	1.23	10.76	0.62
A3-3.	26.28	1750	18.26	17.59	0.96	15.89	0.87	21.28	1.17	11.00	0.60
A4-1.	18.55	1542	12.33	12.95	1.05	11.04	0.90	17.82	1.44	8.72	0.71
B1-1	27.81	1815	20.33	18.93	0.93	17.27	0.85	22.01	1.08	11.43	0.56
C1-1	19.21	1751	16.39	15.86	0.97	13.60	0.83	18.85	1.15	8.93	0.54

Table 4.8 Creep results of pumice concrete

Mix No.		A1.-1	A1.-2	A1.-3	A2.-1	A3.-1	A3.-2	A3.-3	A4.-1	B1.-1	C1.-1
σ_{cy150} , (MPa)		24.3	20.5	26.4	18.1	25.6	24.4	25.3	17.8	26.8	18.1
E_C, (GPa)		17.2	16.2	20.3	13.5	18.1	17.2	18.3	12.3	20.3	16.4
F_a (KN)		183	150	193	133	181	173	178	126	190	128
ε_{ci}^m (microstrain)		680	699	666	670	729	691	690	705	648	520
ε_{ci}^c (microstrain)		565	506	520	536	566	568	552	578	528	441
ε_{ce}^m (microstrain)		495	370	410	440	460	450	410	470	400	380
$\varepsilon_{ci}^m / \varepsilon_{ci}^c$		1.20	1.38	1.28	1.24	1.29	1.22	1.25	1.22	1.23	1.18
$\varepsilon_{ce}^m / \varepsilon_{ci}^m$		0.73	0.53	0.62	0.66	0.63	0.65	0.59	0.67	0.62	0.73
Creep recovery ε^r		112	140	74	155	80	76	50	120	90	190
$\varepsilon^r / \varepsilon_{ci}^c$		0.17	0.22	0.12	0.14	0.13	0.13	0.14	0.14	0.17	0.19
ε_{cc}(t) micro-strain	1	57	59	55	93	42	48	26	34	32	92
	2	83	87	75	125	66	71	32	72	60	128
	3	108	114	89	185	86	95	40	116	108	157
	4	123	130	103	193	104	114	52	149	148	201
	5	140	161	115	199	116	131	60	172	158	241
	6	155	167	133	223	134	147	68	191	172	253
	7	186	197	152	249	150	161	74	207	184	265
	14	255	272	225	391	212	232	108	331	233	370
	21	329	350	300	538	276	282	129	399	277	450
	28	393	417	348	645	333	326	149	459	305	522
	56	537	590	460	848	471	439	219	632	421	767
	84	615	668	546	978	556	500	273	769	485	913
	112	675	717	600	1083	620	556	317	859	534	1040
	140	715	745	650	1163	680	608	358	917	568	1136
	168	740	768	698	1225	709	643	399	958	606	1200

Note: σ_{cy150} is compressive strength of concrete in 150 ×300 mm cylinder in MPa; E_c is the static modulus of elasticity of concrete in MPa; F_a is the applied load in kN ; ε_{ci}^m is the measured values of instantaneous strain; ε_{ci}^c is the calculated values of instantaneous strain; ε_{ce}^m is the instantaneous strain upon unloading; ε^r is the creep recovery; ε_{cc} (t) is the compressive creep under load for duration of t.

Figure 4.1. Compression test setup

(a) Over view of compression test machine **(b) Close-up view of the cylinder during test**

Figure 4-2. 100 (diameter)×200 (height) mm cylinder under compression stress-strain testing

(a) Splitting cylinder test setup **(b) Failure in cylinder after test** **(c) Failure plane of cross section**

Figure 4.3 Pumice specimen undergoing splitting tensile strength

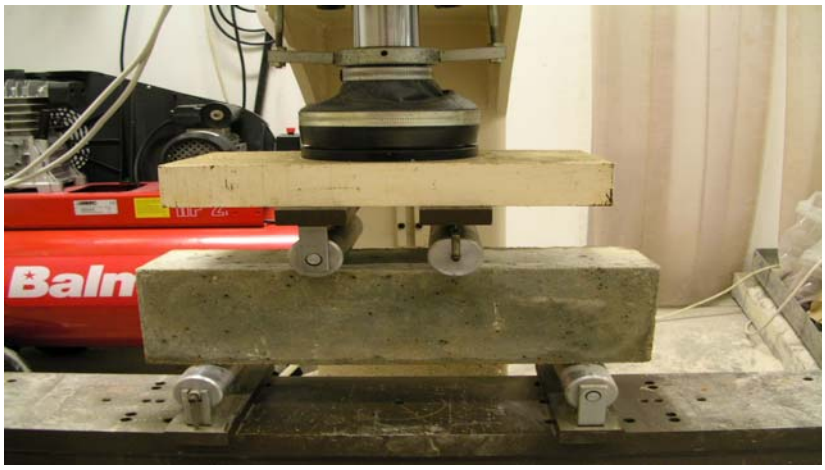

Figure 4.4. Pumice prism 100 ×100× 400 mm under flexure tensile strength

Figure 4.5 Specimen undergoing modulus of elasticity test

Figure 4.6. Demec gage and specimen of drying shrinkage

Figure 4.7. Pumice specimen cylinder (150 mm × 300 mm) under creep test

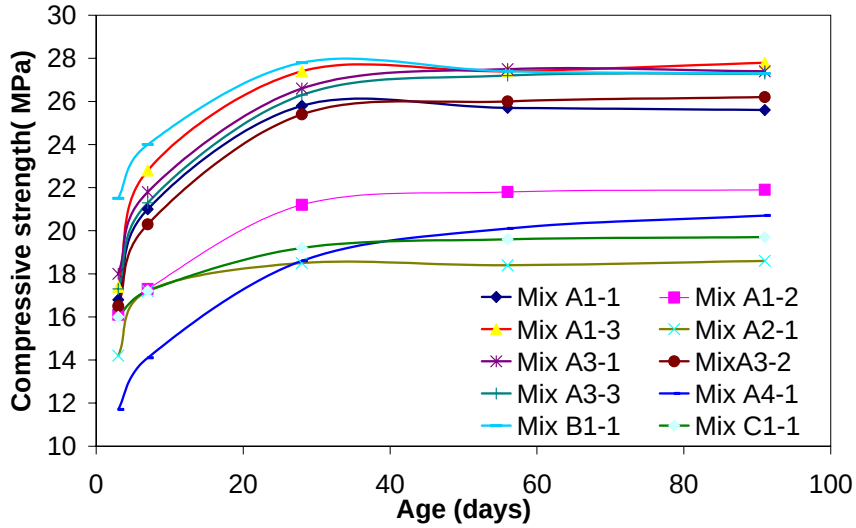

Figure 4.8. Compressive strength development

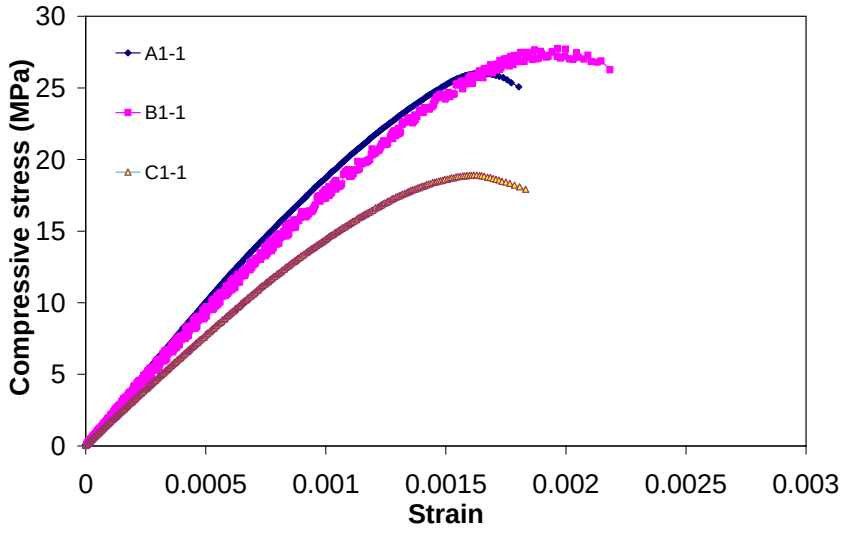

Figure 4.9. Effect of different cement content on the stress-strain curves of pumice concrete

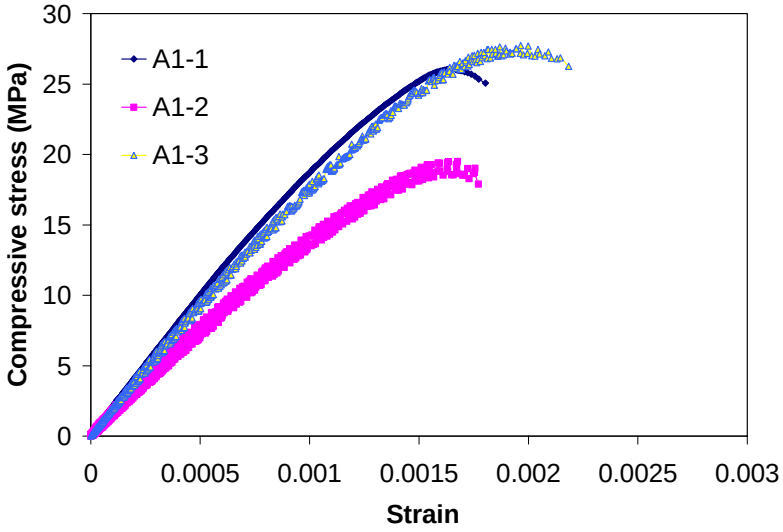

Figure 4.10. Effect of different pumice aggregate content on the stress-strain curves of pumice concrete

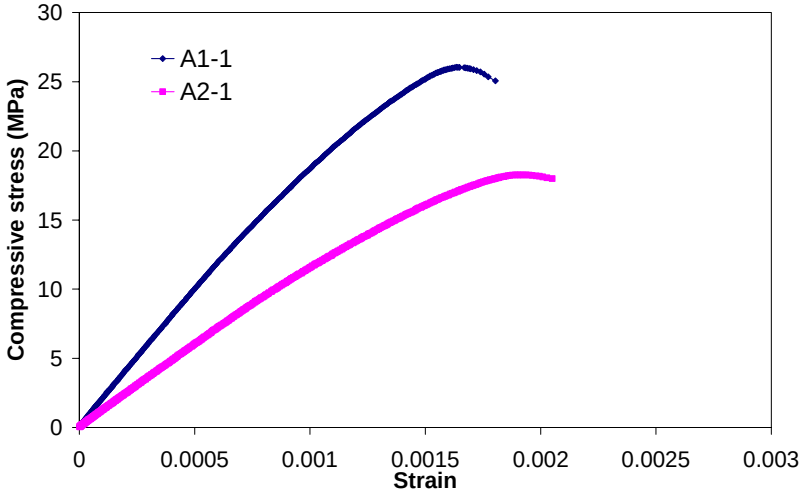

Figure 4.11. Effect of 50 % sand replacement by fine pumice aggregates on the stress-strain curves of pumice concrete

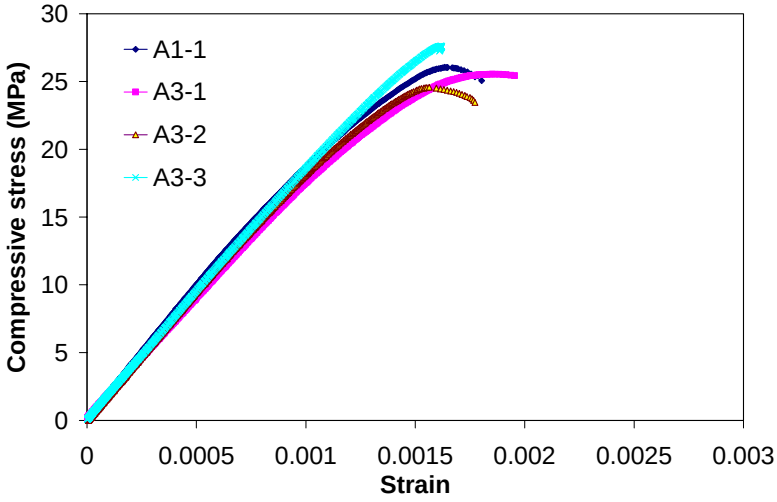

Figure 4.12. Effect of cement replacement by cementitious materials on the stress-strain curves of pumice concrete

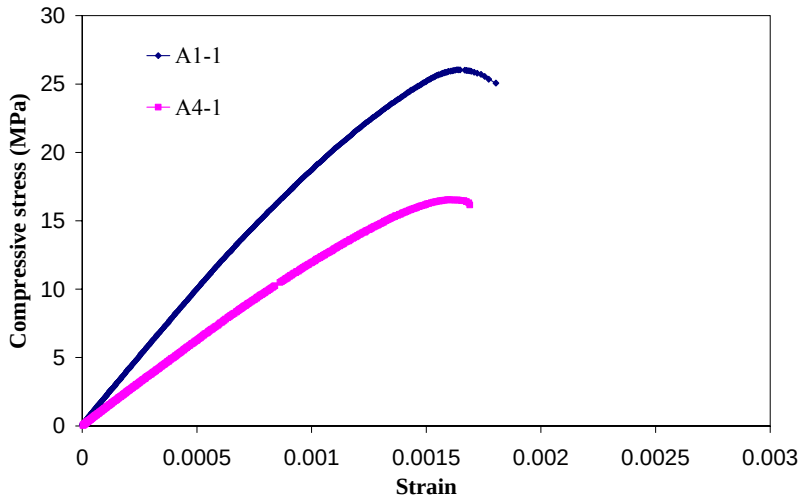

Figure 4.13. Effect of different air content on the stress-strain curves of pumice concrete

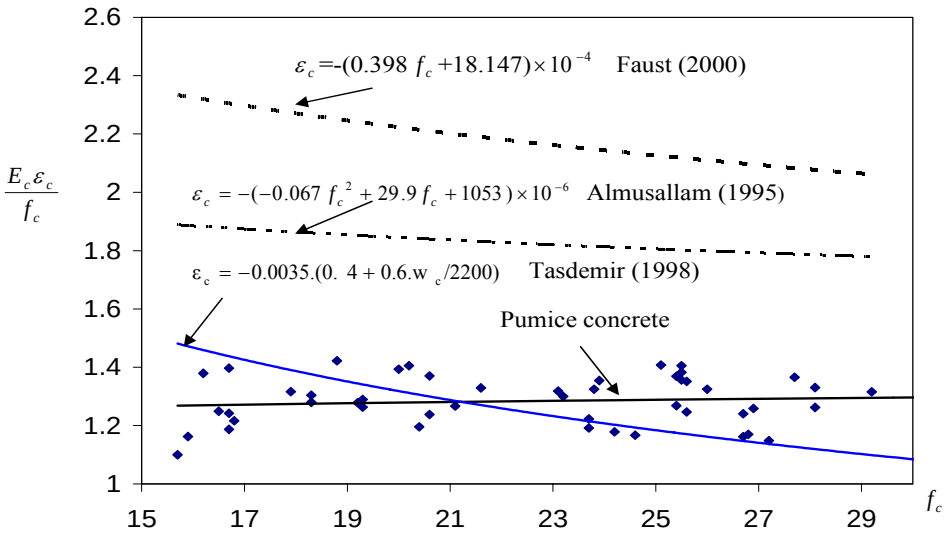

Figure 4.14. Proposed relations between peak stress and cylinder compressive strength for pumice concrete

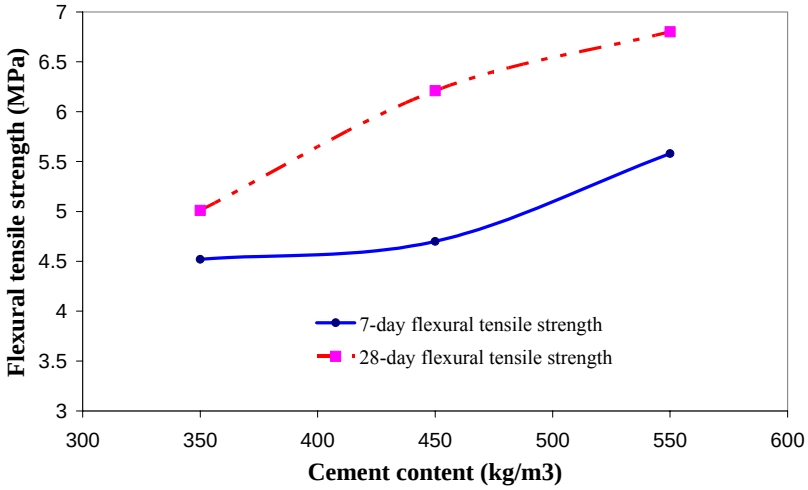

Figure 4.15. Effect of different cement content on the flexural tensile strength of pumice concrete

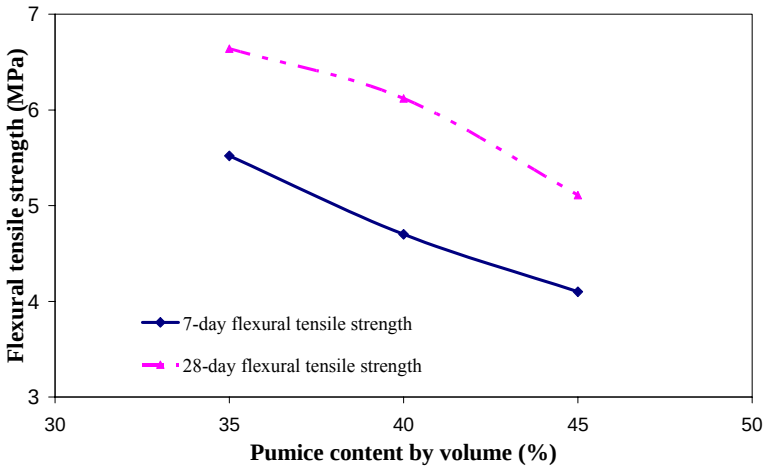

Figure 4.16 Effect of different pumice aggregate content on the flexural tensile strength of pumice concrete

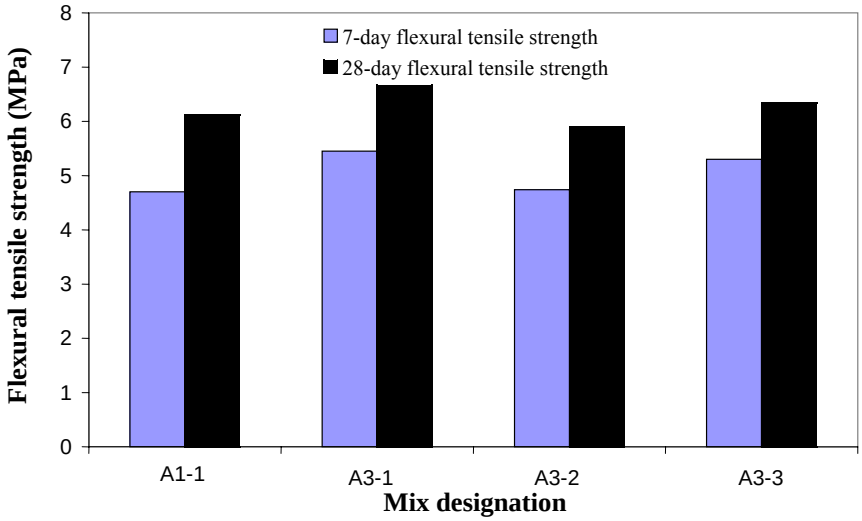

Figure 4.17. Effect of cement replacement by cementitious materials on the flexural tensile strength of pumice concrete

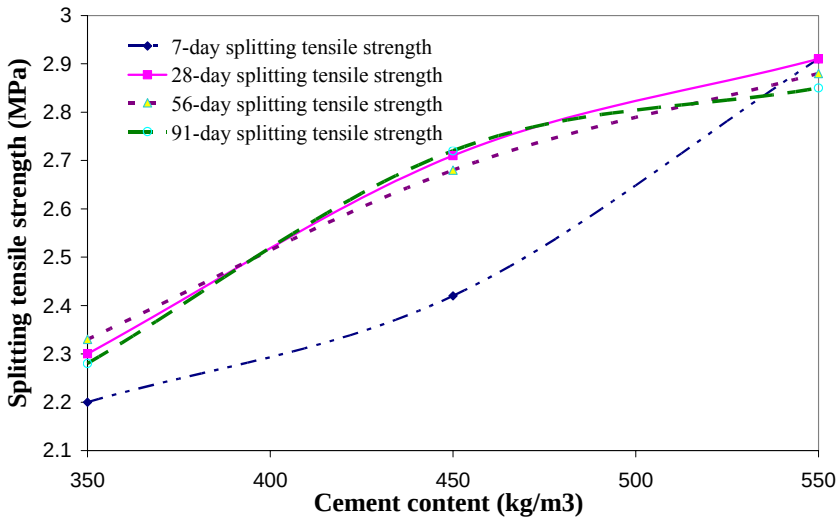

Figure 4.18. Effect of different cement content on the splitting tensile strength of pumice concrete

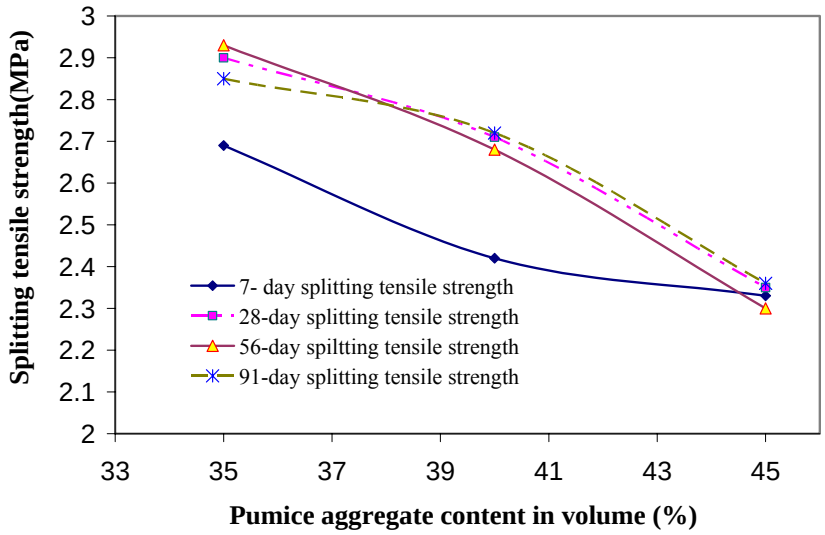

Figure 4.19. Effect of different pumice aggregate content on the splitting tensile strength of pumice concrete

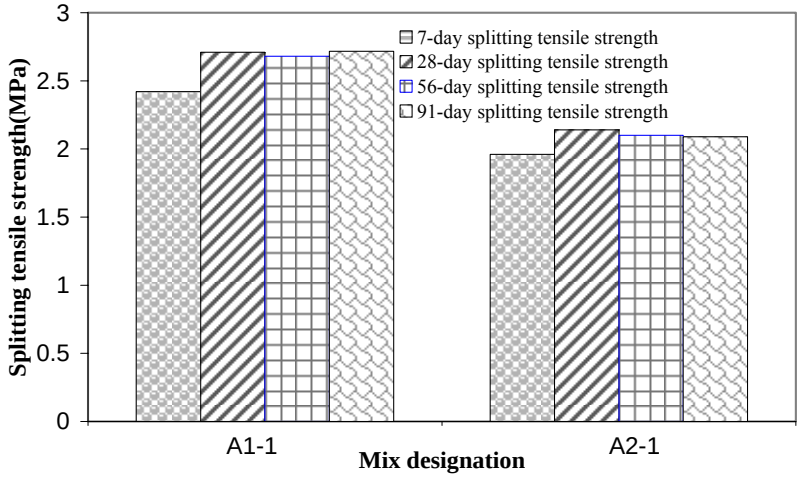

Figure 4.20. Effect of 50 % sand replacement by fine pumice aggregate on the splitting tensile strength of pumice concrete

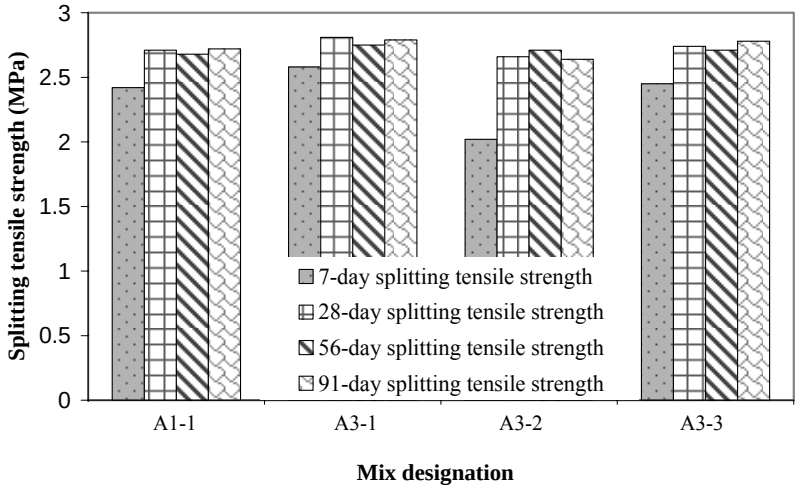

Figure 4.21. Effect of cement replacement by cementitious materials on the splitting tensile strength of pumice concrete

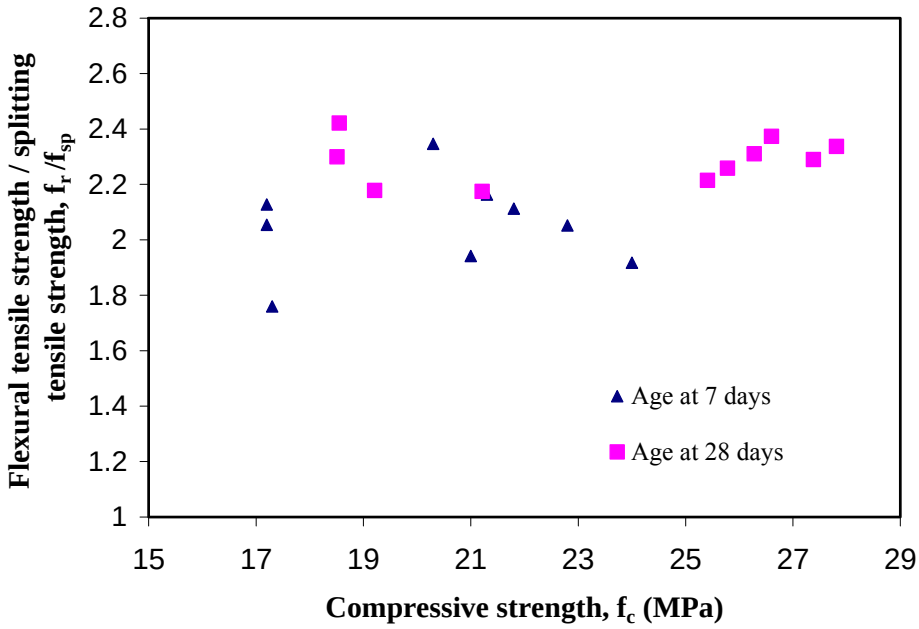

Figure 4.22 Plot of ratio of flexural tensile strength / splitting tensile strength against compressive strength of pumice concrete

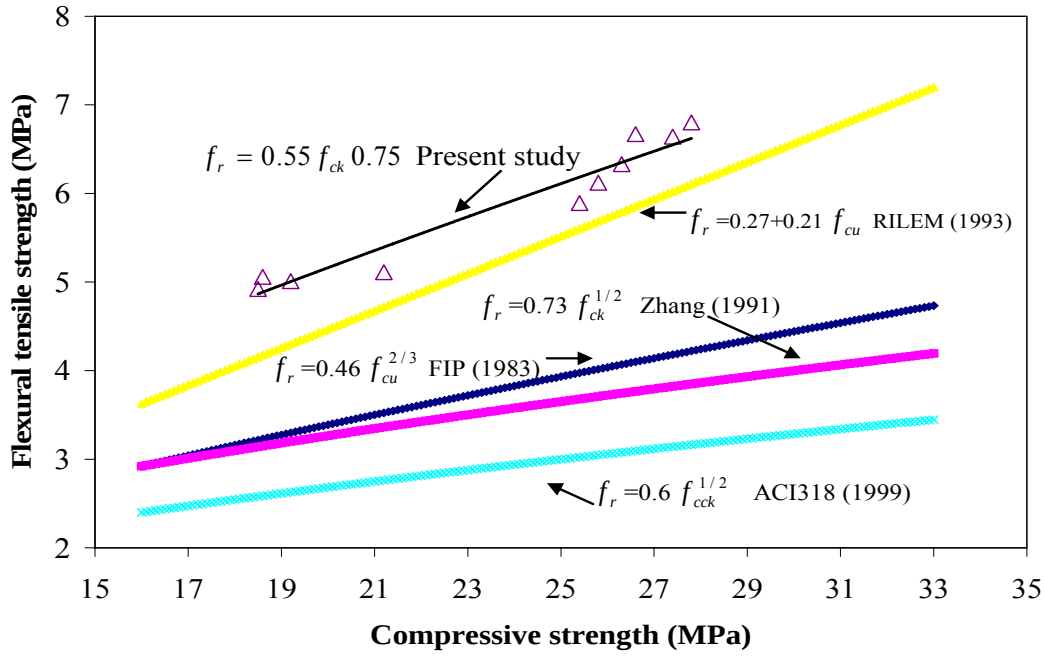

Figure 4.23. Relationship between flexural tensile strength and compressive strength

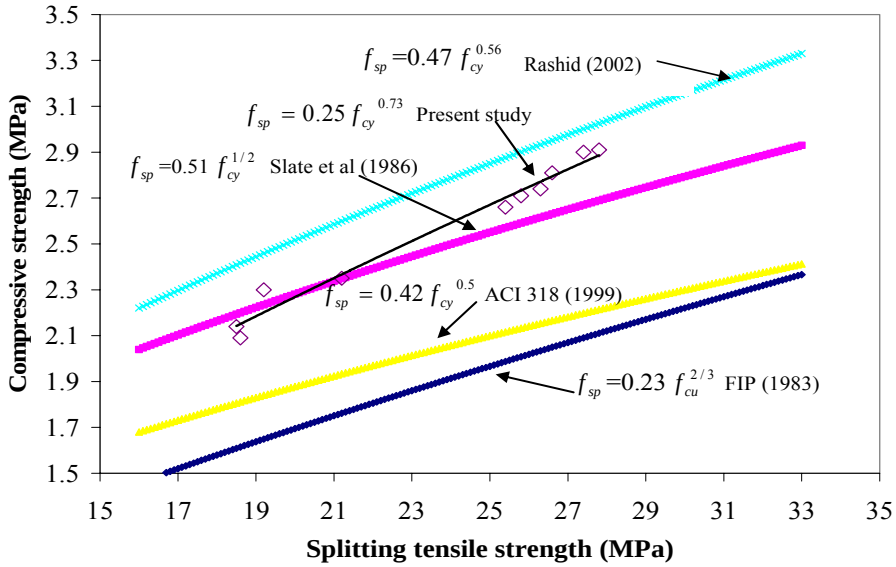

Figure 4.24. Relationship between splitting tensile strength and compressive strength

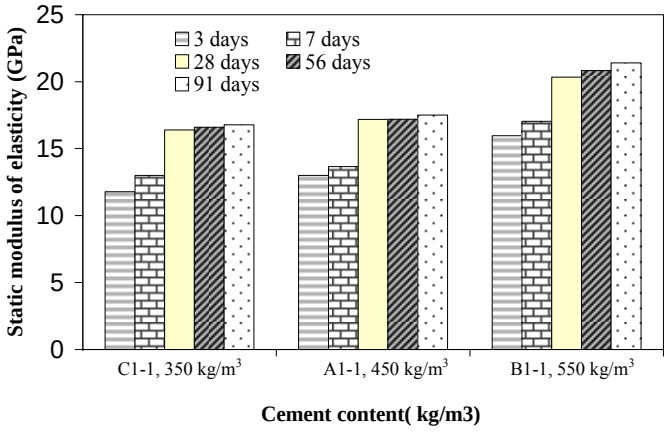

Figure 4.25. Effect of different cement content the modulus of elasticity of pumice concrete

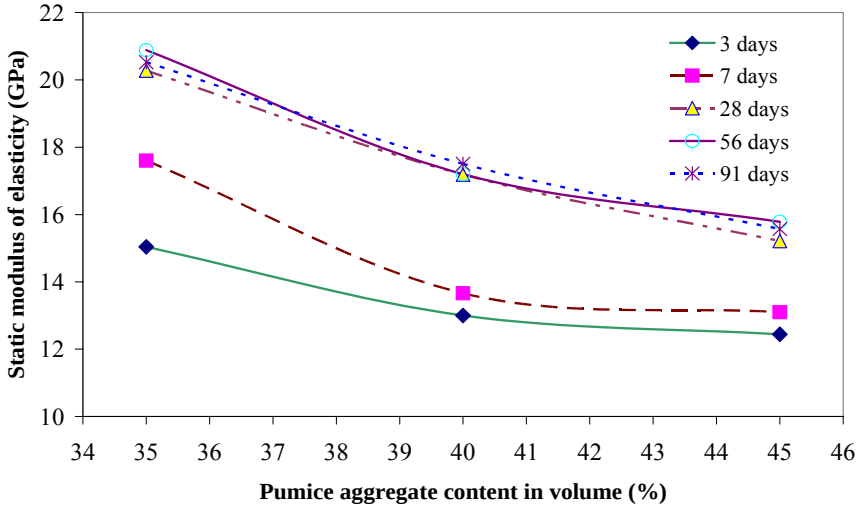

Figure 4.26. Effect of different pumice aggregate on the modulus of elasticity of pumice concrete

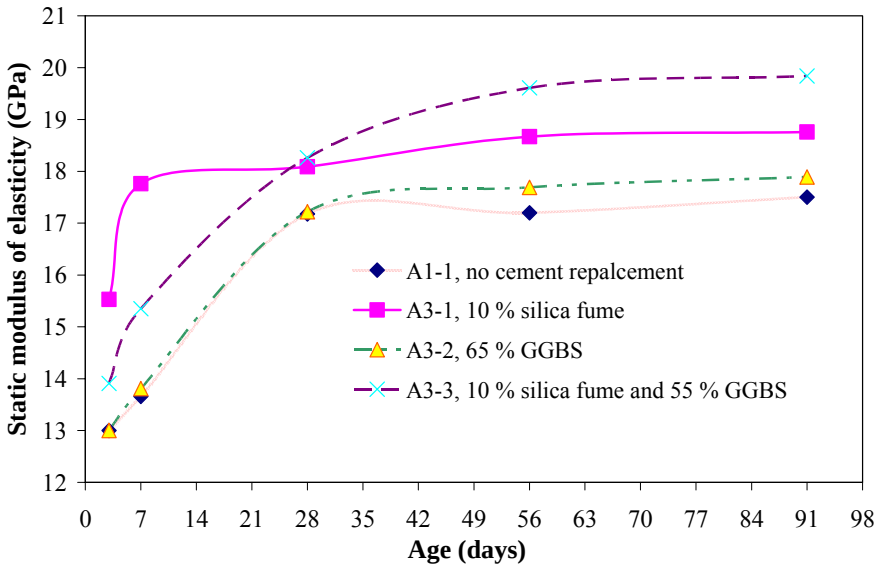

Figure 4.27 Effect of cement replacement by cementitious materials on the modulus of elasticity of pumice concrete

Figure 4.28 Comparison of experimental values of relationship of modulus of elasticity

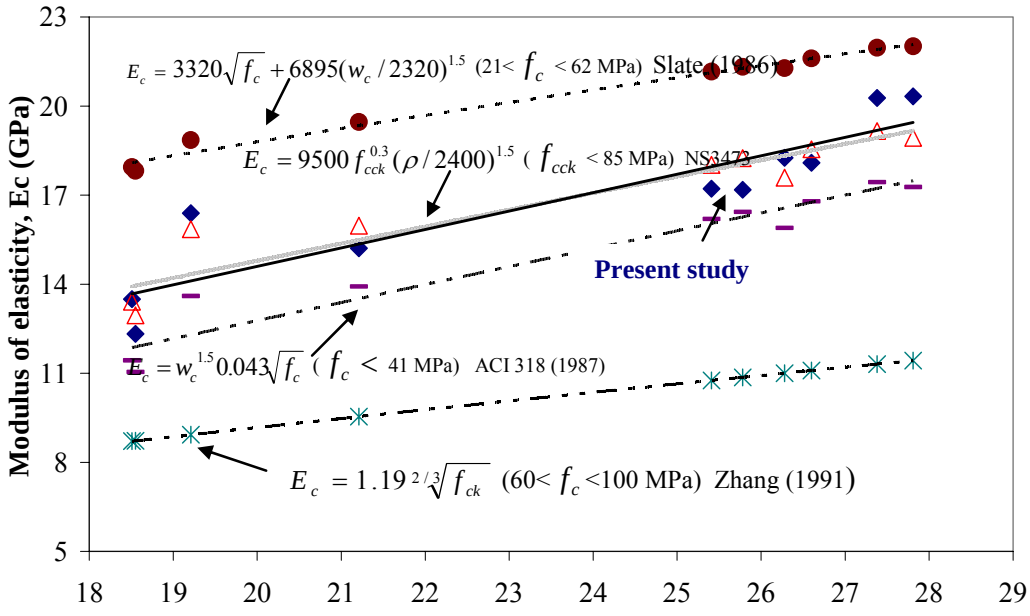

with compressive strength to existing empirical formulae

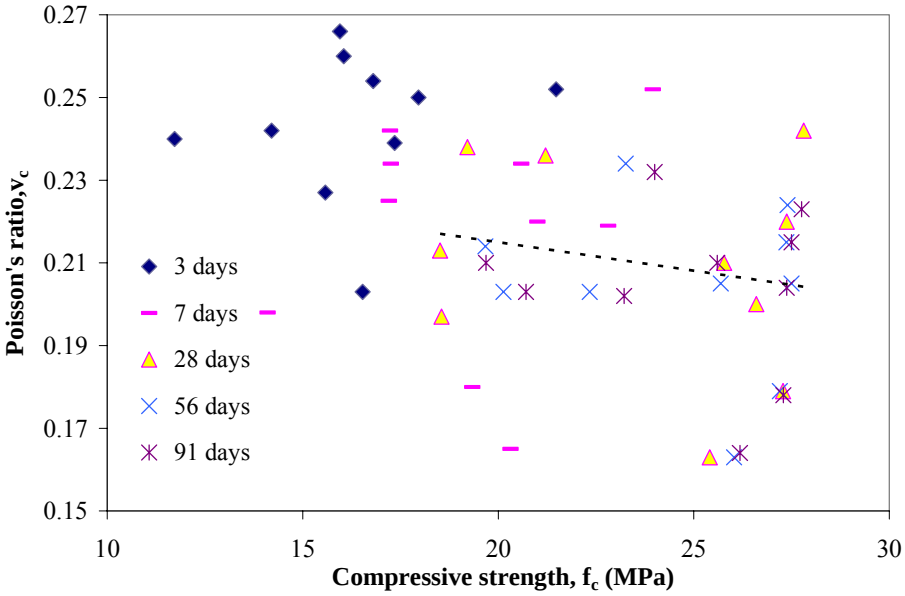

Figure 4-29. Poisson's ratio of pumice concrete with respect to its compressive strength

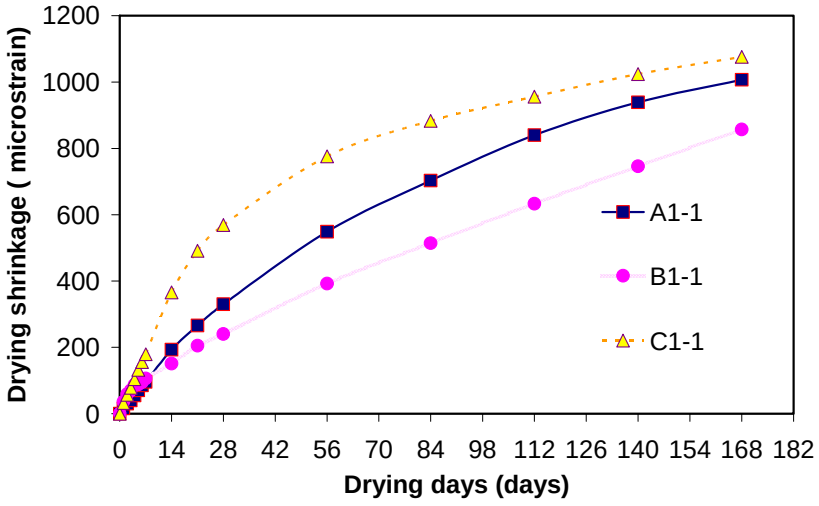

(a)

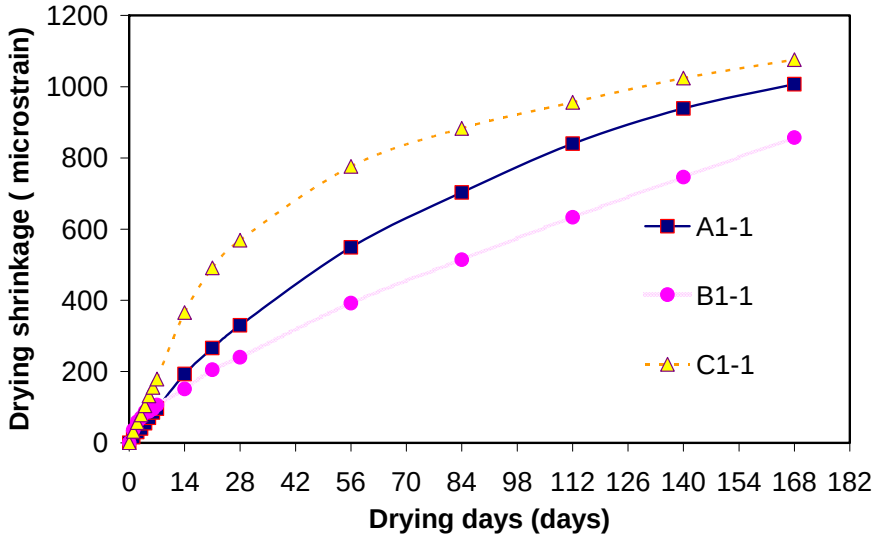

(b)

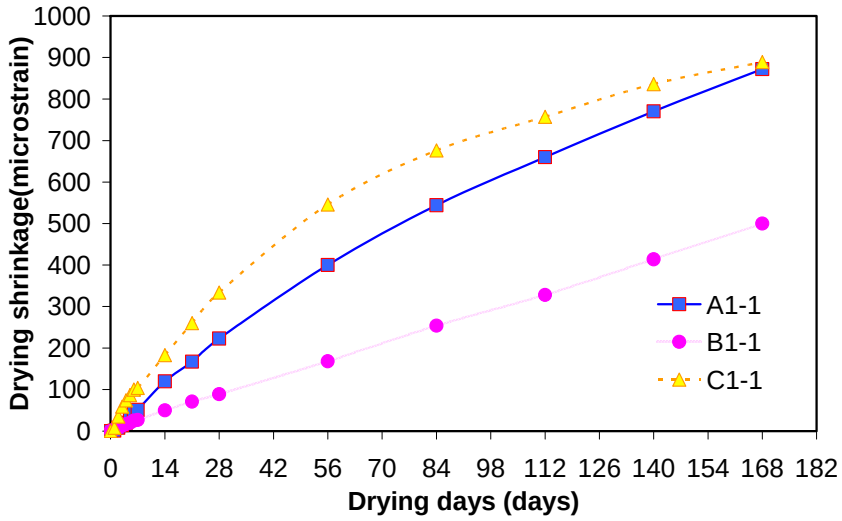

(c)

Figure 4-30 Effect of different cement content on the drying shrinkage of pumice concrete for a curing period of (a) 1-day (b) 7-day (c) 28-day.

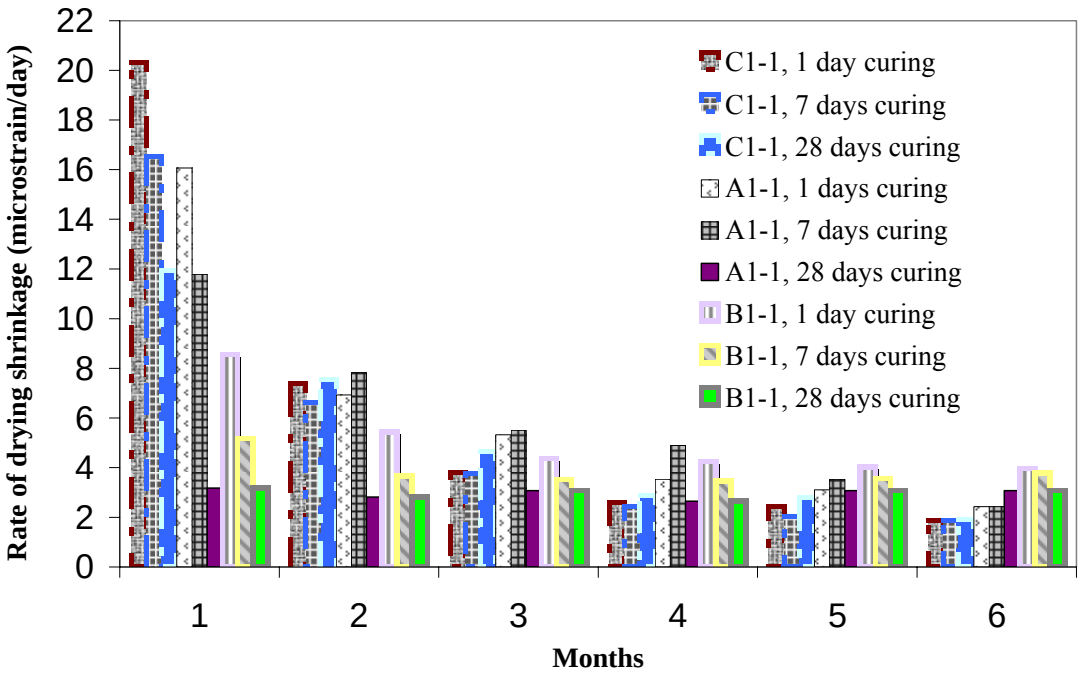

Figure 4-31 Comparison of rates of drying shrinkage of 1, 7, 28 days moist cured pumice concrete with 350, 450 and 550 kg/ m^3

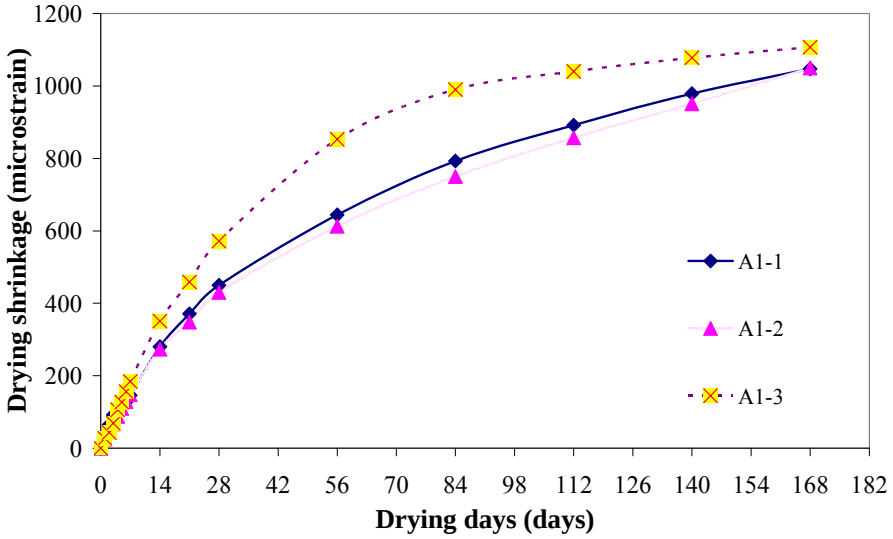

(a)

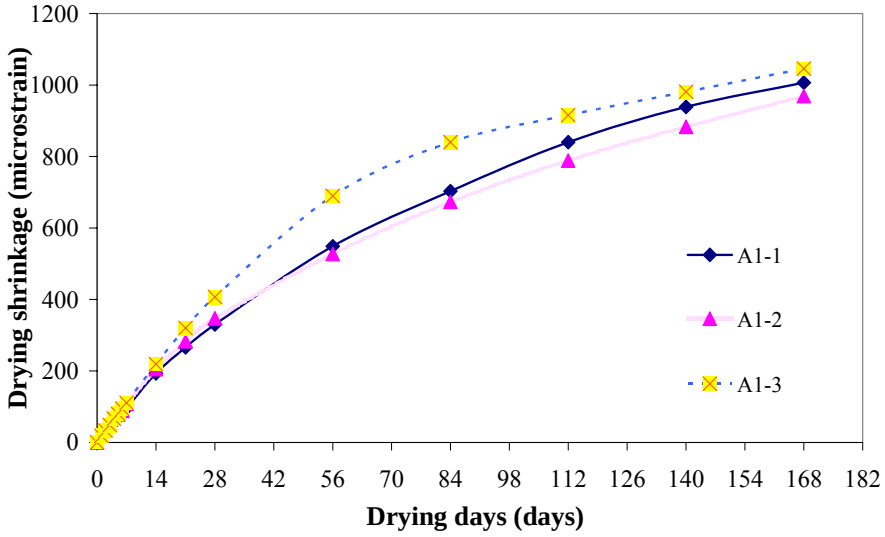

(b)

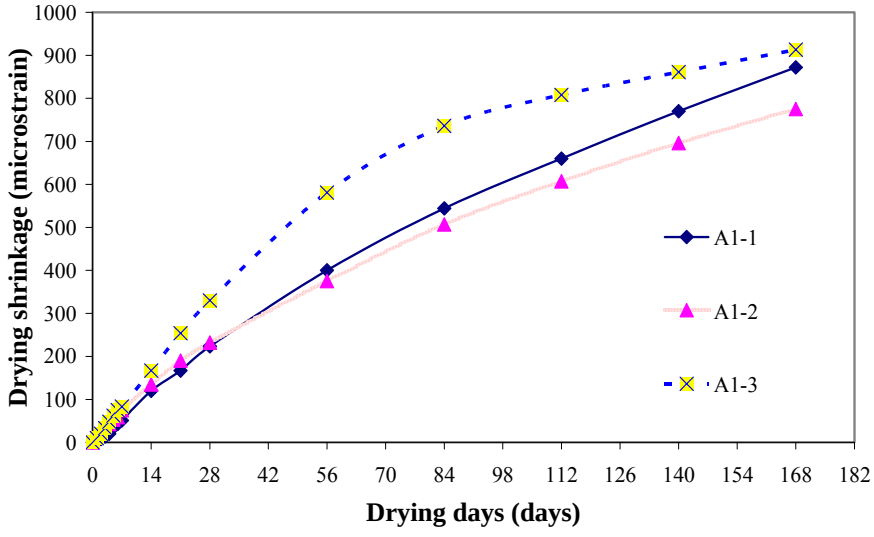

(c)

Figure 4-32 Effect of pumice aggregate content on the drying shrinkage of pumice concrete under duration of curing (a) 1-day (b) 7-day (c) 28-day

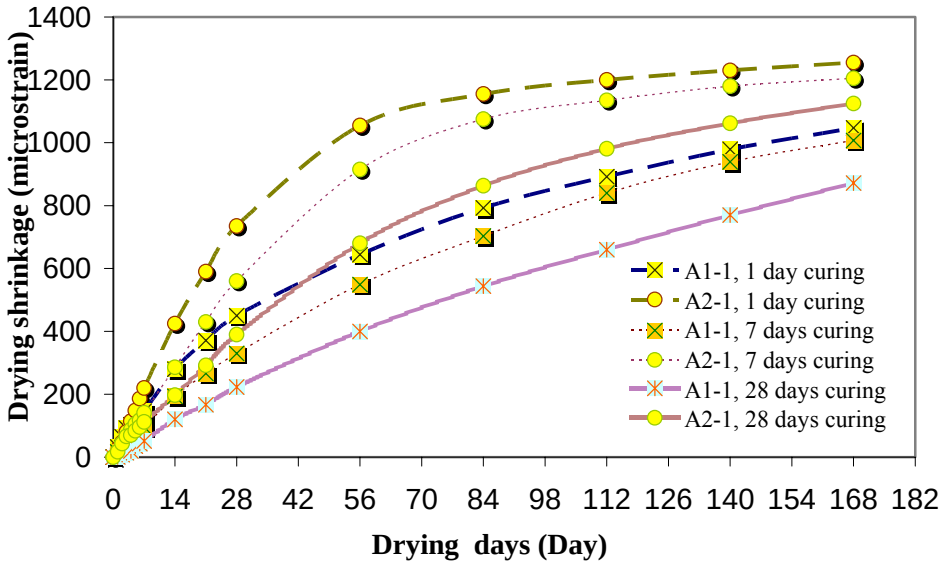

Figure 4-33. Effect of 50 % sand replacement by fine pumice aggregate on the drying shrinkage of pumice aggregate concrete

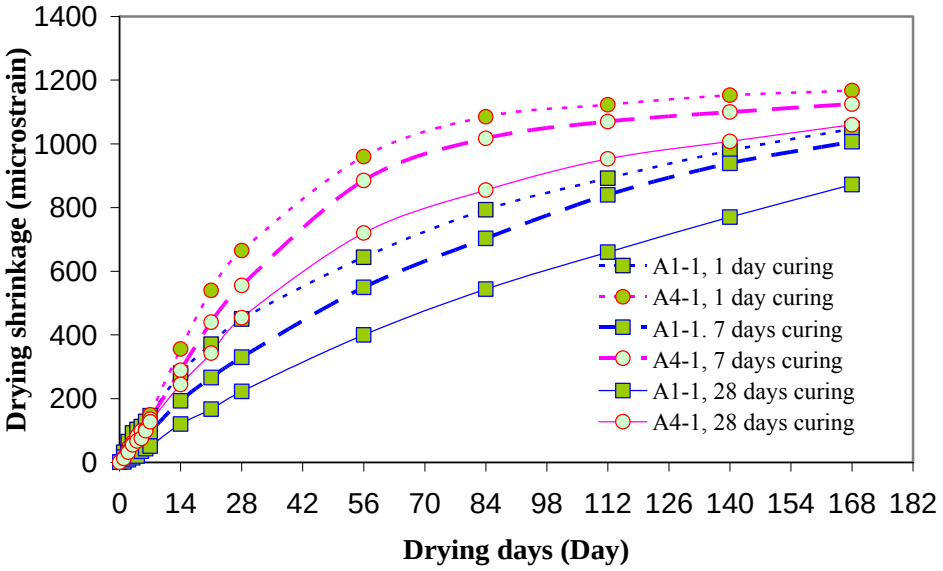

Figure 4-34. Effect of different air content on the drying shrinkage of pumice concrete

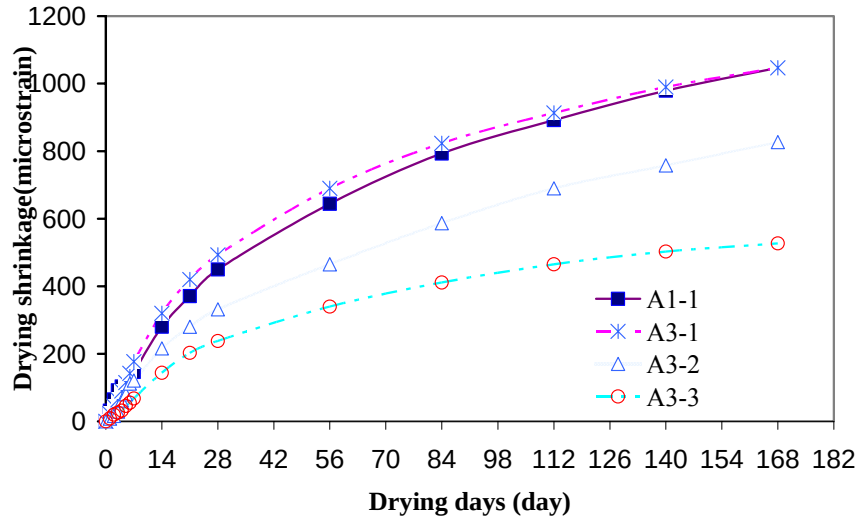

(a)

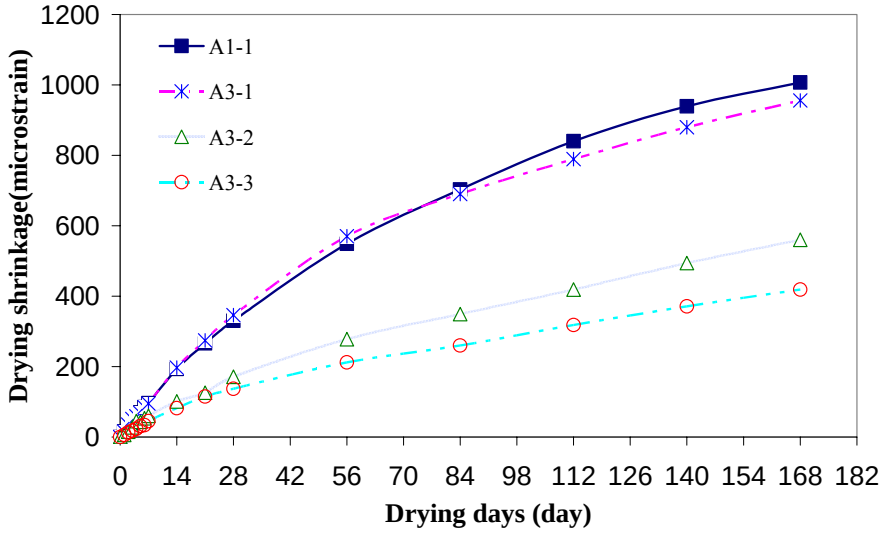

(b)

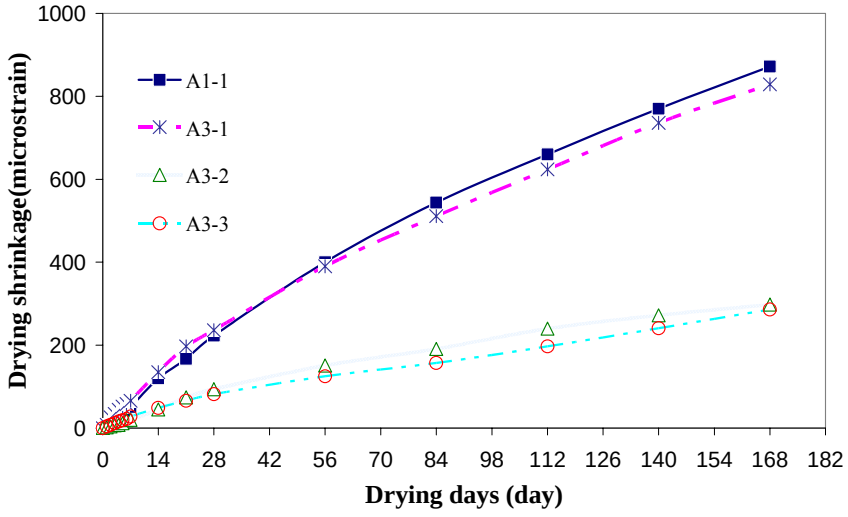

(c)

Figure 4-35. Effect of cement replacement by cementitious materials on the drying shrinkage of pumice concrete under duration of curing (a) 1-day (b) 7-day (c) 28-day

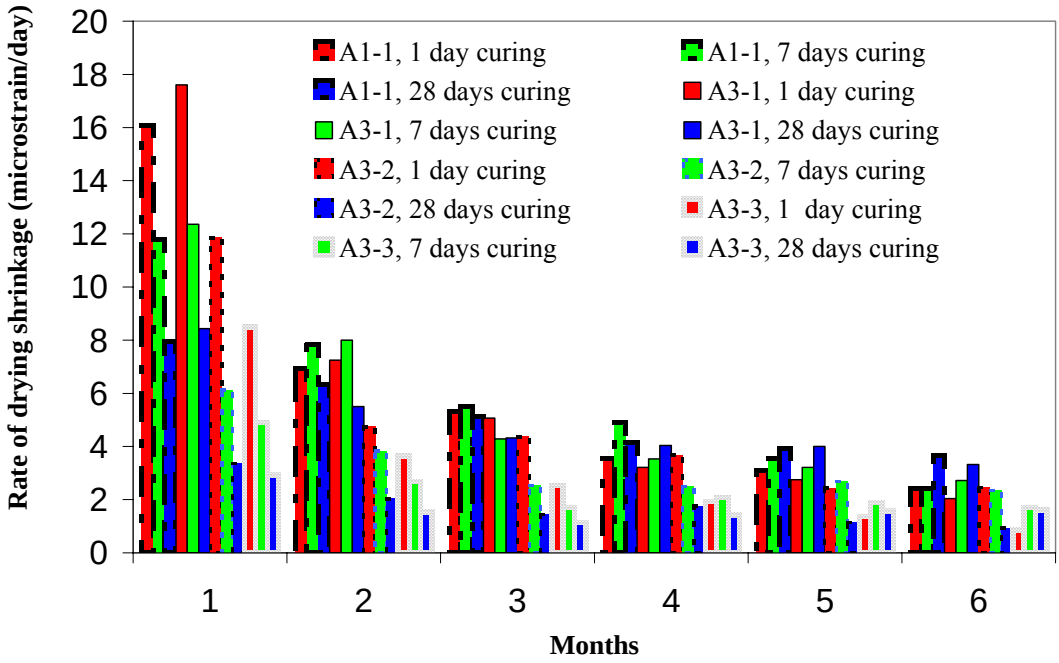

Figure 4.36. Comparison of rates of drying shrinkage of 1, 7 and 28 days moist cured pumice concrete with different cement replacement

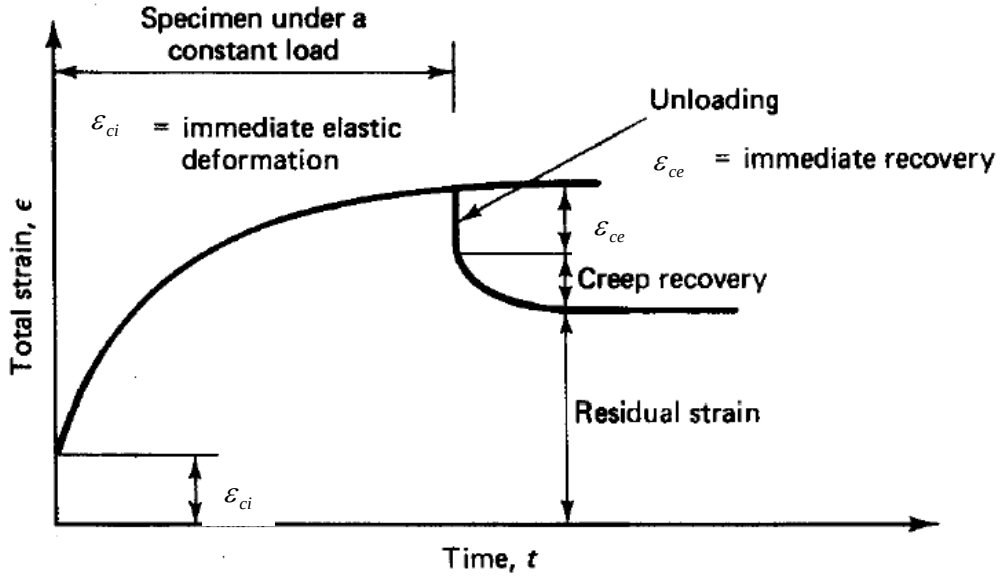

Figure 4.37. Time –dependent deformation in concrete subjected to a sustained

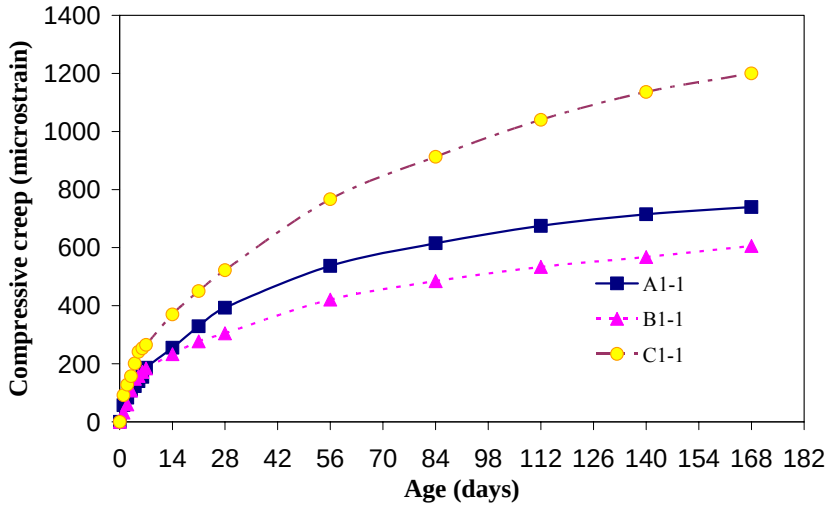

Figure 4.38. Effect of different cement content on the compressive creep of pumice concrete

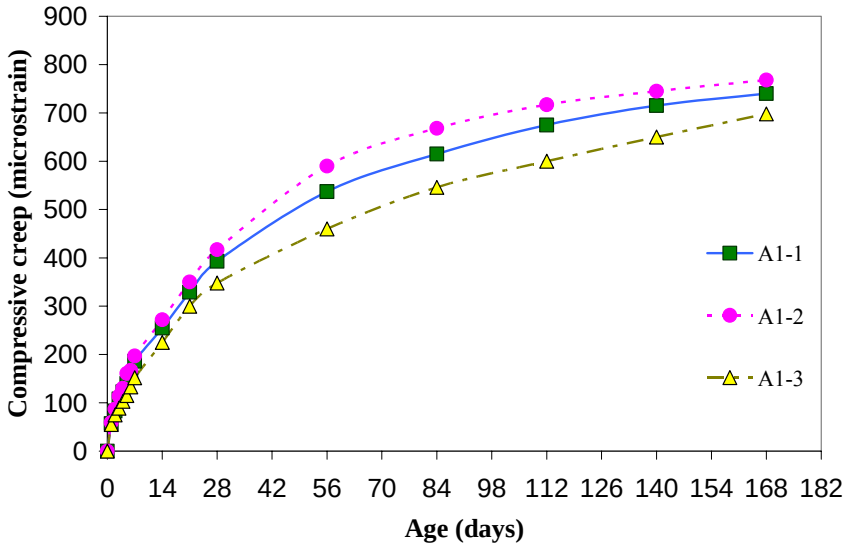

Figure 4.39. Effect of different pumice aggregate content on the compressive creep of pumice concrete

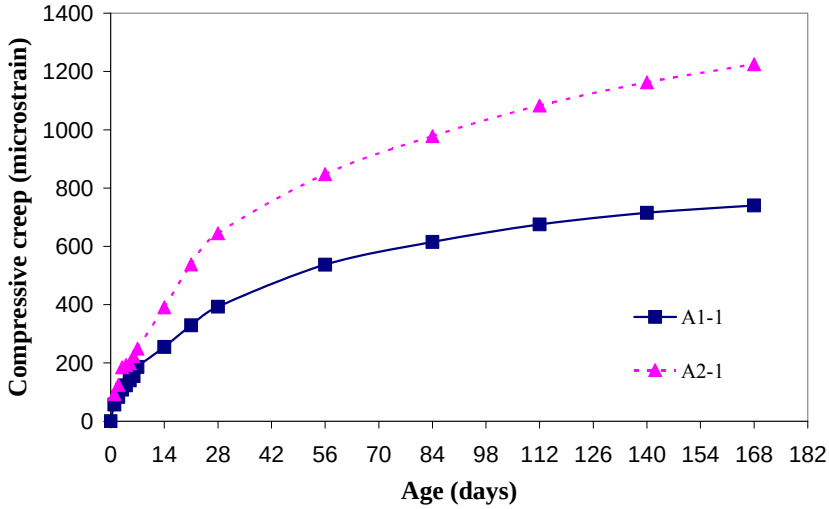

Figure 4.40. Effect of 50 % sand replacement by fine pumice aggregate on the compressive creep of pumice concrete

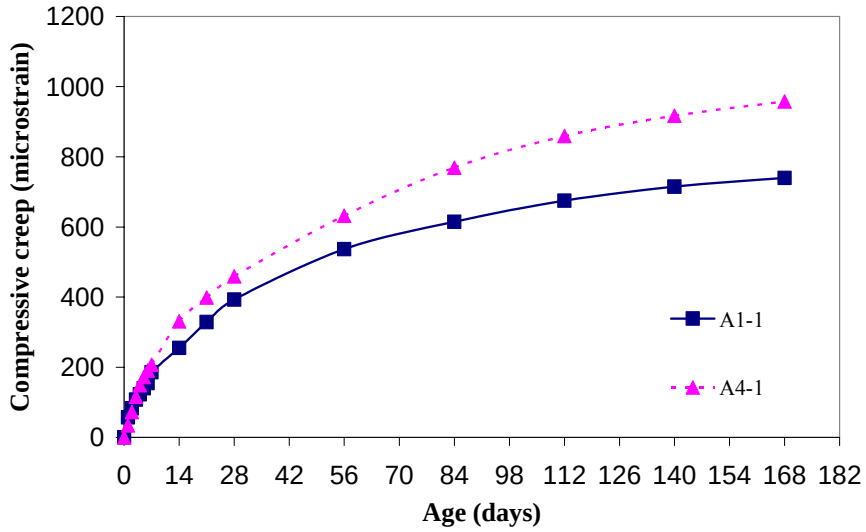

Figure 4.41. Effect of different air content on the compressive creep of pumice concrete

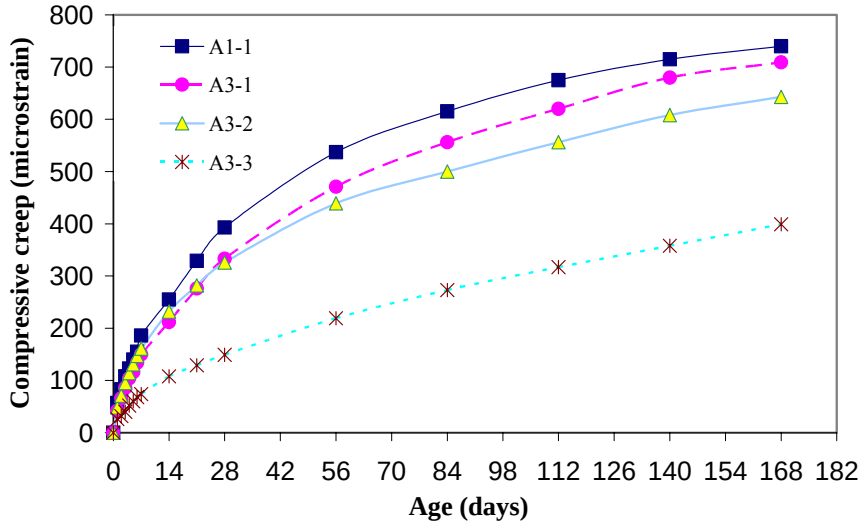

Figure 4.42. Effect of cement replacement by cementitious materials on the compressive creep of pumice concrete

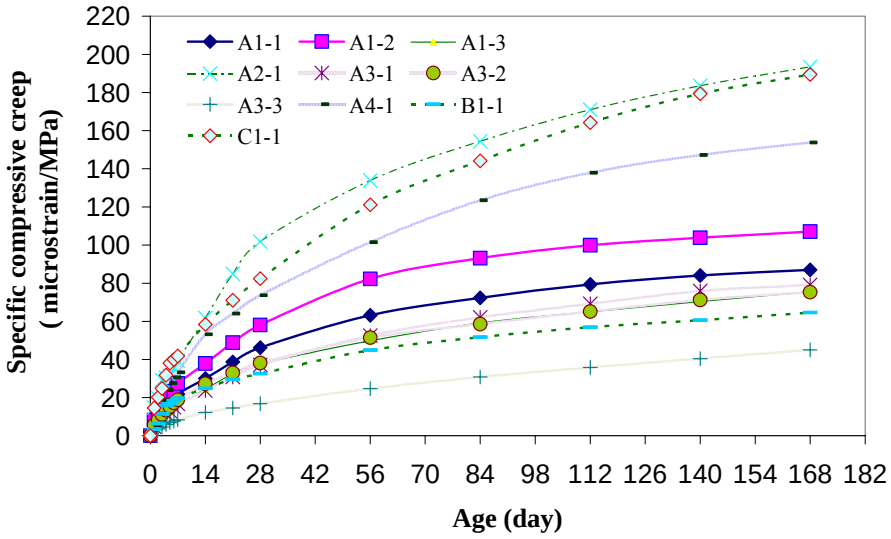

Figure 4.43. Specific creep of pumice concrete

CHAPTER FIVE

FLEXURAL BEHAVIOR OF REINFORCED PUMICE CONCRETE BEAM

5.1 General

Mechanical properties, shrinkage and creep of lightweight pumice aggregates concrete with compressive strengths up to 28 MPa have been investigated in previous chapters, proving the viability of its use in structural application. The present experimental study aims at investigating the full flexural response of pumice concrete beam with compressive strengths ranging from 20 to 25 MPa. Parameters considered include the amounts of longitudinal tensile and compressive steel reinforcements. The effect of these parameters on cracking, stiffness, serviceability, strength and ductility of the beam will be presented and discussed.

Realizing the fact that addressing the consequences of all possible structural actions is a massive task, this study has been narrowed down to the case of reinforced concrete (RC) members subjected to pure bending involving conventional steel bars. High strength pumice concrete under such loadings will be investigated using simply supported beams under a four-point loading system with the following objectives: to check the adequacy of available equations and procedures for predicting the cracking moment, maximum crack-width and deflection at service load, ultimate strength and ductility of high strength pumice concrete beams and suggest modifications wherever necessary to fulfil safety and serviceability requirements.

In the experimental investigations, prototype RC pumice beams of rectangular

cross-section and subject to four-point loading system will be employed. The major parameters considered are the amount of longitudinal tensile reinforcement and compression reinforcement.

5.2 Experimental Program

5.2.1 Test specimens

The experimental program consists of testing 1 doubly reinforced, 3 singly reinforced pumice concrete beam and 1 singly reinforced NWC beam simply supported under a four-point loading system. The nominal dimensions of all specimens are 180×360 mm in cross section and 2700 mm in length. The key parameters considered in the study are longitudinal tensile and compressive reinforcement ratios.

The details of the test program are presented in Table 5.1. All beams are provided with a tensile reinforcement ratio, ρ (area of tensile steel reinforcement/concrete cross sectional area) below the ACI Code 318 (1999) specified maximum value of $0.5\rho_b$, where ρ_b is the steel reinforcement ratio at a balance failure state. The cylinder compressive strength of concrete, f_c is varied from 20 to 28 MPa.

A clear concrete cover of 20 mm is provided on all sides. All longitudinal tensile and compression bars are arranged in one layer. The anchorage length is larger than 40D, where D is the diameter of the steel reinforcement in mm. The amount of lateral reinforcement can be varied by changing the spacing of full-depth rectangular shear links of 10 mm diameter high yield bars (T10).

Shear links are spaced at 100 mm c/c. Sufficient stirrups are provided outside the test zone to ensure a flexural failure mode instead of a shear failure mode.

For doubly reinforced beam, the minimum amount of shear links in the pure

flexural part of the beam is determined in accordance with the maximum spacing of lateral ties for flexural members as specified in Section 7.11.1 of ACI 318 (1999).

5.2.2 Materials and preparations of specimens

The concrete used for the beams has a constant fresh density of 1820 kg/m^3 and compressive strength of 25 MPa. The admixture used is superplasticizer (SP) Acro at a dosage of 40 liter/m^3. The mix design details are presented in Table 5.2.

Concrete mixing procedure: The fine and the coarse aggregates are initially mixed for 2 minutes with half the total amount of water, cement is then added together with the rest of water and mixed for a further 2 minutes. Half of the total amount of SP and air entraining agent (AEA) is then added, mixed for 1 min and then the remaining SP and AEA are added and mixing is continued for a further 1 minute. A cohesive composite concrete is thus obtained. The slump is kept at 75~100 mm with air content up to 2 %.

High strength deformed steel bars of three different sizes are used as longitudinal reinforcement. The yield strength is presented in the footnote at Table 5.1(a). Figure 5.1 (a) and 5.3 show the schematic diagram and the actual steel reinforcement detail used in the test, respectively.

The beams are cast in plywood molds using concrete prepared in the laboratory (see Figure 5.3 (b)). Flexible shaft vibrators are to be used to place and compact the concrete. Once the placing of the concrete is completed, the exposed surface is trowelled smooth. The control cylinder and prisms are cast in steel molds and compacted using a table vibrator. The beam and control specimens are demolded the following day and moist-cured for 14 days followed by air curing for another 14 days.

For the curing purposes, the beams and the control specimens are wrapped with wet hessian and polyethylene sheets to prevent moisture loss. After completion of curing, the beam and the associated cylinders and prisms are kept in air-dry condition (28 C, 100% RH) in the lab prior to testing.

5.2.3 Testing procedure

As seen in Figure 5.1 (b) and Figure 5.2, the beams are simply supported over a span of 2550 mm and tested under two symmetrically placed point loads. The nominal dimensions of the beams are: $180 \times 360 \times 270$ mm. The distance between the two loading points is maintained at 800 mm. The beams are suitably instrumented for measuring deflections at several locations including the mid-span. Curvature of the beam over a central gauge length of 450 mm, and concrete and steel reinforcement strain at critical locations were also measured. The type of electrical resistance strain gauge to measure the strains in steel reinforcement is FLA-10-11 and to measure the strains at the concrete surface, strain gauge type PL-60-11 is used, both from Tokyo Sokki Kenkyujo Co Ltd. Surface crack-widths at the centre-line of the bottommost layer of longitudinal tensile steel are measured over a distance of 480 mm length from the centre-line of the beam using a hand-held microscope with resolution of 0.02 mm.

The load is applied by a 200 kN servo-controlled hydraulic actuator. The beam is monotonically loaded at a displacement rate of 0.15 mm/min up to the ultimate load and after that the rate of loading is increased to 0.30 mm/min. All deformation and strain readings are monitored by a computer at preset load intervals until final failure.

5.3 Results And Discussions

The experimental results are summarized in Table 5.3. The curves showing experimental load vs. bottom tensile reinforcement strain and topmost layer of concrete under compression are presented in Figure 5.4 and 5.5, respectively. The experimental midspan load-deflection curves of all the beams are presented in Figure 5.6. The performance of these test beams has been compared with the ACI 318 (1999) code.

5.3.1 General behaviour of beam under flexural loading

Four distinctly different segments, as shown in Figure 5.7 can idealize a typical load deflection curve. These segments are clearly separated by four significant evens that took place during the process of flexural loading until beam failure. These events, labelled as A, B, C and D in Figure 5.7are identified as first cracking of concrete (A), first yielding of tensile reinforcement (B), first crushing with associated spalling of concrete cover in the compression zone (C) and failure of compression zone due to complete crushing of concrete resulting in disintegration of concrete at this zone (D). The first two events are associated with a reduction in the beam stiffness, while the remaining two events lead to a reduction in the applied load. In between events, a straight line may approximate the curve.

As seen from Figure 5.6, all beams behaved in a manner similar to the above described with the exception of the beam A3 with less ductility. It can be clearly seen that, for reinforced pumice concrete beams, the third and fourth event, C and D take place very close to each other. The first yield of bottom steel reinforcement is determined to be 0.0023 (i.e. E / f_y , where E =200 GPa and f_y =460 MPa). Ultimate

load carrying capacity of the beam is also checked by the measured compressive strain in the extreme compression fiber of the concrete. As shown in Table 5.3, the values of concrete ultimate compressive strain, ε_{cu} for pumice concrete recorded in these beams ranged from 0.0018 to 0.0030 as compared to 0.0030 for that of reinforced NWC beam.

As all test beams are under-reinforced, yielding of main tensile reinforcement occurred before initiation of the crushing of the cover concrete. However, the final failure occurred due to complete crushing of concrete in compression zone resulting in disintegration of concrete at this portion. Figure 5.8 presents photographs of the test beams at failure.

5.3.2 Cracking moment

The load at which first crack occurred in a beam, p_{cr} is determined by visual inspection using a magnifying glass, counterchecked by noting any change in gradient of the corresponding load-deflection curves. The experimental cracking moment, $M_{cr,\exp}$, which includes the effect of self-weight of the beam in addition to that of applied super-imposed load, is presented in Table 5.4

Analysis is made to estimate the cracking moments for the beams tested in this program. An accurate assessment of cracking moment is necessary mainly for two reasons. Firstly, cracking moments provide the basis for setting a minimum limit to longitudinal tensile reinforcement ratio to prevent failure by rupture of the steel at the onset of cracking. Secondly, it affects the analytical evaluation of service load deflections. In the analysis, a representative expression for modulus of rupture, is used to estimate the modulus of rupture for the whole range of concrete strength. The

equation is presented in Chapter 4 Section 4.2.3.4, Equation 4.14, f_r =0.55 $f_{cu}^{0.75}$, where f_r is the modulus of rupture of concrete and f_{cu} is the cube compressive strength.

The calculated cracking moment using Equation 5.1, are presented and compared with test results in Table 5.4. It may be seen that the ratio of experimental to calculated cracking moments, $M_{cr,\exp} / M_{cr,cal}$, has a mean value of 0.80 with a standard deviation of 0.346.

$$M_{cr,cal} = \frac{f_r I_g}{y_t} \tag{5.1}$$

where, $M_{cr,cal}$ is cracking moment in beam in N.m , f_r is the modulus of rupture of pumice concrete in N/mm^2 and f_r =0.55 $f_{cu}^{0.75}$ (Equation 4.14) for pumice concrete, I_g is the gross moment of inertia of concrete in m^4 and y_t is the distance of bottom extreme tension fibre from the neutral axis in m.

5.3.3 Flexural stiffness

It is shown from Figure 5.6 that uncracked stiffness of the beams remains essentially the same irrespective of the test parameters employed. This is because at this stage, structural action of reinforcing steel bars not yet been fully mobilized.

In reinforced concrete structures, post-cracking stiffness is of more significance. As such a structure exhibits cracking when put into service; post-cracking stiffness governs the associated deflections and affects its serviceability limit state. It may be observed in Figure 5.6 that the amount of longitudinal tensile reinforcement has

significant effect on post cracking stiffness of the beams by comparing the behaviour of beams A1, A2 and A3. Beams with higher ρ values for e.g. A3 demonstrate a higher post cracking stiffness due to the associates increase in cracked moment inertia for the same concrete strength, i.e. stiffness, k $\propto$ EI/L, where E is modulus of elasticity of concrete in N/mm^2, I is crack moment of inertia of concrete in mm^4, L is the beam span in mm.

5.3.4 Serviceability limit state

Cracking is inevitable in reinforced structures when they are put into full service. As large deflection and/or excessive cracking during service may cause unnecessary alarm or discomfort to users of the structures and facilities deterioration of concrete due to carbonation, chloride ingress and steel corrosion Limiting these values to some tolerable limits e.g. 0.3 mm is one of usual design requirements. Although indirect methods of limiting the span-effective depth ratio (l/d) and appropriate detailing of reinforcement is used, respectively, to ensure that the maximum deflection and service crack-widths are not excessive, numerical calculation is sometimes unavoidable. The intention here is to find whether values from typical design codes for e.g. ACI 318 could be predicted accurately for Pumice concrete. For this purpose, service load is assumed to be the experimental ultimate load $P_{u,\exp}$, divided by a factor 1.7

(a) Maximum deflection at serviceability limit state

The service loads and the corresponding maximum midspan deflection, $\delta_{s,\exp}$ obtained experimentally for the test beams are shown in Table 5.5.

Based on the elastic bending theory for deflection, the predicted values of

deflection are calculated and shown in Table 5.5. The equations for deflection calculation following ACI 318 (1999) are shown bellow.

$$\delta_{s,max} = \frac{M_a}{24E_c I_e}(3L^2 - 4a^2) \quad (5.2)$$

$$I_e = I_{cr} + (I_g - I_{cr})\left(\frac{M_{cr}}{M_a}\right)^3 \leq I_g \quad (5.3)$$

$$I_{cr} = \frac{b\bar{y}^3}{3} + nA_s(d - \bar{y})^2 \quad (5.4)$$

$$\frac{b\bar{y}^2}{2} + nA_s'\bar{y} - nA_s'd' - nA_s d + nA_s\bar{y} = 0 \quad (5.5)$$

where δ_s is the maximum deflection at the assumed service load in m, M_a is the middle span moment at serviceability limit state in N.m and $M_a = M_{ultimate}/1.7$; $M_{ultimate}$ is the calculated ultimate (mid-span) moment in kNm; M_{cr} is the cracking moment capacity of the beam obtained by using gross concrete section in Nm; E_c and E_s are the elasticity of modulus of concrete and steel reinforcement respectively in N/m^2 ; I_e is the effective moment of inertia of the beam section in m^4; I_g is the gross moment of inertia of beam section in m^4 (taking into account all the concrete section and ignoring the steel present); I_{cr} is the cracked moment of inertia of beam in m^4, ignoring the concrete section below the neutral axis and transforming the bottom steel area into equivalent concrete area; L is the beam span in m; a is the shear span in m; b is the width of the beam in m; $\bar{y}$ is the distance of the neutral axial to the extreme

compression face in the beam section in m; d is the effective depth of the beam in m; d' is the distance of the centroid of compressive reinforcement from the extreme compression face in a beam section in m; n is the modulus ratio and $n = \frac{E_S}{E_C}$.

For a given beam, the maximum deflection depends on the loading and support conditions and is inversely proportional to its flexural rigidity $E_c I$. An accurate estimation of maximum deflection under service load depends on correct assessment of E_c and I. It has been shown in Chapter 4 that the Norwegian Code NS 3473 (1998) expression for elastic modulus, E_c =9500f$_{cck}^{0.3}$ ($\frac{\rho}{2400}$) $^{1.5}$ MPa (where f_{cck} is the 28 day compressive strength of 100 mm (diameter) × 200 mm (height) cylinder specimen in MPa and ρ is the air dry density of concrete in kg/m^3) can give a fairly good prediction of the static modulus of elasticity of the pumice concrete used in this study.

With regard to the moment of inertia, the use of the value based on gross concrete section, I_g for calculation is generally acceptable as long as the beam remains uncracked. Cracking reduces the beam stiffness. However, the use of a moment of inertia, I_{cr} based on a fully cracked section may not be appropriate. This is because cracks occurs only at discrete locations and the intact concrete between two adjacent cracks will carry tensile stress which can contribute a significant portion of the concrete tensile strength due to the bond between the steel and concrete, providing a tensile stiffening effect. The effects of tensile stresses in the concrete is usually accounted for in design by an empirical adjustment of inertia, called effective moment of inertia, I_e. The value of I_e depends on the extent of cracking in the beam i.e. stage of loading considered relative to the first cracking stage. It usually lies between I_g and I_{cr}. The expression of I_e adopted in ACI code (ACI 318, 1999) is shown in

Equation 5.3.

Using the simplified effective moment of inertia, I_e in ACI 318 (1999), but employing a more representative expression for the modulus of rupture of concrete in Equation 5.2 to obtain M_{cr}, the maximum deflection at the assumed service load, $\delta_{s,\max}$ is calculated for each test beam.

The calculated values, as denoted by $\delta_{s,cal}$, are presented and compared with the corresponding experimental values, $\delta_{s,\exp}$ in Table 5.5. It may be seen that the method from ACI code gives safe predictions for service load deflections with a mean and standard deviation of ratio of experimental to calculated deflection, $\frac{\delta_{s,\exp}}{\delta_{s,cal}}$ as 1.27 and 0.0032, respectively.

The ACI code shows the maximum permissible middle span deflection for a beam in practice. For conservative estimates, the maximum permissible deflection is $l/240$, where l is the effective beam span in m, For this study, the maximum permissible deflection is 5.3 mm (for beam supporting non structural elements likely to be damaged by large deflection) and 10.6 mm (for beam supporting nonstructural elements not likely to be damaged by large deflection). The test beams satisfy the allowable deflection limit of 10.6 mm.

(b) Maximum crack width and spacing

For each test beam, the central 800 mm length is selected as the test zone to study its cracking behaviour. Since spacing of cracks is often required for the assessment of crack-width, it may be relevant to have a brief discussions on the number and spacing of cracks observed in the present tests before discussion on the maximum crack width.

The numbers of cracks, their maximum, minimum and average spacing (at the

central portion of the bottommost layer of longitudinal reinforcement) observed in each beam at the assumed service load are presented in Table 5.6. At this load, both primary and secondary cracks are observed, the total number of which ranged from seven to eleven. It is interesting to note that all beams, other than B1 and N1, exhibit exactly the same number of eight cracks for which the average spacing varied from 104 to 115 mm. Beam B1 has a higher amount of compressive steel and demonstrates a total of eleven cracks with average spacing of 90 mm. Compared to NWC beam N1, pumice concrete beam A2 shows more cracks with smaller crack spacings.

As ACI 318 (1999) does not include any requirement on the prediction of crack spacing for crack control, experimental values of average crack spacing ($s_{av,\exp}$) are compared with the predictions of EC2 (1991) as denoted as $s_{av,EC2}$ .The expression for $s_{av,EC2}$ is shown in Equation 5.6 and 5.7.

$$s_{av,EC2} = 50+k_1k_2\frac{d_b}{4\rho_r} \tag{5.6}$$

$$\rho_r = \frac{A_s}{A_{cef}} \tag{5.7}$$

where d_b is the bar diameter in mm; k_1 is a coefficient depending upon bond quality (0.8 for high bond bars); k_2 is a coefficient which depends upon the shape of strain diagram (0.5 for bending without axial force); A_s is the area of longitudinal tensile reinforcement in mm^2 ; A_{cef} is the effective tension area having the full width of the beam and having the depth equal to the lesser of 2.5(h-d) and $\frac{h-c}{3}$; h is the total

depth of the beam; c is the cover of rebar.

It is seen in Table 5.6, that calculated values $s_{av,EC2}$, are, on average, 10 % lower than the experimental values for pumice concrete beams. The mean and SD of ratio ($s_{av,\exp} / s_{av,EC2}$) for pumice concrete have been found to be 0.89 and 0.119.

In structural concrete members, restrictions are placed on the maximum crack width at service load for purpose of durability and aesthetic aspects of the structure. Therefore, control of cracking or prediction of maximum crack width, $\omega_{cr,\max}$, represents one vital design considerations. The allowable maximum crack is 0.3 mm. In this study, surface crack-widths are measured at the centre of the bottommost layer of the main tensile reinforcement. The effect of tensile reinforcement ratio, ρ , on the maximum crack width at this load level may be seen to be insignificant although a trend of decreasing experimental crack width, $\omega_{cr,\exp}$ is observed with an increase in ρ values. The beams tested have a crack width less than 0.3 mm at service load. This shows that reinforced pumice beam satisfies the serviceability limit state of cracking.

5.3.5 Ultimate strength

It has been described previously that crushing of the concrete in the extreme compression fiber zone with associated spalling of concrete cover usually marked the attainment of ultimate strength. The experimental values of ultimate strength, expressed as moment, $M_{u,\exp}$ are listed in Table 5.7.

The effect of various parameters considered in this study on the ultimate strength of the beam may be investigated qualitatively from the load-deflection curves presented in Figure 5.6. It may be seen by comparing behaviour of beams A1, A2 and

A3 in Figure 5.6 that an increase in the amount of tensile reinforcement increased the ultimate strength. Although a higher amount of tensile steel requires more concrete area in the compression zone, the effect of the resulting reduction in lever arm is fully offset by an increase in tensile stress resultants, thus demonstrating a net gain in strength. As with flexural stiffness, the ultimate strength is hardly affected by the addition of compressive reinforcement comparing the behaviour of beams B1 and A2. With the same tensile reinforcement as Beam N1 of normal weight concrete, the pumice concrete beam A2 shows a similar ultimate strength but with a decease in ductility.

It may be of interest to check whether the provisions contained in structural concrete code ACI 318 (1999) may be used to predict the ultimate strength of pumice concrete beams tested in this program. The ultimate moment, $M_{u,ACI}$ calculated using Whitney's rectangular stress block and ε_{cu} of 0.003 for NWC and pumice concrete, as contained in ACI 318 (1999) are presented and compared with the test results in Table 5.7. The ACI recommendation of 0.003 for the maximum concrete strain appears to be an acceptable lower bound for LWAC with compressive strength not exceeding by 75.9 MPa (Ahmad and Barker, 1991). The equation used to calculate $M_{u,ACI}$ is as shown as follows:

$$M_{u,ACI} = f_c^{'} bd^2\omega(1-0.59\omega) \quad \text{for singly reinforced beam} \tag{5.8}$$

$$M_n = C_c(d-\frac{a}{2}) + C_s(d-d^{'}) \quad \text{for doubly reinforced beam (from equilibrium of moment about the centroid of tensile steel reinforcement)} \tag{5.9}$$

$0.85 f_c^{'} ba + E_s A_s^{'}(1 - \frac{\beta_1 d^{'}}{a})0.003 = A_s f_y$ (from equilibrium of horizontal forces across concrete section) (5.10)

where $\omega = \rho f_y / f_c^{'}$ and is referred to as the mechanical reinforcement ratio; ρ is the tensile reinforcement ratio; b is the beam width in m; d is the effective depth of the beam in m; C_c is the compressive force in the concrete in N and C_c=0.85 $f_c^{'} ba$; C_s is the compressive force in the compressive reinforcement in N and C_s=$(E_s \varepsilon_s^{'}) A_s^{'}$; E_s is the modulus of elasticity of steel in GPa; $\varepsilon_s^{'}$ is the strain in the steel in N in the compression zone; a is the depth of the stress block and is calculated from Equation 5.5; β_1 is the ratio of depth of rectangular stress block, a to depth to neutral axis, c and $\beta_1 = 0.85$; A_s is the area of tensile steel reinforcement in m^2; $A_s^{'}$ is the area of compressive steel reinforcement in m^2.

It may be seen ACI 318 (1999) provisions give a reasonable and conservative estimate of the ultimate moment capacity of the test beams. For the 5 beam tested, the ratio of experimental to calculated value ranges from 1.14 to 1.27, with an average of 1.20 and standard deviation of 0.055 for pumice concrete beam whereas the corresponding value is 1.14 for the single NWC beam. As the prediction is on the safe side and the difference is not so large (conservative difference averaging 20 %) for pumice concrete, no revision of the Whitney‘s stress block parameters and associated failure criterion is needed for the beams tested.

5.3.6 Ductility

In structural design, ductility may be defined as the ability of a material, a particular section of a member, the member itself or the structure as a whole to deform at or near the ultimate load without a significant loss in strength and this represents another important design objective. In the case of a flexural member, the ductility is usually determined based on deflection parameter. The following discussion on the influence of various test parameters is therefore based on displacement ductility index, μ_d and it is defined as the ratio of maximum (central) deflection at ultimate, δ_u, to that at significant yield of the main tensile reinforcement, δ_y (Kong, 2003). That is,

$$\mu_d = \frac{\delta_u}{\delta_y} \tag{5.12}$$

Figure 5.9 shows a schematic diagram for determining the characteristic yield load and ductility. Figures 5.10 and 5.11 show the effect of tensile steel reinforcement on the displacement ductility.

Limiting the tensile reinforcement ratio ρ is one of the most commonly used means of guaranteeing adequate ductility. According to ACI 318 (1999), in flexural members, ρ should be limited to 0.75 ρ_b for common situation and to 0.5 ρ_b for structures in which redistribution of moments is considered; in case of doubly reinforced section, the above limitations should be applied to ($\rho - \rho'$) where ρ' is the compressive steel reinforcement ratio. ρ_b is the balance steel reinforcement ratio for a singly reinforced section and based on the ACI code, it may be obtained as:

$$\rho_b = \frac{0.85\beta_1 f_c^{'}}{f_y}\left(\frac{0.003}{0.003+\varepsilon_y}\right) \tag{5.12}$$

where β_1 is the ratio of depth of rectangular stress block, a to depth to neutral axis, c; $\beta_1 = 0.85$; ε_y is the yield strain of tensile steel reinforcement.

A displacement ductility index μ_d in the range of 3 to 5 is considered imperative for adequate ductility, especially in the area of seismic design and the redistribution of moment (Park, Robert, and Pauley, Thomas 1984). Assuming a μ_d of 3 represents an acceptable lower bound to ensure adequate ductility of flexural member (Ahmad and Barker, 1991). Assuming E_s = 200 GPa and f_y = 460 MPa, the requirement of $\rho \leq 0.5\ \rho_{bs}$ translates into a minimum deflection ductility index, μ_d of 3 for singly reinforced concrete beam (Section 8.4.3, ACI 318, 1999). The same number is also frequently referred to as the minimum requirement for displacement ductility index, μ_d, for the study of reinforced pumice concrete beam. It can be analytically shown that the displacement ductility index, μ_d decreases with an increase in tensile steel content, ρ (see Figure 5.9). It is shown that the minimum target value (μ_d = 3) can be achieved at a value of about 0.21 for ρ/ρ_b (see Figure 5.10). Further more, compared to NWC beam N1, pumice reinforced concrete beam A2 presents a relatively lower μ_d value, 42 % lower than that of Beam N1. This is expected since pumice concrete material is less ductile as compared with normal weight concrete of the same strength.

The longitudinal bars placed in the compression side of a flexural RC member, due to its higher strength and elastic modulus as compared to surrounding concrete,

help to reduce the depth of neutral axis, thus improving the ability of the beam to deform more before final collapse. Figure 5.9 showed that the ductility index, μ_d of beam B1 increased up to 4.15, as compared to 1.71 for beam A2.

5.3.7 Complete load-deflection response

In this study, an attempt has been made to predict the short-term complete load-deflection response of the beams tested ignoring creep and shrinkage. It is based on the second moment-area theorem in which the distribution of curvature along the length of the beam at a particular stage of loading has been determined using the general principles of mechanics with some idealization of actual $M-\phi$ relationship as proposed by Rashid (2002).

For a given section, the moment and the corresponding curvature at each critical event can be obtained from usual flexural theory based on equilibrium and Bernoulli's compatibility. The concrete stress resultant and its location are determined using the trapezoidal rule and the longitudinal compression reinforcement is assumed to remain buckled for the whole range of the loading history.

When the applied load is gradually increased, the moment diagram passes through 4 regimes, depending on the loading stage. These regimes are shown in Figures 5.13 (a) - (c). In the first regime, the maximum moment, $M1$ is less than M_{cr}, and the beam remains uncracked . In regime 2, cracks appears in the beam and the maximum moment, M_2 within the constant moment region lies between M_{cr} and M_y. In the third regime the tensile reinforcing steel yields and the maximum moment, M_3 is in the range between M_y and M_u.

In view of the idealized tetra-linear moment-curvature behavior (Figure 5.12), the

four moment regimes result in the corresponding curvature diagrams shown in the accompanying moment diagrams in Figure 5.13 (a) - (c). The mid-span deflection can then be determined by taking moment, about one of the supports, of the area under each curvature diagram between the support and the mid-span section.

Regime 1

For a simply supported beam with two symmetrically applied point loading, as used in this study, the mid-span deflection, δ_1 is simply given by

$$\delta_1 = \frac{L^2}{24}\phi_1(3-4\alpha^2) \tag{5.13}$$

where $\alpha = a/L$, in which a and L are the shear span and total span, respectively, of the beam. The corresponding load is

$$P_1 = \frac{2M_1}{a} \tag{5.14}$$

Regime 1 ends when ϕ_1 equals ϕ_{cr} and moment M_1 equals M_{cr}

Regime 2

In this regime (Fig 5.13 (b)), the deflection at mid-span, δ_2, can be expressed as

$$\delta_2 = \frac{\alpha^2 L^2}{6}\left[\phi_{cr}(1+\gamma_1) + \phi_2\left(\frac{3}{4\alpha^2} - 1 - \gamma_1 - \gamma_1{}^2\right)\right] \tag{5.15}$$

where ϕ_2 lies in the range $\phi_{cr} \le \phi_2 \le \phi_y$. γ_1 is the ratio M_{cr}/M_2. The load, P_2 at this

stage is still given by Equation 5.16, except that M_1 is replaced by M_2 and P_1 by P_2.

Regime 3

$$\delta_3 = \frac{\alpha^2 L^2}{6}\left[\phi_{cr}\gamma_2(\gamma_1+\gamma_2)+\varphi_y(1-\gamma_1)(1+\gamma_1+\gamma_2)+\phi_3(\frac{3}{4\alpha^2}-1-\gamma_2-\gamma_2{}^2)\right] \qquad (5.16)$$

where $\gamma_1 = M_{cr}/M_3$, $\gamma_2 = M_y/M_3$ and ϕ_3 lies in the range $\phi_y \le \phi_3 \le \phi_u$. The corresponding load is calculated form Equation 5.16 with P_3 and M_3 in place of P_1 and M_1 respectively.

The load –deflection relations thus obtained are compared with the experimental curves up to the ultimate load for all of the test beams in Figure 5.14 (a) to (e), Although a stiffer post cracking gradient is obtained in most of the cases, ultimate strength and the general shape of the load-deflection curves obtained, depicting the deformation capacity of the beams with critical evens in the loading history, are in good agreement with the corresponding experimental values.

5.4 Conclusions

The following are conclusions reported from the experimental program of simply reinforced concrete pumice beam under flexural loading.

1, The ACI code 318 (1999) underestimates the experimental cracking moment up to 12 % on average for reinforced pumice concrete beam, whereas for NWC beam, it underestimates the cracking moment up to 19%. ACI code is more conservative.

2. The ACI 318 (1999) code underestimated the experimental deflections of reinforced concrete pumice beam under short term service loads up to about 27 %. For reinforced NWC beam, the underestimation is by up to 23 %.

3. Crack widths at service loads varied from 0.16 to 0.26 mm and these are within 0.3 mm, the maximum allowable crack width for durability requirements. The crack spacing is closer when compared to the reinforced NWC beam with crack width of 1.29 mm.

4. ACI 318 (1999) code gives a conservative prediction of the ultimate flexural strength of the beams, 20 % on average lower than the experimental results.

5. Unlike reinforced NWC beam, reinforced pumice concrete beam exhibit insufficient displacement ductility (less than 3) when reinforced with ρ / ρ_b > 0.31. With pumice concrete strength of about 25 MPa, singly reinforced beam with ρ / ρ_b of 0.21 and doubly reinforced beam with $(\rho - \rho^{'})/\rho_b$ of 0.10 showed adequate ductility of 3.67 and 4.15, respectively.

6. The complete load-deflection response up to the ultimate of the reinforced pumice concrete beams can be fairly predicted based on the second moment –area theorem from usual flexural theory based on equilibrium and Bernoulli's compatibility.

Table 5.1 Details of beam tested

Beam	Beam width b (mm)	Beam height h (mm)	Effec-tive depth d (mm)	Age of concrete at testing (days)	Cylinder compre-ssive strength $f_c^{'}$ (MPa)	Elastic modulus of concrete E_c (GPa)	Tensile steel rebar	Compre-ssive steel rebar	Steel rebar ratio ρ (%)	Steel Rebar at ratio at balance state ρ_b (%)	$\frac{\rho}{\rho_b}$ or $\frac{\rho-\rho^{'}}{\rho_b}$
N1	180	360	322	28	25	23.6	2No.T16 401.9 mm^2	----	0.69	2.22	0.31
A1	180	360	324	38	25	18.6	2No.T13 265.3 mm^2	----	0.39	2.22	0.21
A2	180	360	322	39	25	18.6	2No.T16 401.9 mm^2	----	0.69	2.22	0.31
A3	180	360	320	42	25	18.6	2No.T20 628 mm^2	2No.T13 265.3 mm^2	1.09	2.22	0.49
B1	180	360	322	43	25	18.6	2No.T16 401.9 mm^2	----	0.69	2.22	0.10

Note: Yield strength of T20, T16 and T13 bars are 537 MPa, 466 MPa and 472 MPa, respectively.

(1) $\rho = A_s / bh \times 100\%$, A_s is the area of longitudinal tensile reinforcement.

$\rho^{'} = A_s^{'} / bh \times 100\%$, $A_s^{'}$ is the area of compressive tensile steel reinforcement.

(2) The steel reinforcement ratio must be $\leq 0.5\rho_b$ (according to ACI 318, 1999).

For singly reinforcement section, $\rho \leq 0.5\rho_b$; for doubly reinforced section, $\rho - \rho^{'} \leq 0.5\rho_b$

Table 5.2 Concrete mix design of concrete

Mix proportion of pumice concrete for beams A1, A2, A3 and B1

Fresh Density (kg/m^3)	Water Cement ratio	Cementitious material (kg/m^3)		Water (kg/m^3)	Sand (kg/m^3)	Pumice aggregates at SSD (kg/m^3)			Super plasticizer (litre/m^3)	Slump (mm)
		Cement	GGBS			5mm	10mm	20mm		
1766	0.33	225	225	150	763	123	144	186	1.3	150~200

Mix proportion of normal weight concrete for beam N1

Fresh Density (kg/m^3)	Water Cement ratio	Cementitious materials(kg/m^3)		Water (kg/m^3)	Sand (kg/m^3)	Gravel aggregate	Slump (mm)
		Cement	GGBS				
2310	0.62	336	------	208	1008	769	75~100

Note: GGBS means ground granulated blast-furnace slag; SSD means saturated surface dry.

Table 5.3 Summary of experimental results

Beam	N1	A1	A2	A3	B1
Measured $f_c^{'}$ (MPa) (cylinder compressive strength)	27.5	24.4	23.8	25.1	24.2
First cracking load, P_{cr} (kN)	32	24	29	42	40
Deflection at first crack, δ_s (mm)	1.1	0.8	1.2	1.67	1.9
First yielding load, P_y (kN)	129	98	127	211	130
Deflection at first yield load, δ_y (mm)	9.2	9.1	9.0	13.1	9.2
Ultimate load, P_u (kN)	147	106	145	220	148
Ultimate deflection, δ_u (mm)	26.2	30.1	15.5	15.0	26.7
Failure load , P_f (kN)	137	99	130	220	148
Deflection at failure, δ_f (mm)	42	32.4	21.2	14.8	42
Ultimate concrete compressive strain capacity, ε_{cu} (microstrain) at P_u	3486	3036	2460	1800	2931
Age of concrete (day) at testing	28	38	39	40	41

Table 5.4 Cracking moment capacity of test beams

Beam	Experimental cracking moment, $M_{cr,\exp}$ (kN.m)	Calculated cracking moment, $M_{cr,cal}$ (kN.m)	Ratio $\frac{M_{cr,\exp}}{M_{cr,cal}}$
N1	14.0	13.1	1.07
A1	11.6	19.6	0.56
A2	13.8	19.6	0.70
A3	19.5	20.4	0.96
B1	18.7	19.6	0.95

Table 5.5 Service load deflections of the test beams

Beam	Experimental deflection $\delta_{s,\exp}$ (mm)	Calculated deflection $\delta_{s,cal}$ (mm)	Ratio, $\frac{\delta_{s,\exp}}{\delta_{s,cal}}$
N1	3.8	3.1	1.23
A1	4.9	3.8	1.29
A2	5.6	4.5	1.14
A3	6.1	4.9	1.24
B1	5.6	4.3	1.30

Table 5.6 Cracks width and crack spacing within the central 800 mm region of test beams

Beam	N1	A1	A2	A3	B1
Experimental crack width $\omega_{cr,\exp}$ (mm)	0.28	0.26	0.22	0.26	0.16
Numbers of primary cracks from experiment	7	5	4	7	6
Numbers of secondary cracks from experiment	0	3	4	1	5
Maximum crack spacing (mm) from experiment	190	165	170	150	150
Minimum crack spacing (mm) from experiment	119	50	65	70	60
Experimental average crack spacing (mm), $s_{av,\exp}$	153	115	104	105	90
Calculated crack spacing (mm), $s_{av,EC2}$	118	130	118	101	118
Ratio, $\frac{s_{av,\exp}}{s_{av,EC2}}$	1.29	0.88	0.88	1.04	0.76

Table 5.7 Ultimate moment capacity of test beams

Beam	Experimental ultimate moment $M_{u,\exp}$ (kN.m)	Calculated ultimate moment $M_{u,ACI}$ (kN.m)	Ratio $\frac{M_{u,\exp}}{M_{u,ACI}}$
N1	64.3	56.2	1.14
A1	46.4	37.5	1.24
A2	63.4	54.8	1.18
A3	96.3	81.6	1.19
B1	64.7	57.6	1.14

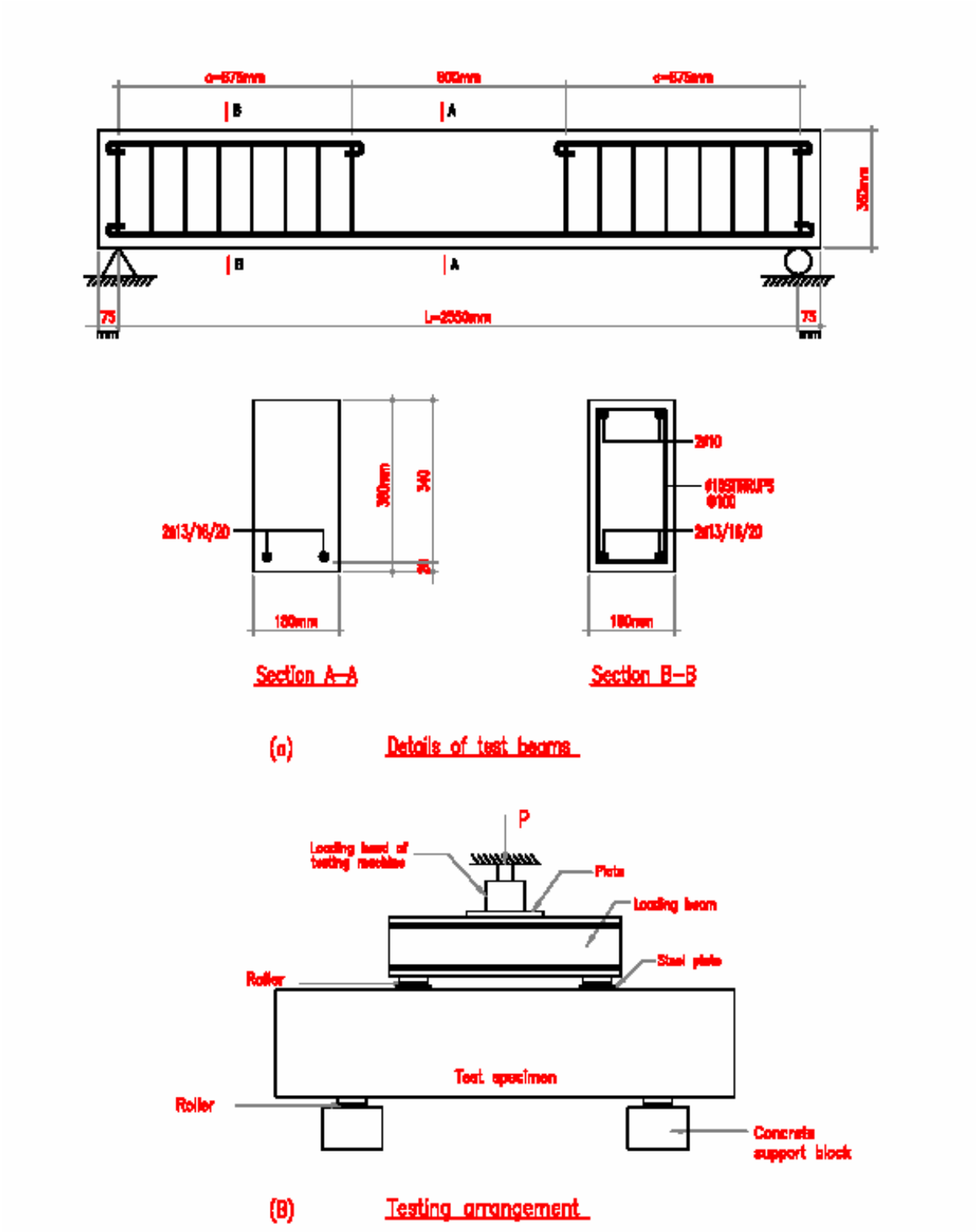

Figure 5.1. Details of test beam and reinforcement

Figure 5.2. Setup of the beam test

Figure 5.3. Steel cage and concreting of reinforced pumice concrete beam

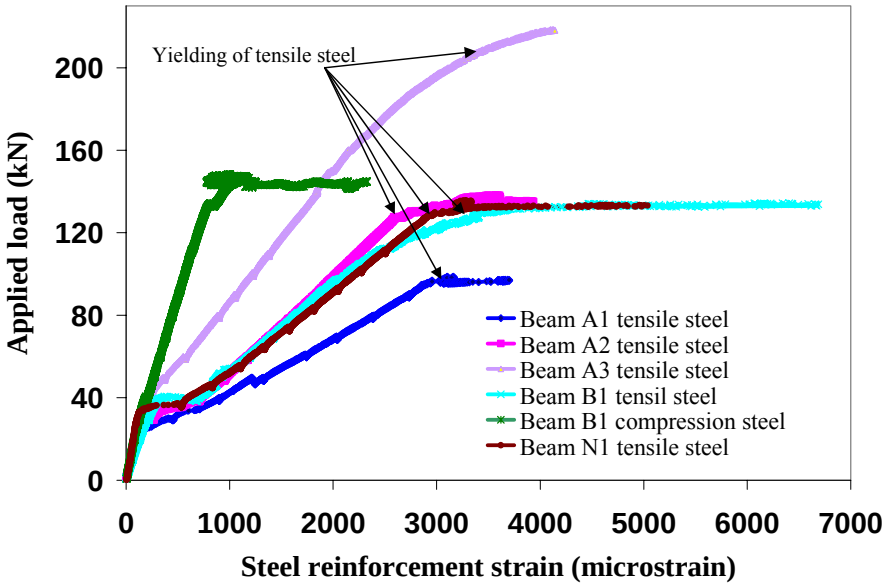

Figure 5.4. The curves of applied load - steel reinforcement strain

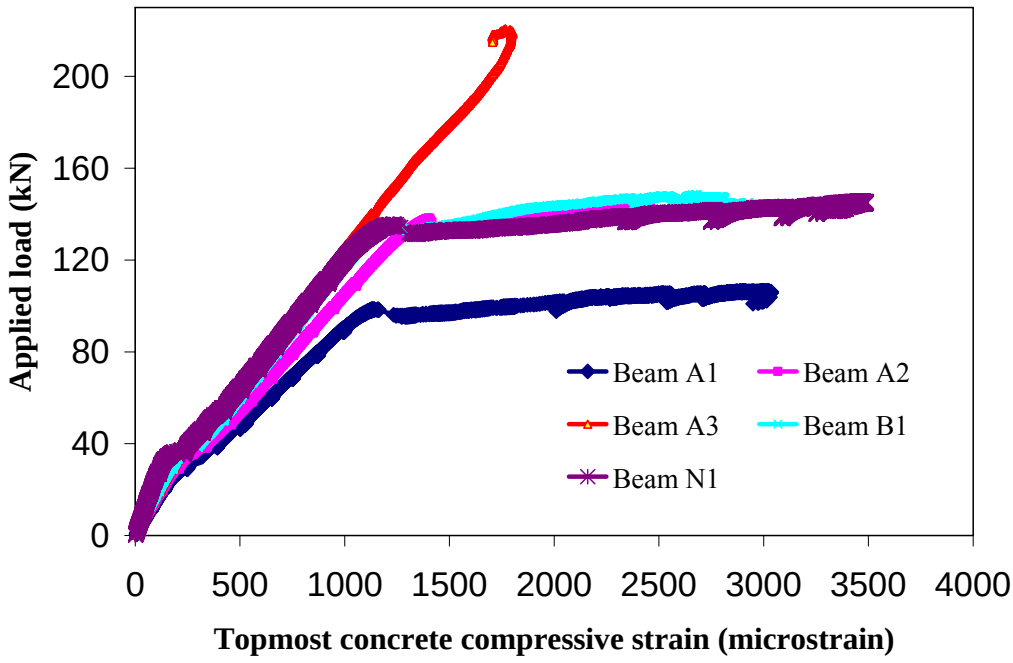

Figure 5.5. The curves of applied load vs topmost concrete compressive stain

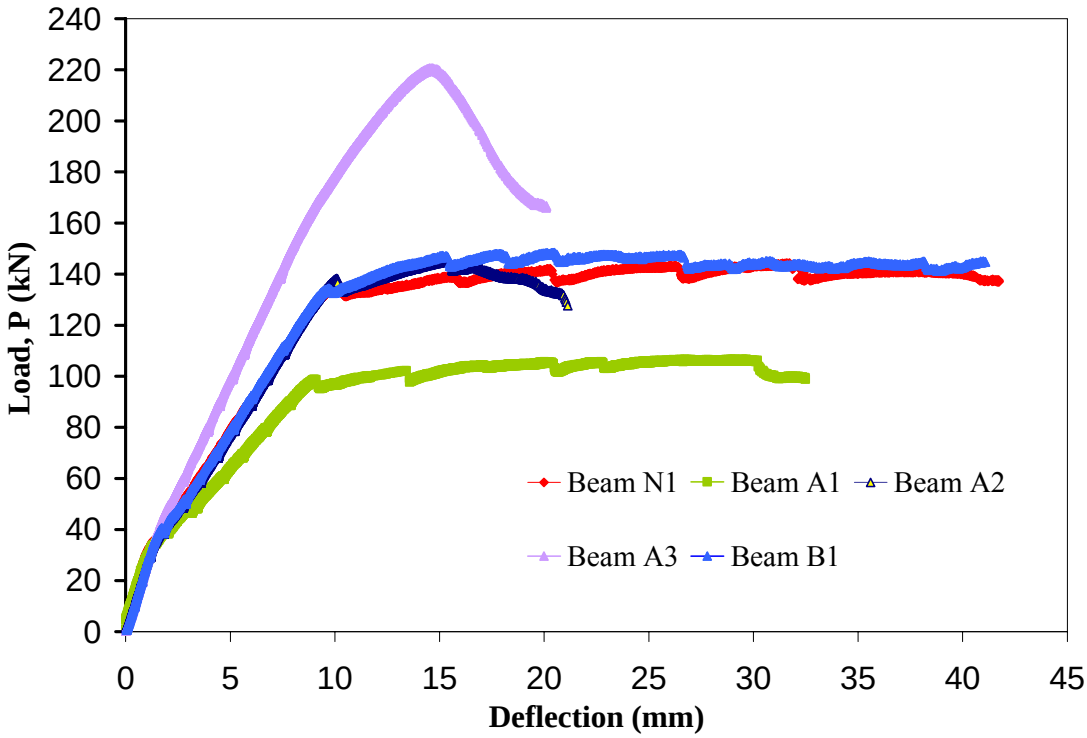

Figure 5.6. Midspan load-deflection curves of reinforced pumice and NWC beams

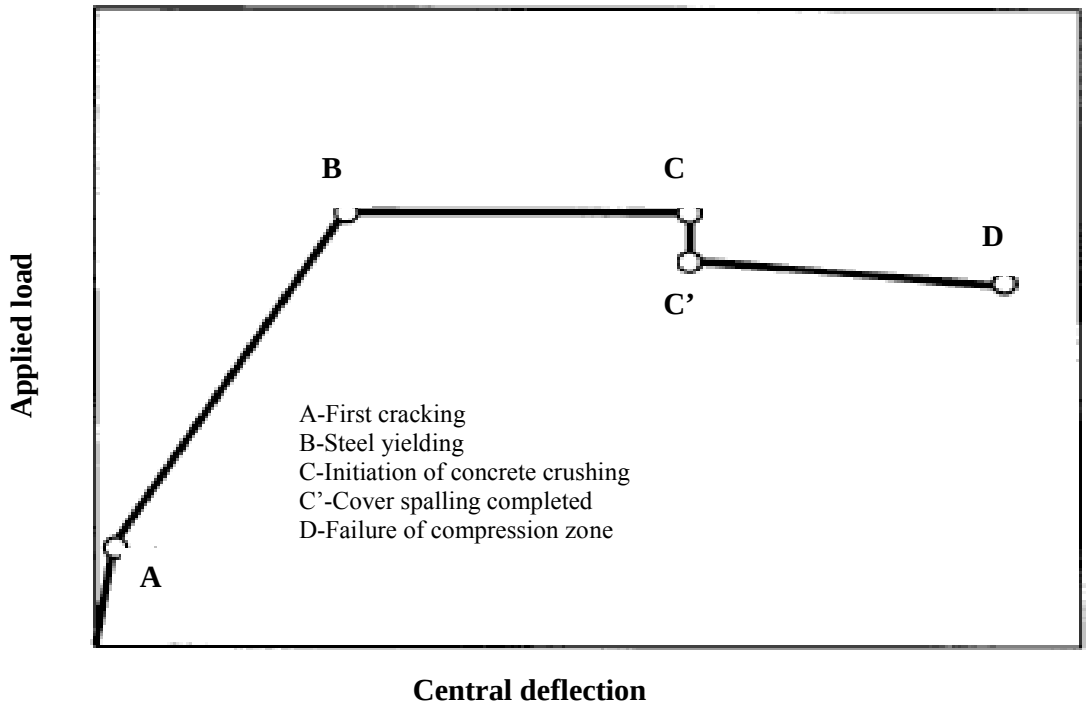

Figure 5.7. Idealized curve of load-deflection behaviour of RC beams

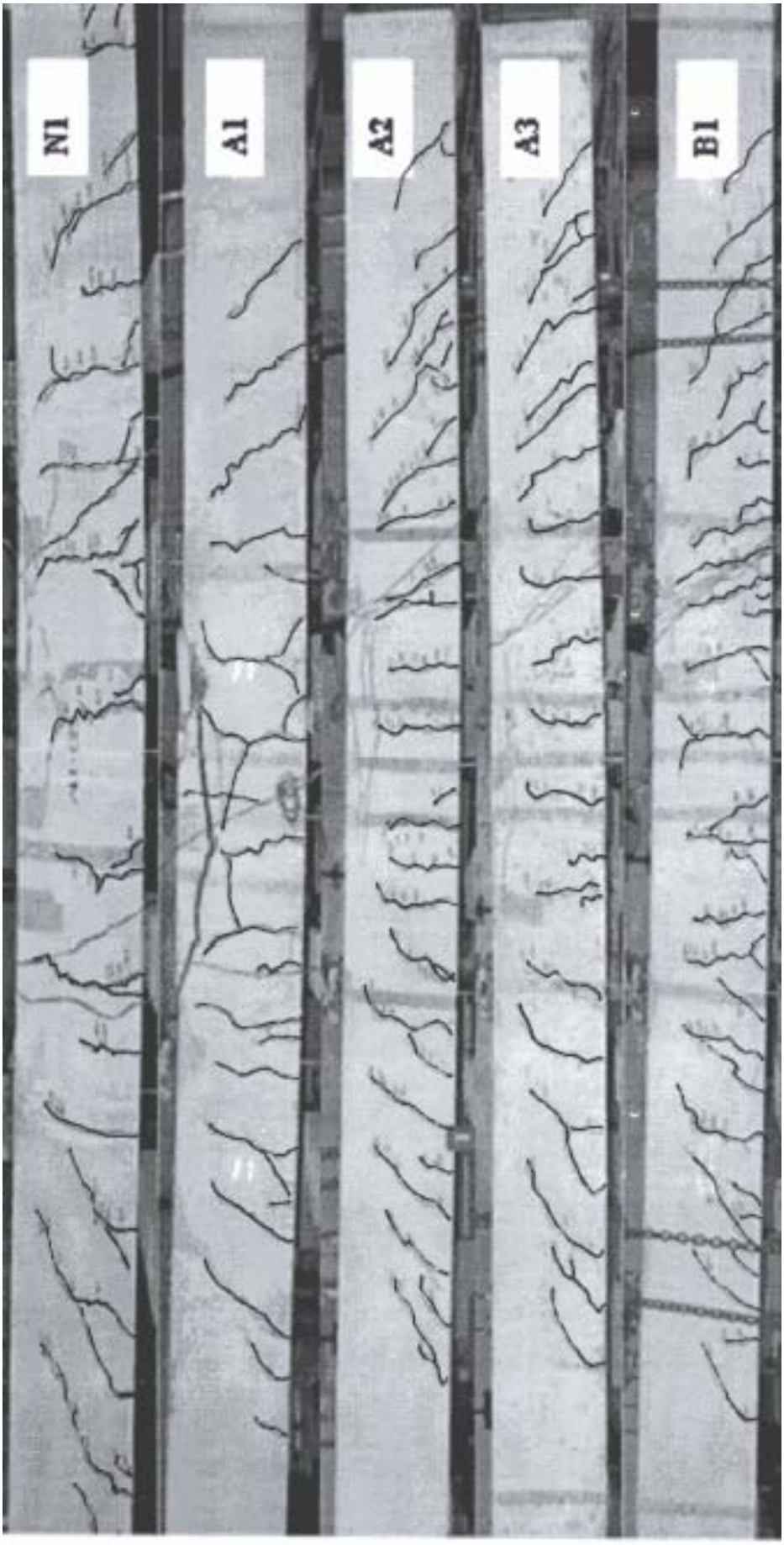

Figure 5.8. Crack failure pattern of test beam at failure load

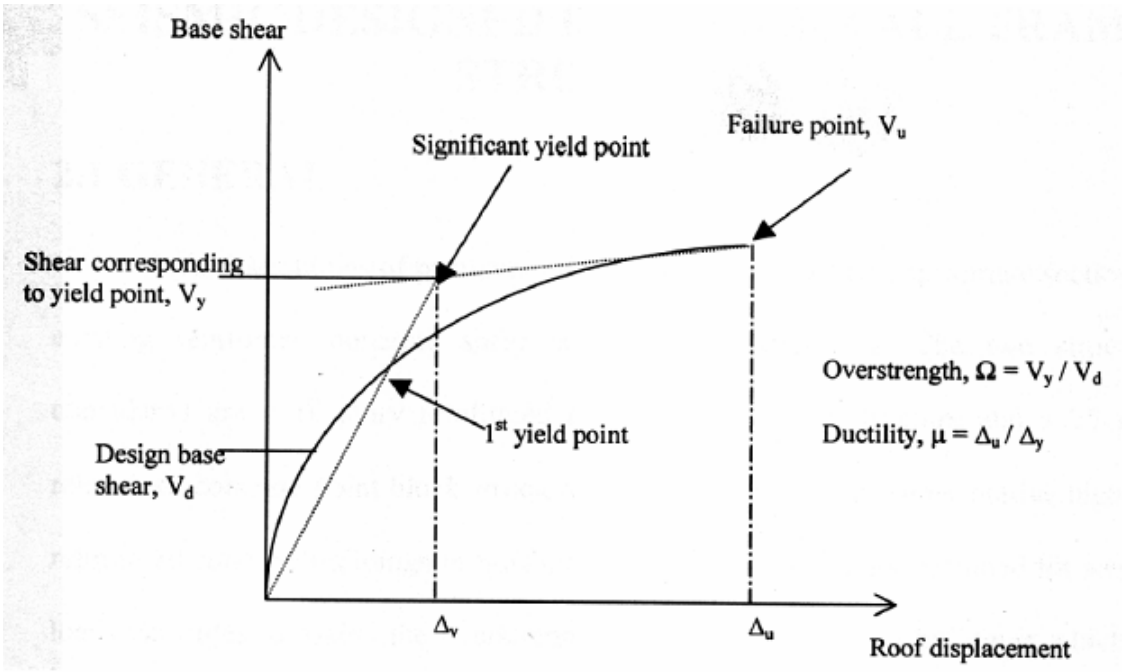

Figure 5.9 Over strength and ductility factor of a building (Kong, 2003)

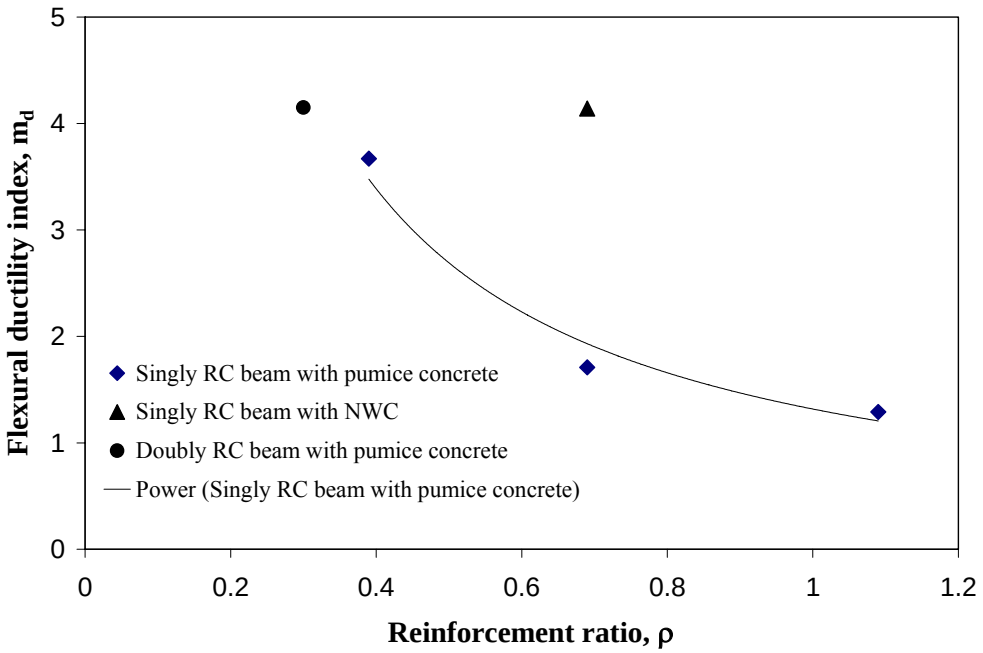

Figure 5.10. Effect of tensile steel reinforcement ratio ρ on the displacement ductility

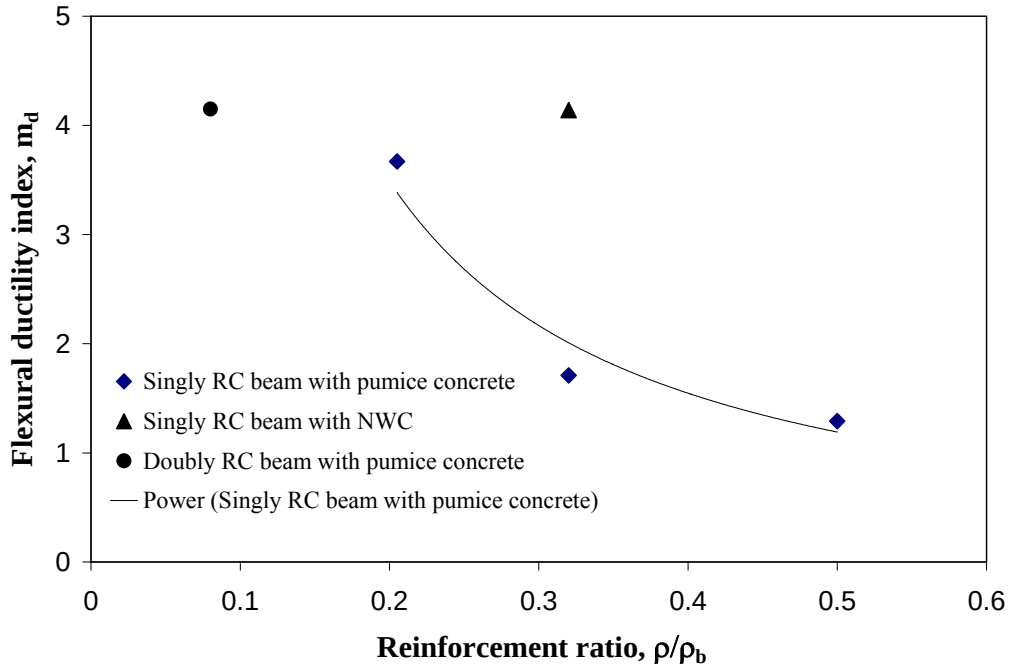

Note for beam B1, reinforcement ratio is defined as $(\rho - \rho')/\rho_b$

Figure 5.11 Effect of reinforcement ratio ρ/ρ_b on displacement ductility μ_d

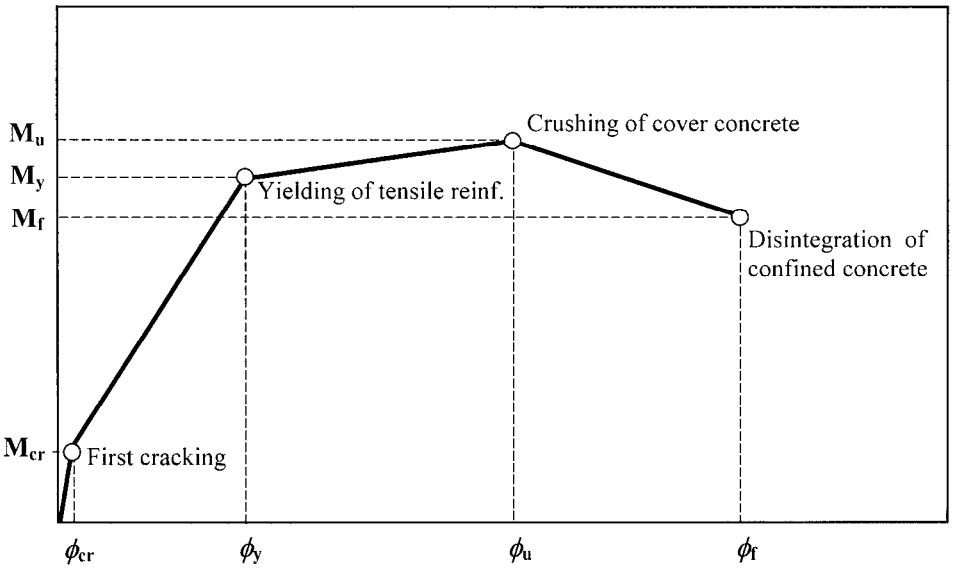

Figure 5.12. Idealized moment-curvature relationship

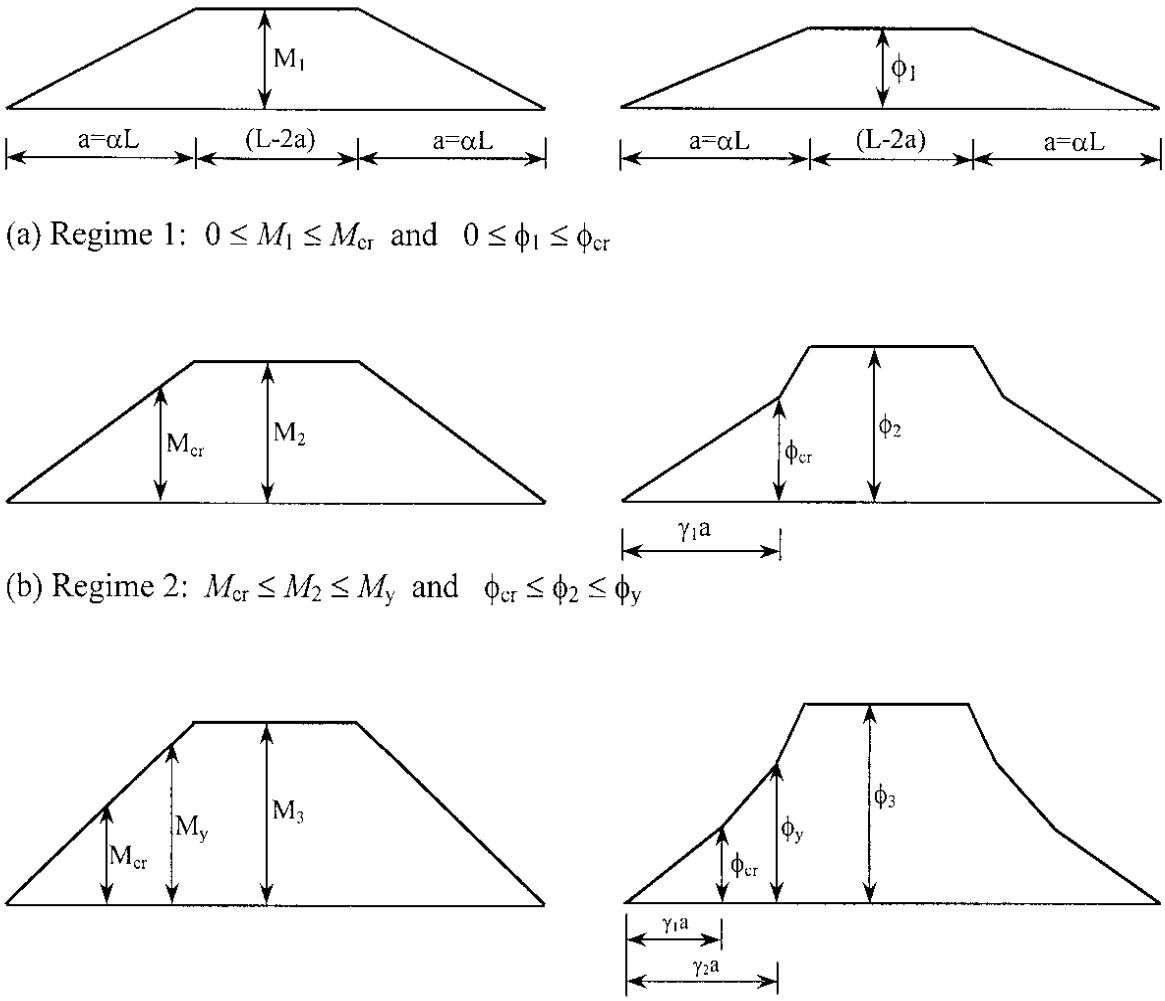

Figure 5.13 Bending moment and curvature distribution along the beam (Rashid, 2002)

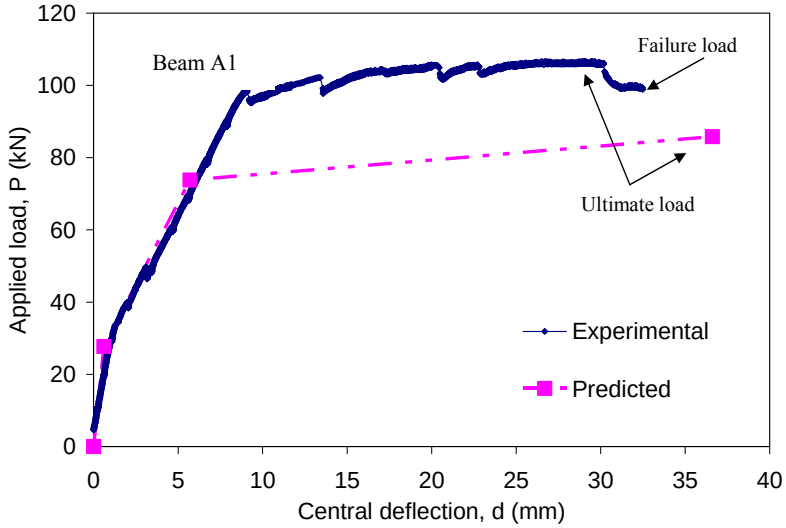
Beam A1
Failure load
Ultimate load
Experimental
Predicted
Applied load, P (kN)
Central deflection, d (mm)
0
20
40
60
80
100
120
0
5
10
15
20
25
30
35
40

(a)

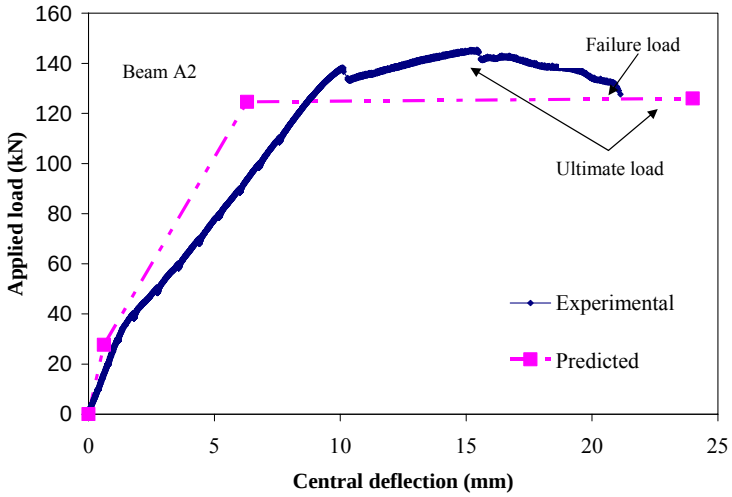
Beam A2
Failure load
Ultimate load
Experimental
Predicted
Applied load (kN)
Central deflection (mm)
0
20
40
60
80
100
120
140
160
0
5
10
15
20
25

(b)

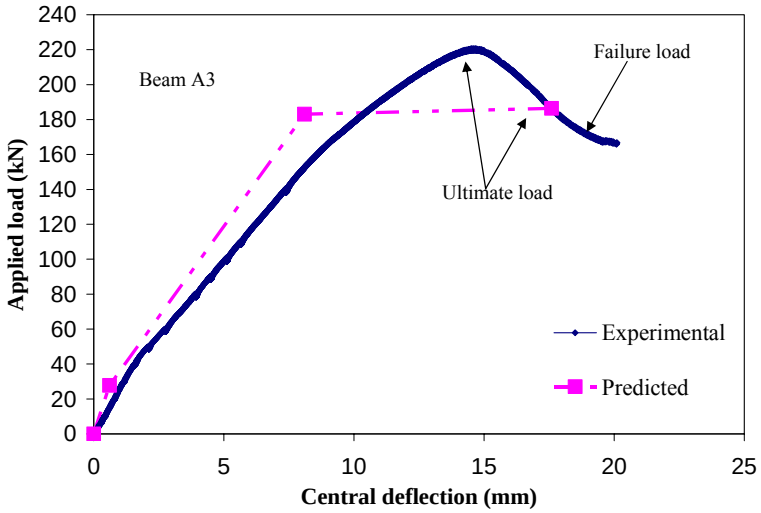
Beam A3
Failure load
Ultimate load
Experimental
Predicted
Applied load (kN)
Central deflection (mm)
0
20
40
60
80
100
120
140
160
180
200
220
240
0
5
10
15
20
25

(c)

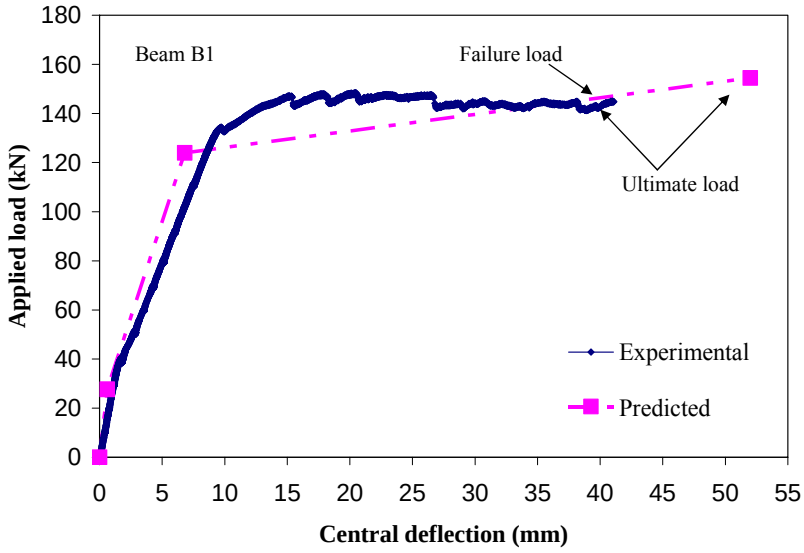

(d)

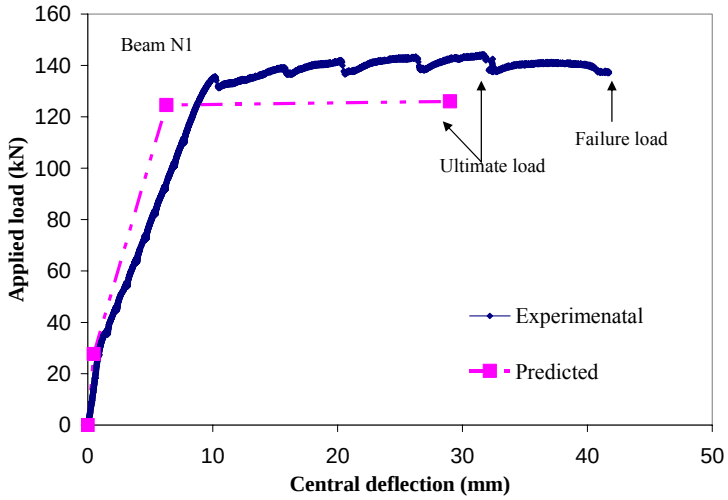

(e)

Figure 5.14. Predicted load –deflection relationship

CHAPTER SIX

CONCLUSION

This thesis provides a study on the behavior of pumice concrete under uniaxial compression, splitting & flexural tensile stress, drying shrinkage and creep. The viability of pumice concrete for structural application is also studied through flexural loading of a simply supported reinforced pumice concrete beam.

The following conclusions are made for pumice concrete.

(1) The strength of pumice aggregate is the primary factor controlling the strength of lightweight concrete with pumice aggregates. Compressive strength level of 18.5 to 27.4 MPa with the corresponding air-dry density of 1579 to 1836 kg/m^3 is observed.

(2) The flexural and splitting tensile strength vary from 2.14 to 2.9 MPa and from 4.92 to 6.64 MPa respectively. Thus the tensile/compressive strength ratio is higher for pumice concrete than that for NWC and lightweight concrete with artificial lightweight aggregates.

(3)The elastic modulus of pumice concrete varies from 13.5 to 20.3 GPa, which is much lower than that of NWC of similar compressive strength. For the various concrete mixes, the Norwegian concrete code, NS 3473 (1998) appears to give a fairly good prediction of the elastic modulus, while the ACI Code underestimate the elastic properties. The Poisson's ratio of the pumice concrete had a high scatter with values varying from 0.16 to 0.27.

(4) The ultimate concrete compressive strain, ε_{cu} at peak load based on the uniaxial compression test for the pumice concrete varies from 0.00162 to 0.00200, which is

much lower than that of NWC with ε_{cu} of 0.003 or LWAC with artificial aggregates with ε_{cu} of 0.003 to 0.0035. The shape of ascending part of stress-strain curve is more linear than that of lightweight concrete with artificial aggregates.

(5) The measurement of drying shrinkage for pumice concrete with 7 days fog curing varies from 168 to 1290 microstrains at 168 days drying, which is generally higher than that of NWC with 300 to 700 microstrains (Shacklock and Keene, 1957)..

(6) In the creep test under 168 days loading, the creep values are between 339 and 1225 microstrains. Specific creep presented a larger range of 45-193 microstrain/MPa, much higher than that of LWAC with artificial LWA reported by CEB/FIP (1977) with creep values of 65 to 90 microstrains/MPa. Values of creep recovery between 0.13 and 0.22 are found.

The following conclusions are made for steel reinforced pumice concrete beams:

(1) The ratio of ρ/ρ_b where ρ = steel reinforcement ratio in a beam cross section and ρ_b = the balance steel reinforcement ratio in a beam cross section, plays an important role in determining the shape of the load-deformation curves starting from cracking stage to ultimate failure.

(2) Unlike reinforced NWC beam, for reinforcement ratio, ρ/ρ_b of 0.21, the flexural ductility index (μ_d) of reinforced pumice concrete beam (with an average $f_c^{'}$ = 23.8 MPa) is significantly less than 3, the value specified by code. The provision of compressive reinforcements in the beam does not affect the ultimate strength but increases the value of μ_d. Doubly reinforced beam with $(\rho-\rho^{'})/\rho_b$ at 0.10 shows adequate deflection ductility of 4.15.

(3) ACI 318 (1999) code gives a safe prediction of the ultimate flexural strength, 20 % on average lower than the experimental results.

(4) ACI 318 (1999) code underestimates the experimental deflections of steel reinforced concrete beam under short term service loads up to about 21.5 % on average. For reinforced NWC beam, the underestimated experimental deflection value of beam as compared to the calculated value is 23 %.

(5) Crack widths at service loads for steel reinforced pumice concrete beam vary from 0.10 to 0.18 mm, and are within maximum allowable crack width 0.3 mm for the durability requirements. The crack spacing of the pumice concrete beams is closer than the NWC beam.

(6) ACI code underestimates the experimental crack moment up to 12 % on average for reinforced pumice concrete beam, whereas the underestimated cracking moment for reinforced NWC beam is 19 %.

(7) The short-term complete load-deflection response up to the ultimate load of the reinforced pumice concrete beams can be fairly predicted based on the second moment–area theorem from the usual flexural theory based on equilibrium and Bernoli's compatibility..

6.1 Recommendations For Future Research

The following studies need to be investigated:

(1) the thermal conductivity of pumice concrete.

(2) the behavior of laterally confined pumice concrete.

(3) stress-strain relationship of pumice concrete under triaxial compression.

(4) the experimental and analytical investigations on long-term response of pumice

concrete beams in flexure taking into creep and shrinkage.

(5) the behavior of pumice concrete under cyclic and fatigue loading.

(6) the shear behavior of reinforced pumice concrete beam.

(7) pumice concrete has potential application for use in column and slab but the behaviour needs further investigation.

REFFERENCES

ACI Committee 211.2. Standard Pactical for Selecting Proportions for Structural Lightweight Cncrete,1998.

ACI, Committee 213R-87. Guild for Structural Lightweight Aggregate Concrete, ACI Manual of Concrete practice, Part 1, Materials and General Properties of Concrete, Detroit, Michigan., 18 pp.,1994.

ACI Committee 233R-95. Ground Granulated Blast-furnace Slag as a Cementitious Constituent in Concrete and Mortar. American Concrete Institute, Farmington Hills, MI, 1996.

ACI Committee 304.5R. Batching, Mixing, and Job Control of LWAC. 1991.

ACI Committee 318-83. Building Code Requirements for Reinforced Concrete. American Concrete Institute, Detroit, Michigan., 1983.

ACI Committee 363R . State- of –the –Art Report on High-Strength Concrete. 1992

ACI Committee 435. Deflections of Reinforced Concrete Flexural Members, Journal of the ACI, V63, No.6, pp.737-674, 1966.

ACI Committee 523, ACI 523.1R-92, Guide for Cast-in-Place Low Density Concrete, 1992.

Ahmad, S.H. and Shah, S.P. Structural Properties of High Strength Concrete and Its Implications for Precast Prestressed Concrete. PCI Journal, V. 30, No. 4-6, pp. 92-119, 1985.

Ahmad, S.H and Batts J. Flexural Behavior of Doubly Reinforced High Strength Lightweight Concrete Beams with Web Reinforcement, ACI Structural Journal, No. 88-S38, pp. 351-358, 1991.

Ahmad, S.H. and Barker R. Flexural Behavior of Reinforced High Strength Lightweight Concrete Beams, ACI Structural Journal, No. 88-S9, pp. 69-77, 1991.

Aitcin, P.C. and Mehta, P.K. Effect of Coarse Aggregate Characteristics on Mechanic Properties of High Strength Concrete. ACI Material Journal, V.87, No.2, pp. 103-107, 1990.

Alfes, C. Mechanical Properties of High Strength Concrete. State of the Art Report on High Strength Concrete, RILEM, pp. 2-7, 1990.

Almusallam, T.H. Stress-Strain Relationship of Normal and High-Strength and Lightweight Concrete, Magzine of Concrete Research, V. 47, No, 170, pp. 39-44, 1995.

Anson, M. and Newman, K. The Effect of Mix Proportions and Method of Testing on the Poisson's Ratio of Mortar and Concrete. Magazine of Concrete Research, V.18, No. 44, pp. 115-130, 1966.

Asgeirsson, H. Hekla pumice in Lighweight Concrete. IBRI, 45 pp., 1994.

Ashour, S.A. Effect of Compressive Strength and Tensile Reinforcement Ratio on Flexural Behavior of High Strength Concrete Beams. Engineering Structure, Surrey, UK, V. 22, Issue 5, pp. 413-213, 2000.

ASTM C39. Standard Specification for Ready-Mixed Concrete,

ASTM C127. Test Method for Specific Gravity and Absorption of Coarse Aggregate, 2001

ASTM C128. Test Method for Specific Gravity and Absorption of Fine Aggregate

ASTM C136-01. Standard Test Method for Sieve Analysis of Fine and Coarse Aggregate.

ASTM C150. Specification for Portland Cement, 1994.

ASTM C173. Air Content of Freshly Mixed Concrete by the Volumetric Method, 2001.

ASTM C33. Specification for Concrete Aggregates, 1993.

ASTM C260. Specification for Air-Entraining Admixtures for Concrete, 1994.

ASTM C469. Standard Test Method for Static Modulus of Elasticity and Poisson's Ratio of Concrete in Compression, 2002.

ASTM C494. Specification for Superplaticiser for Concrete, 1994.

ASTM C496. Standard Test Method for Splitting Tensile Strength of Cylindrical Concrete Specimens, 1990.

ASTM C 512. Standard Test Method for Creep of Concrete in Compression, 1994.

ASTM C566. Standard Test Method for Total Evaporable Moisture Content of Aggregate by Drying. 1997

Baalbaki, W; Benmokrane, B. Chaallal, O. Aitcin, P.C. Influence of Coarse Aggregate on Elastic Properties of High Performance Concrete. ACI Material Journal, V.88 No. 5, pp. 499-503, 1991.

Bardhan-Roy, B.K. Lightweight Aggregate Concrete in the UK. CEB/FIP International Symposium on Structural Lightweight Aggregate Concrete, Sandefjord, Norway, pp. 52-69, 1995.

Bentur, A. The Contribution of the Transition Zone to the Strength of High Quality Silica Fume Concretes. Bonding in Cementitious Composites, Proc. Symp., Materials Research Society, V. 114, pp. 97-103, 1993.

Beutur, A, and Cohen, M.D. The Effect of Condensed Silica Fume on the Microstructure of the Interfacial Zone in Portland –Cement Mortars. Journal of American Ceramic Society, V. 70, No.4, pp. 738-743, 1987,

Branson, D.E. Instantaneous and Time-Dependent Deflections of Simple and Continuous Reinforced Concrete Beams. Report No.7, Part 1, Albama Highway Research Department, Bureau of Public Roads, pp. 1-78, 1963.

BS 8110: Part 2:1985 British standard Structural Use of Concrete, Part 2. Code of Practice for Special Circumstance. British Standard Institute.

Bremner, T.W. and Holm, T.A. Elasticity, Compatibility, and the Behavior of Concrete ACI Material Journal, V.3, No. 2, pp. 244-250.

Brooks, J. J and Neville, A.M. A Comparison of Creep, Elasticity and Strength of Concrete in Tension and in Compression. Magazine of Concrete Research, V. 29, No. 100, pp. 131-141, 1977.

Burnett, I. High Strength Concrete in Australia-State of the Art. Sydney, 1990.

Carrasquillo, R.L., Slate, F.O., Nilson, A.H. Microcracking and Behavior of High Strength Concrete Subjected to Short Term Loading. ACI Journal, V. 78, No. 3, pp. 179-186, 1981.

Carrete, G.G. and Malhotra, V.M., Mechanism Properties, Durability and Drying Shrinkage of Portland Cement Concrete Incorporating Silica Fume. Cement Concrete and Aggregates V. 5, No.1, pp 3-13, 1983.

CEB-FIP Manual. Lightweight Aggregate Concrete. CEB-FIP Manual of Design and Technology, The Construction Press, London, pp. 169. 1977.

CEB/ FIP International Symposium on Structural Lightweight Aggregate Concrete, Sandefjord, Norway, pp. 154-163, 1995.

CEB-FIP Bulletin 4. Lightweight Aggregate Concrete Codes and Standards, 1999.

Chelouah N., Forst-Tausalz-Widerstand von hochfesten luftporenfreien Portlandzement-betonen, Dessertation, Weimar, 1996.

Cembureau. Lightweight Aggregate Concrete - Technology and World Applications. Editor G. Bologna, Paris, 1974.

CEN prEN 206 Concrete - Performance, Production and Conformity, 1997.
Chandra, S. and Berntsson, L. Lightweight Aggregate Concrete Science, Technology and Applications, William Andrew Publication, pp. 100-103, 2001

Chi, J. M. and Huang, R. Effect of Aggregate Properties on the Strength and Stiffness of Lightweight Concrete, Cement Concrete Composite, V. 25, pp. 197-250, 2003.

Clarke, J.L. Design Requirements. Structural Lightweight Aggregate Concrete, Chapman & Hall, London, pp. 45-74, 1993.

Kordina, K. (Experiments on the Influence of the Mineralogical Character of Aggregates on the Creep of Concrete. RILEM Bulletin, Paris, No. 6, pp. 7-22, 1960.

Counto, U.J. The Effect of the Elastic Modulus of the Aggregate on the Elastic Modulus. Creep and Creep Recovery of Concrete. MCR, V. 16, No. 48, pp. 129-138, 1964.

CUR, Centre for Civil Engineering Research and Codes Structural Behaviour of Concrete with Coarse Lightweight Aggregates. Report 173, Gouda, Netherlands, 1995.

Curcio, F., Galeota, D., Gallo, A., Giammatteo, M. High-performance Lightweight Concrete for the Precast Prestressed Concrete Industry. Proc.4th. Int. CANMET/ACI/JCI Symposium, Japan, pp. 389-406,1998.

Davis, H.E. Autogenous Volume Changes of Concrete, Proc. ASTM., 40 PP.1103-1110, 1940.

DIN 4219, Leichtbeton und Stahlleichtbeton mit geschlossenem, 1979.

DIN 4226 Teil 3 (Zuschläge für Beton Prüfung von Zuschlag mit dichtern oder porigen Gefüge. 1983.

Dossier TécnicoHormigones Ligeros Estructurales. 1997.

EI-Hindy, E., Miao, B.Q., Chaalla, O. and Aitcin, P.C., Drying Shrinkage of Ready Mixed High-Performance Concrete, ACI Material Journals, V.63, No.63, pp. 111-116, 1994.

Feldman, R.F. and Sereda, P.J. A Model for Hydrated Portland Cement Paste as Deduced from Sorption –Length Change and Mechanical Properties. Materials and Structures Bulletin RILEM, No.6, pp. 509-522, 1968.

Faust, T. The Behavior of Structural LWAC in Compression, pp512-521, 2000.

Finn, E.V. Guide to Structural Use of Lightweight Aggregate Concrete. The Institute of Structural Engineers, October, 1987.

FIP. Manual of Light Weight Aggregate Concrete, 2nd. Edition, 1983.

Fulton, F.S. The Properties of Portland Cement Containing Milled Granulated Blast-furnace Slag, Monograph, Portland Cement Institute, Johannesburg, pp. 4-46, 1974.

Glucklich, J. Creep Mechanism in Cement Mortar. Journal of ACI, Vol. 59, pp. 923-948, 1962.

Gjerde, T. Structural Lightweight-Aggregate Concrete for Marine and Offshore Applications, Norwegian Contractors, Oslo, Norway, 1982.

Gopalaratman, V.S. and Shah, S.P. Softening Response of Plain Concrete in Direct Tension, ACI Journal, V. 8, No.3, 1985, pp. 310-323.

Haktanir, T. and Altun, F. Structural Lightweight Concrete with Pumice Aggregate of Erciyes Region. Innovations and Development in Concrete Materials and Construction, Dhir Hewlett Csetenyi, 2002.

Hammer, T.A. and Smeplass, S. The Influence of Lightweight Aggregate Properties on Material Properties of the Concrete. In International Symposium on Structural Lightweight Aggregate Concrete, Norway, pp. 517-532, 1995.

Helm, T. A. Physical Properties of High Strength Lightweight Aggregate Concretes. Proceedings, Second International Congress of Lightweight Concrete, London, 1980.

Hirsch, T.J. Modulus of Elasticity of Concrete Affected by Elastic Moduli of Cement Paste Matrix and Aggregate. ACI Journal V.59, No. 3 , pp. 427-450, 1962.

Hoff, G. C. High Strength Lightweight Aggregate Concrete for Arctic Applications. ACI SP 136 American Concrete Institute, Detroit, PP. 1-245, 1992.

Hoff, G.C., Walum, R., Weng, J.K., Nu ez, E. The use of Structural Lightweight Aggregate in Offshore Concrete Platforms. CEB/FIP International Symposium on Structural Lightweight Aggregate Concrete, Sandefjord, Norway, pp. 349-362, 1995.

Hoff, G.C. The Development of High-Performance Concrete for Offshore Concrete Structures. Concrete for Infrastructure and Utilities, pp. 383-394, 1996.

Hofmann, P., Stöckl, S. Versuche zum Kriechen und Schwinden von hochfestem Leichtbeton. Deutscher Ausschuss für Stahlbeton, H. 343, pp. 1-20. 1983.

Holm, T.A. Structural Lightweight Concrete. Handbook of Structural Concrete. London, 1983.

Holm, T.A. and Bremner, T.W. High Strength Lightweight Aggregate Concrete. High-Performance Concrete and Applications, Edward Arnold, London, pp. 341-774, 1994.

Holm, T.A. Lightweight Concrete and Aggregates, ASTM Standard Technical Publication STP 169C, 1995.

Holm, T.A.. State-of-the-Art Report on High-Strength, High-Durability Structural Low-Density Concrete for Applications in Severe Marine Environments, pp. 29-31, 2000.

Hossain, K.M.A. Properties of Volcanic Pumiced Based Cement and Lightweight Concrete, Cement and Concrete Research, V. 24, No, 78, 2003.

Hua, C., Acker, P., and Ehrlacher, A. Analysis and Models of Autogenous Shrinkage of Hardened Cement Paster, Modelling at Microscopic Scale. Cement and Concrete Research, V. 25, No. 7, pp. 1457-1468, 1995.

Isserman, R. and Bentur. A. Interfacial Interactions in Lightweight Aggregate Concretes and Their Influence on the Concrete Strength, Cement and Concrete Composites V.18, pp. 67-76, 1996.

Jackson, N. Civil Engineering Materials, 3rd ed., Macmillan Press, Hong Kong, 1983.

Jones, R. and Kaplan, M.F. The Effect of Coarse Aggregate on the Mode of Failure of Concrete in Compression and Flexural. Magazine of Concrete Research, V. l.9, No. 26, pp. 89-94, 1957.

Johnsen, H. Construction of the Støvset Free Cantilever Bridge and the Nordhordland Cable Stayed Bridge. CEB/FIP International Symposium on Structural Lightweight Aggregate Concrete, Sandefjord, pp. 517-532. 1995.

Klieger, P. and Isberner, A.W. Laboratory Studies of Blended Cement-Portland Blast-Furnace Slag Cements. Journal of PCA Research and Development Department laboratories, V.9, No.3, pp. 2-22, 1967.

Klink, S.A. Actual Elastic Modulus of Concrete, ACI Journal, Vol.82 (5) pp. 630-633, 1985.

Kong, KH. Ph.d thesis, Overstrength and Ductility of Reinforced Concrete Shear Wall Frame Structures in Low Seismic Regions., pp. 1-22, National University of Singapore, 2003.

Kotsovos, M.D. Effect of Testing Techniques on the Post Ultimate Behavior of Concrete in Compression. Materials and Construction, V. 16, No.91, pp. 3-12, 1983.

Kruml, F. Short- and Long-Term Deformation of Structural Lightweight Aggregate Concrete. First International Congress of Lightweight Concrete, V. 1, London, 1968.

Lazarus, D. Lightweight Concrete in Buildings. Structural Lightweight Aggregate Concrete. London, pp. 106-149, 1993.

Liu, X., Yang, Y., Jiang, A. The Influence of Lightweight Aggregate on the Shrinkage of Concrete. CEB/FIP International Symposium on Structural Lightweight Aggregate Concrete, Sandefjord, Norway, pp. 555-562, 1995.

Malhotra, V.M. Are 4x8 Concrete Cylinders As Good As 6x12 for Quality Control of Concrete. ACI Journal, V.73, No. 1, pp33-36, 1976.

Manmohan, D., Mehta .P.K. Influence of Pozzolanic, Slag and Chemical Admixtures on Pore Size Distribution and Permeability of Hydrated Cement Pastes, Cement, Concrete, and Aggregates. V. 3, No. 1, 1981, pp. 63-67., 1981.

McNeely, D.J. and Lash, S.D. Tensile Strength of Concrete. ACI Journal, Proceedings, V. 60, No. 6, pp. 751-761,1963.

Mehtha, P.K. Concrete Structure Properties and Materials. Prentice Hall Inc, Englewood Cliffs, NJ. 1986.

Mehta, P.K and Aitcin, P.C. Microstructural Basis of Selection of Materials and Mix Proportion for High Strength Concrete. ACI SP-121, pp. 265-286, 1990,

Narayanan N. and Ramamurthy K.,Structure and Properties of Aerated Concrete: A Review, Cement & Concrete Composites, v. 22, pp. 321-329, 2000.

Newman, J.B. Properties of Structural Lightweight Concrete in Structural Lightweight Concrete. Chapman & Hall, London, pp. 19-44, 1993.

Neville, A.M. The Relation between Creep of Concrete and the Stress-Strain Ratio. Applied Scientific Research, The Hague, Section A.9. pp. 285-92, 1960.

Neville, A.M., Creep of Concrete as a Function of Its Cement Paste Content. Magagine of Concrete Research. V. 16, No. 46, pp. 21-30, 1964.

Neville, A.M., and Hirst, G. Mechanism of Cyclic Creep of Concrete. Douglas McHenry International Symposium on Concrete and Concrete Structures, ACI SP-55, American Concrete Institute, Detroit, pp. 83-101, 1978.

Neville, A.M., Dilger, W.H., Brooks, J.J., Creep of Plain & Structural Concrete. Construction Press, London, 361 pp, 1982.

Neville, A.M. Brooks, J.J. Concrete Technology. University Press, Belfast, pp. 438. 1987.

Nevile, A.M. Properties of Concrete, 4th ed., Longman, Harlow, England, 1995.

Nilsen, A.U. Elastic Behavior of Concrete. Dr.ing. Dissertation 1992:66, The Norwegian Institute of Technology, NTH, 1992.

NS 3473. Concrete Structures – Design Rules, 1998.

Olarfur, H.W. Air Entrainment as a Measure to Reduce Density of High Performance Lightweight Aggregate Concrete with a Main Emphasis on Natural Lightweight Aggregates. Preceedings Second International Symposium on Structural LWAC, Kristiansand, Norway, pp. 933-949, 2000.

Oluokun, F.A. Burdette E.G and Deatherage J.H., Splitting Tensile and Compressive Strength Relationships at Early Ages. ACI Material Journal, V.88, No. 2, pp115-121, 1991.

Oluokun, F.A. Prediction of Concrete Tensile Strength from Compressive Strength: Evaluation of the Existing Relations for Normal Weight Concrete. ACI Materials V. 88, No. 3, pp. 302-309. 1991.

Pankhurst, R.N.W. Construction. Structural Lightweight Aggregate Concrete. Chapman & Hall, London, pp. 75- 105, 1993.

Park, R., and Paulay, T., Reinforced Concrete Structures. John Wiley & Sons, New York, Feb, 1984, 311 pp.

Pastor, J.A., Nilson, A.H and Slate, F.O. Behavior of High Strength Concrete Beam. Research Report No. 84-3, Department of Structural Engineering, Cornell University, Ithaca, 311 pp., 1984.

Paulson, K.A.; Nilson, A.H; and Hover, K.C., Immediate and Long-Term Deflection of High-Strength Concrete Beams, Research Report No, 89-3, Department of structural engineering, Cornell University, Ithaca, 230pp,1989.

Penttala, V., Rautanen, T., Microporosity. Creep and Shrinkage Prediction from Short-term Tests. ACI SP-121, ed, Hester. W.T American Concrete Institute, Detroit, pp. 409-432, 1990.

Popovics, S. Effect of Porosity on the Strength of Concrete, Journal of Materials, V. 4, pp. 356, 1969.

Power, T.C. Some Observations on the Interpretations of Creep Data, Bulletin RILEM, No.33, pp. 381-344, 1968.

Power, P.C. Mechanism of Shrinkage and Reversible Creep of Hardened Cement Paste. In Structure of Concrete and Its Behavior under Load: Proc. of An International Conference, Sept, 1965, London, Cement and Concrete Association, pp. 319-344, 1968.

Punkki, J., Gjørv, O.E. Effect of Water Absorption by Aggregate on Properties of Highstrength Lightweight Concrete. CEB/FIP International Symposium on Structural Lightweight Aggregate Concrete, Sandefjord, Norway, pp. 604-616, 1995.

Rachel, D., Javed, Bhatty. Supplementary Cementing Materials for Use in Blended Cements. Research and Development Bulletin RD112T, Portland Cement Association, 1996.

Ramachandran, V.S. Concrete Admixture Handbook, Properties, Science and Technology, Second edition, pp. 686-690, 1995.

Ramazan Demirboga. Effect of Expanded Perlite Aggregate and Mineral Admixture on the Compressive Strength of Low-Density Concretes, Cement and Concrete Research, V. 31, pp. 1627-1623, 2001.

Rashid, M.A. Flexural Behavior of High Strength Concrete Beam. Ph.d Thesis, pp. 55. Singapore, 2002.

Rapheal, J.M. Tensile Strength of Concrete, ACI Journal Proceedings, Vol.18, No. 2, pp. 158-165, 1984,.

Reichard, T. W. Creep and Drying Shrinkage of Lightweight and Normal Weight Concretes. National Bureau of Standards, Monograph 1964, U.S. Department of Commerce, Ishington, DC, pp. 30, 1964.

Remzi Sahin and Habib Uysal. Effect of Different Cement Dosage, Slump, and Pumice Aggregate Ratio on the Compressive Strength and Density of Concrete, Cement and Concrete Research, V.1, No. 5, pp. 2318, 2003.

Rønne, M.; Hammer, T.A. LWA Concrete for Floaters. SP3 Mechanical Properties. Report 3.1 Mechanical Properties of Concretes with Strength Grades LC30 and LC40. SINTEF Report STF70 A93040, 1993.

Roy, RL. and Larrard, F.D. Creep and Shrinkage of High-Performance Concrete: the LCPC Experience. Creep and Shrinkage of Concrete, Proceedings of the Fifth International RILEM Symposium., pp. 499-504, 1993.

Ruetz, W. A Hypothesis for the Creep of Hardened Cement Paste and the Influence of Simultaneous Shrinkage. In Structure of Concrete and Its Behavior under Load: Pro. Of an International Conference, Sept. 1965, London, Cement and Concrete Association, pp. 365-387, 1968.

Sahin, R. and Uysal, H. Effect of Different Cement Dosage, Slump, and Pumice Aggregate Ratio on the Compressive Strength and Density of Concrete. Cement Concrete Research, V. 1, No. 5, pp. 2318, 2003.

Setunge, S., Attard M.M., Ultimate Strength Criteria for Confined High Strength Concrete, ACI Structural Journal, 1993.

Shacklock, B.W. and Keene, P.W. The Effect of Mix Proportions and Testing Conditions on Drying Shrinkage and Moisture Movement of Concrete. Cement Concrete Association. Technical Report TRA/266, London, 1957.

Shideler, J.J. Lightweight Aggregate Concrete for Structural Use, Journal of American Concrete Institute, V. 54, pp. 299-238, 1954.

Smith G.M and Young L.E. Ultimate Flexural Analysis Based on Stress-Strain Curves of cylinders. ACI Journal, Proceedings, V.53 (6), pp. 597-610, 1956.

Swammy, R.N. Mix Design and Properties of Concrete Made from PFA Coarse Aggregates and Sand. International Journal of Cement Composite and Lightweight Concrete, V. 5, No. 4, 1983.

Short, A; Kinniburgh, W. Lightweight Concrete. MCMLXIII, London, pp. l-14, 1963.

Slate, F.O; Nilson, A.H., Martinez, S. Mechanical Properties of High-Strength Lightweight Concrete. AC1 Journal, pp. 606-613, 1986.

Shideler, J. J. Lightweight Aggregate Concrete for Structural Use, Joumal, American Concrete Institute, Oct. 1957; Proceedings, Vol. 54, pp. 298-328, 1957.

Smeplass, S. Mechanical Properties - Lightweight Concrete. Report 4.5, High Strength Concrete. SP4 - Materials Design, SINTEF, 1992.

Smeplass, S. Materialutvikling Høyfast Betong, Report 5.6 Effect of the Aggregate Type on the Compressive Strength and E-modulus of the Aggregate, SINTEF-report STF70 A92051 Trondheim, Norway,1992.

Spitzner, J. A Review of the Development of Lightwieght Aggregate - History and Actual Survey. CEB/FIP International Symposium on Structural Lightweight Aggregate Concrete, Sandefjord, Norway, pp 13-21, 1985.

Smeplass, S. Lightcon Rapport. DP2: Materialegenskaper. Delrapport 2.9: Effekt av Masse-Forholdet på Lettbetongens Trykkfasthet, SINTEF-rapport STF22 A97829, 1997.

Smeplass, S. Lightcon Rapport. DP3 Konstruktiv virkemåte og Dimensjonering. Fasthet un-der Langtidslast. SINTEF-rapport STF22 A97835, 1997.

Smeplass, S. Pumpbarhet av Lettbetong med Impregnerte, Forfuktede og Ubehandlede Lettilslag. LettKon report 4.x, Sintef, Trondheim, Norway, 1998.

Swamy, R.N, and Lambertt, G.H. Flexural Behavior of Reinforced Concrete Beams Made with Fly Ash Coarse Aggregates, The International Journal of Cement Composites and Lightweight Concrete, V. l.6, No. 3, 1984.

Shrive, N.G. Compression Testing and Cracking of Plain Concrete, Magazine of Concrete Research, V. 35, No. 122, pp. 27-39, 1983.

Sugair, F.H. Analysis of the Time –Dependent Volume Reduction of Concrete Containing Silica Fume. Magazine of Concrete Research, V. 47, No.170, pp. 78-81, 1995.

Sutherland, A. Air Entrained Concrete, Publication 45022, Cement and Concrete Association, 1974.

Tasdemir, M. A. Elastic and Inelastic Behaviour of Structural Lightweight Aggregate Concretes, Ph.D. Thesis, Faculty of Civil Engineering, Istanbul Technical University,

1982 (in Turkish with English Summary).
Theissing, E.M., et al. Lichtbeton (Light weight concrete). CUR-report 48, pp. 208, 1971.

Thorenfeldt, E., Design Criteria of Lightweight Aggregate Concrete. CEB/FIP Internationaln Symposium on Structural Lightweight Aggregate Concrete, Sandefjord, Norway, pp. 720- 732, 1995.

Thomas, Telford. State of Art Report, Condensed Silica Fume in Concrete, FIP Commission on Concrete, 1988.

Troxell, G.E., Paphael, J.M. and Davis R.E., Long-Time Creep and Shrinkage Tests of Plain and Reinforced Concrete. Proc. ASTM, V. 58, pp. 1101-1120, 1958.

Tucker, J. Effect of Dimensions of Specimensnupon the Precision of Strength Test Data. Proceedings , ASTM, V. 45, pp 952-959, 1945.

Uijl, J.A. den, Stroband, J., Walraven, J.C. Splitting Behaviour of Lightweight Concrete. CEB/ FIP International Symposium on Structural Lightweight Aggregate Concrete, Sandefjord, Norway, pp. 154-163, 1995.

Valore, R. C. North American Lightweight Concretes, pp. 1-37. 1988.

Videla, C and Lopez, M. Mixture Proportioning Methodology for Structural Sand-Lightweight Concrete. AC1, 97-M34, 1997.

Walker S. Modulus of Elasticity of Concrete, Structural Materials Research Laboratory. Bulletin 5 Lewis Institute, Chicago, 1923.

Weber, S., Reinhardt, H.W., A Blend of Aggregate to Support Curing of Concrete. CEB/FIP International Symposium on Structural Lightweight Aggregate Concrete, Sandefjord, Norway, pp. 662-671, 1995.

Weigler, H. and Karl, S. Stahlleichtbeton. Bauverlag GMBH, Wiesbaden and Berlin, pp. 38-43, 1972.

Wethers G. Aufnahme von Druckkraften in Schwerbeton und in Leichtbeton. Beton s: 184,1967.

Wiegrink, K., Marikunte, S and Shah, S.P. Shrinkage Cracking of High Strength Concrete, ACI Material Journal, V. 93. No.5, pp. 409-415, 1996.

Wolsiefer, J., and Clear, K., Long Term Durability of Silica Fume Structural Concrete, Shotcrete, Grout, Slab Overlays and Patches," Second CANMET/ACI International Symposium on Advances in Concrete Technology, Las Vegas, NV. 1995.

Wright ,P.J.F. Statistical Methods in Concrete Research. Magazine of Concrete Research, V. 16, No, 15, pp. 139-149,1954.

Yeginobal, A. and Sobolev, A. High Strength Natural Lightweight Aggregate Concrete

with Silica Fume. ACI, SP178-38.
Yang, C.C. and Huang, R. Double Inclusion for Approximate Elastic Moduli of Concrete Material, Cement and Concrete Research V. 26, No. 1, pp.83-91, 1996.

Zhang, M.H. Microstructure and properties of High Strength Lightweight Concrete. PhD Thesis, The Norwegian University of Science and Technology, N-7034 Trondheim, Norway. 1989

Zhang, M.H. and Gjorv, O. E. Pozzolanic Reactivity of Lightweight Aggregates. Cement Concrete Res., V. 20, pp. 884-990, 1990.

Zhang, M.H. and Gjorv, O. E. Microstructure of Interfacial Zone between Lightweight Aggregate and Cement Paste. Cement Concrete Research., V. 20 610-618, 1990.

Zhang M.H and Gjorv O.E. Characteristics of Lightweight Aggregates for High Strength Concrete. AC1 Materials Journal, pp. 150-158, 1991

Zhang, M.H., Gjørv, O.E. Permeability of High-Strength Lightweight Concrete. ACI Materials Journal, V. 88, No. 5, pp.463-469, 1991.

Zhang M.H. and Gjorv, OE. Mechanical Properties of High-Strength Lightweight Concrete. AC1 Materials Journal 1991, pp. 240 -247, 1991.

Zhang, M.H. Characteristics of Light Weight Aggregates for High Strength LWA Concrete. SINTEF Report STF65 A92022, Trondheim, Norway. 1992

Zhang, M-H et al. Materialutvikling Høyfast Betong, report 2.3. The Interfacial Zone between High Strength Lightweight Aggregate and Cement Paste, SINTEF-report A92023 Trond-heim, Norway, 1992.

Zhang, M.H. and Gjørv, O.E. Properties of High-strength Lightweight Concrete. CEB/FIP International Symposium on Structural Lightweight Aggregate Concrete, Sandefjord, Norway, pp. 683-693, 1995.